KAUNAS UNIVERSITY OF TECHNOLOGY

INDRĖ DRULYTĖ

APPLICATION OF THE STATISTICAL POST - PROCESSING METHODS IN ORDER TO ESTIMATE THE PARAMETERS OF LESIONS OF HUMAN TISSUE AND INCREASE THE ACCURACY OF ULTRASONIC MEASUREMENTS

Doctoral dissertation
Technological sciences, Measurement engineering (T 010)

2019, Kaunas

This doctoral dissertation was prepared at Kaunas University of Technology, Prof. K. Baršauskas Ultrasound Research Institute during the period of 2014–2018.

Scientific Supervisor:

Prof. Dr. Renaldas RAIŠUTIS (Kaunas University of Technology, Technological Sciences, Measurement Engineering – T 010).

Scientific Advisor:

Assoc. Prof. Dr. Tomas RUZGAS (Kaunas University of Technology, Natural Sciences, Mathematics – N 001).

Doctoral dissertation has been published in:
http://ktu.edu

Editor:

Tony Bexon (Publishing Office "Technologija")

ISBN 978-609-02-1572-2

The bibliographic information about the publication is available in the National Bibliographic Data Bank (NBDB) of the Martynas Mažvydas National Library of Lithuania.

KAUNO TECHNOLOGIJOS UNIVERSITETAS

INDRĖ DRULYTĖ

STATISTINIŲ APDOROJIMO METODŲ TAIKYMAS ŽMOGAUS AUDINIŲ STRUKTŪROS PAŽEIDIMŲ PARAMETRAMS VERTINTI IR MATAVIMŲ TIKSLUMUI ULTRAGARSU PADIDINTI

Daktaro disertacija
Technologijos mokslai, matavimų inžinerija (T 010)

2019, Kaunas

Disertacija rengta 2014-2018 metais Kauno technologijos universiteto Prof. K. Baršausko ultragarso mokslo institute.

Mokslinis vadovas:

prof. dr. Renaldas RAIŠUTIS (Kauno technologijos universitetas, technologijos mokslai, matavimų inžinerija – T 010).

Mokslinis konsultantas:

doc. dr. Tomas RUZGAS (Kauno technologijos universitetas, gamtos mokslai, matematika – N 001).

Interneto svetainės, kurioje skelbiama disertacija, adresas:
http://ktu.edu

Redagavo:

Tony Bexon (leidykla “Technologija”)

ISBN 978-609-02-1572-2

Leidinio bibliografinė informacija pateikiama Lietuvos nacionalinės Martyno Mažvydo bibliotekos Nacionalinės bibliografijos duomenų banke (NBDB).

CONTENTS

THE LIST OF ABBREVIATIONS

AMISE - asymptotic mean integrated squared error
GMM - Gausian mixture model
MAPE - mean absolute percentage error
PRESS - prediction sum of squares
EM - expectation – maximization algorithm
ROC - receiver operating characteristics
MLE - maximum likelihood estimation
MCM - Monte Carlo method
PDF - Probability density function
GUM - Guide to the Expression of Uncertainty in Measurement
TOF - Time of flight
k - space frequency of wave
T - period of time
c - speed of ultrasound
ρ - density
p_i - amplitude of wave moving through the interface
p_r - amplitude of reflected wave
p_t - amplitude of transmitted wave
θ - angle
W_{kr} - energy of moving wave
W_{at} - energy of the reflected wave
W_{pr} energy of transmitted wave
J_{kr} - intensity of moving wave
J_{at} - intensity of reflected wave
J_{pr} - intensity of transmitted wave
Z_1 - acoustic impedance of the first environment
Z_2 - acoustic impedance of the second environment
V_{ref} - voltage output due to the reflective wave at the transducer
V_s - received voltage signal from the scattering volume
D_{ref} - acoustic coupling function from the transducer surface to the reference plane and back to the transducer surface
D_s - mean diffraction correction coefficient for backscattering
z_{ref} - acoustic axis
w - angular frequency
η_s - coefficient of shear viscosity
η_B- coefficient of bulk viscosity
γ - ratio of specific heats
C_p - heat capacity
B - thermal conductivity

q - number of components in the mixture model
p_k - priori probability
$f_k(x)$ - distribution density function
n - size of sample
Ω - volume of area is histogram
K - kernel function
h - fixed (global) bandwidth
$\hat{f}(x)$ - kernel estimator
$\overline{X}$ - empirical mean
$S \epsilon R^{d \times d}$ - empirical covariance matrix
$Z = (Z(1), \ldots, Z(n))$ - sample of standardized data
V_d - volume of the d-dimensional unit sphere
K_{New} - new proposed kernel function
$\varphi(x)$ - distribution of normal
$R(g) = \int_{-\infty}^{\infty} g(u)^2 du$ is the roughness of a function.
v - order of a kernel
$\kappa_j(K) = \int_{-\infty}^{\infty} u^j K(u) du$ – non-zero moment
g_0 - reference density
$\hat{\sigma}$ - sample standard deviation
$\epsilon g(x)$ - arbitrary distribution
$\sigma^2{}_f$ - variance of distribution f
U - density of ultrasonic thicknesses distribution of the skin tumours
H - density of histological thicknesses distribution of the skin tumours
N - Normal distribution density
R_t - particular region
q_t - group-specific densities
$D_t^2(x)$ - generalized squared distance from x to group t
r - fixed radius
Γ - Gamma function
z - p-dimensional vector
$v_r(t)$ - volume of a p-dimensional ellipsoid
s - smoothing parameter
$A(K_t)$ - optimal constant for kernel
m_i - matrix
α - intercept parameter
$\beta = (\beta_1 \ldots \beta_s)'$ - vector of s slope parameters
μ - mean
σ - variance.
T - global threshold.

$\hat{O}$ - maximum likelihood estimator
$I_n(\hat{O})$ - expected Fisher information
l - rank of the parameter.
Δd_p - difference between results of measurements of the two methods
$\overline{\Delta d}$ - mean of the differences of two methods
$d_{1,p}$ - thickness of an application of proposed automatic statistical post – processing method
$d_{2,p}$ - thickness of non – invasive ultrasound examination (made by dermatologist)
$d_{3,p}$ - thickness of invasive histological analysis examination
$\overline{d_\iota}$ - average thickness of one of the 4 indexed groups
$d_{i,p}$ - thickness of the invasive histological examination ($i = 1,...,4$)
Δc - difference between the maximum and minimum ultrasound velocities
Δt_d - discretisation time interval
$u_{\Delta td}$ - uncertainty of ultrasonic signal sampling frequency
W - sensitivity coefficient
d - value of measured thickness
m - coverage factor

INTRODUCTION

Research object

Application of a newly developed automatic statistical post–processing method in order to analyse the characteristics and improve the classification of skin tumours from ultrasonic and digital dermatoscopy images.

Relevance of research and scientific problem

The number of people who are diseased by skin melanoma has been increasing faster and faster during the last three decades. When comparing the numbers of skin melanoma during the period of 2005 – 2014, it has shown that the number is increasing by 3% every year. The most vulnerable group are people are 50 years old or older. Skin melanoma rates are quite low and account for just 1% of all skin cancers, however it influences a high number of skin cancer deaths [1]. The most significant factors that strongly influence skin cancer are genetics and the health history of family, as well as other environmental factors [2, 3, 4]. A focus on the selection of the features and characteristics of lesions of skin tissue provides the possibility to achieve a faster diagnosis, to have a more accurate prediction of the disease, to save more people lives and to select an appropriate method of treatment, along with the possibility to diminish the cost of treatment. The first attempts of diagnosing melanoma in dermatology were introduced by Spitz in 1948. Spitz nevus received a name of "melanoma of childhood" due to the lack of technologies and undisturbed histopathologic features at that time [5].

Accurate data ensures the higher accuracy of analysis, which is one of the tools used for diagnosing and decision making. The storage of medical information and its statistical analysis have been carried out since the middle ages. The first known statistical journal of medicine was published in London, in 1662 [6]. In 1863, F. Nightingale, the pioneer of todays nursing, raised the problem regarding the lack of medical statistical records and non-systematic storage in hospitals, as a consequence of treatment effectiveness and costs limited analysis. In 1977 the US Congress published a study "Medical information systems practitioner's consequences" [7]. It states that medical information systems can be a useful tool for training, also to help medicine and health care specialists leading to a higher quality of facilities and optimization of health care institution activity. The authors of this study also confirmed that a medical information system would be a useful tool for researchers and health governing institutions. From 2000, an active global implementation of regional and national electronic health records systems started. The aim of these systems is to save all important patients medical records. The Lithuanian health sector also applies information technologies, creating a national electronic health services and information system for a cooperation infrastructure, in addition to a subsystem for national medical image archiving and exchange. Health care institutions implement and improve the information systems of hospitals, along with systems for radiological images preview and archiving, with information systems of laboratories

[8]. An information system of health care records structured information about the patient; such as diagnosis, demographic patient data, vital functions, test results and etc. The data analysis and mining are very important for all patients, especially when visiting various medical facilities. The smart analysis of patient records helps to faster diagnose an ailment, consequently choosing the optimal treatment, prediction of treatment periods and results, identifying the risk of complications and side effects, along with resource optimization of the health care institutions. In the last decade, data mining research in biomedicine has been highly considered [9, 10]. Data mining methods and algorithms can be useful if researchers clearly understand the scopes, types of data and peculiarities. The most common tasks mentioned in literature are classification, clustering, prediction, association, visualization, identification of deviations and analysis of internal links. For these data mining tasks, researchers need to choose a suitable algorithm. Choosing a method or an optimal algorithm depends on the aims of the task analysis and data characteristics. Over the last decade, many methods of data mining application in medicine have been identified. In diagnosis there are widely applied neural networks, decision trees, decision rules [11], methods for search of associative rules (for costs analysis) [12], prediction of patient health and treatment probability, also it is very popular to use assesment based on synergy of prediction algorithms [10]. In 2014, N. Esfandiari et al. [9], carried out a literature review, where there are examples of described applications of data mining in medicine based on analysis of the structured data. It is stated that classification (neural networks, decision trees, decision rules, support vector machine), clustering (k-means, hierarchical clustering) and associative search (*a priori* associative rules search) models are the most popular in medicine. Lalayants et al. [13] wrote that the solution of successful medical data mining is to identify the right activity of the health care institution or to find the clinical problem. Data mining methods are usually used in biomedical data analysis and visualization tasks in order to facilitate decision-making [14]. If the data mining process could be simple enough, the management of information problems would have been solved a long time ago (R. Bellazzi, B. Zupan [10]). Practical data mining application in medicine has some obvious barriers, such as technological problems, trans-disciplinary communication, ethics and patient data security [12, 14, 15]. Medical research leads to a lot of data characterizing the condition of a patient. However, all this data is dynamically changing and depends on the patient's illness, patient's biological condition, environment, the quality of life, related diseases and other actual reasons, which can be described as a random factor. The change of medical statistic observations is described by primary statistics analysis. The results lead to further ideas of medical research and affect the application of the appropriate statistical method. The reliability of the above mentioned methods usually depends on the assumption of data distribution – normal, binomial and etc. This study will present a simple, effective method of nonparametric statistics and a hypothesis criteria about the variable distribution and identity checking of two distributions. These hypotheses are called goodness of fit test hypotheses. Therefore, the purpose of this research is to determine the connection between the thicknesses of the skin tumours measured by non-invasive ultrasonic technique and after a surgical

intervention measured histologically by optical microscope. In addition, the research will compare the compatibility of the likely density of histological thicknesses distribution of the skin tumours and Normal distribution density. Conseuently, this method is effective for a structured large data matrix and simple to use. There is no reason to check the sample that is distributed by well-known theoretical distribution, because these cases have already been examined both theoretically as well as empirically. The greatest challenge is to check the identity between two samples. As a solution, the most commonly used techniques relies on the differences of density distribution. Even in todays data analysis there are a lot of evaluation methods of density distribution, but in practice it is not easy to find an effective evaluation procedure if the data distribution is multimodal and the volume of the sample is small. Kernel smoothing is the most frequently used nonparametric estimation method (see Jones, et al., 1996 [16], Marron and Wand, 1992 [17]; Silverman, 1986 [18]). Thus far, there is no generally accepted method for kernel estimation, which outperforms the other in all cases. Although many adaptive selection procedures have been proposed (Bashtannyk and Hyndman, 1998 [19]; Jones, 1992 [20]; Zhang et al., 2004 [21]), their efficiency has not yet been well established, especially for samples of a moderate size.

On the basis of Lithuanian cancer registered data, Lithuania diagnosed more than 250 melanomas cases every year. Although Lithuania is not included in the list of the largest melanomas risk countries, the statistics show that the number of melanomas cases in Lithuania is increasing every year. The main reason is that diagnosis occurs too late. The mortality of melanoma in Lithuania is larger than in other Europe countries [22, 23]. Melanoma is a rapidly growing and spreading malignant tumour, rarely amenable to treat through the spread of time. Usually melanoma is diagnosed in 2 – 4 stages, however in the absence of effective treatment of metastatic melanoma, a patients survival chance decreases. A key factor of survival of melanoma is early diagnosis and urgent surgical removal of the primary tumour. The late diagnosis of melanoma can be prevented by regular checks of nevus and disposal nevus, which could also be malignant. Surgical removal of melanoma that has a thickness of 1 mm increases the probability of survival for 10 years by 90 – 97 percent [24, 25].

Ultrasound technologies allow medical staff to capture high accuracy images of the human skin. Scanning the human body by ultrasound, echo and its differences are captured, because bones, fat and muscles reflect differently. Reflected ultrasound waves are translated to electric impulses, which help to shape an image and to analyze the surface of lesion. Images of deeper skin layers can identify very informative data related to the analysis of diagnosing the early stage of melanoma, but most of the published research is based only on the analysis of the thickness measurements of malignant skin tumours [26, 27] and not on the other characteristics of skin layers. This research presents a newly developed automatic algorithm by enabling the analysis and estimate of more features of skin tumours.

The question that will be answered at the end of this research is, can the accuracy of ultrasonic B-scan and digital dermatoscopy measurements be improved by using an automatic measurement technique based on the assessment of synergy of these different technologiesand can the proposed method be used in the field of dermatology as a decision support tool?

The **working hypothesis** of the thesis is whether the assessment of synergy of the ultrasonic B-scan and digital dermatoscopy imaging based on an automatic post-processing method can increase the accuracy of measurements of skin lesion tumours. Additionally, whether the proposed automatic post-processing method can be used as a reliable decision support tool in the field of dermatology, and help to reduce the numbers of invasive histological examinations and surgeries in such a way to save more people's lives.

The aim of the research is to develop an automatic analysis and measurement technique based on the application of a set of statistical post – processing methods and the synergy of different imaging technologies; in order to estimate the parameters of human skin lesions and increase the accuracy of ultrasonic B-scan and digital dermatoscopy measurements.

Goals of the research

The following goals were formulated in order to achieve the objective:

1. The development of an automatic statistical post–processing measurement technique based on the different technologies of ultrasonic and digital dermatoscopy imaging in order to estimate the multimodal set of the most informative parameters of lesions, as well as to identify benign and malignant nevus and increase the accuracy of measurements.
2. The simulation and application of the proposed automatic statistical post–processing measurement technique based on the different technologies of ultrasonic and digital dermatoscopy imaging in order to identify the features of lesions of human tissue and to assess the results.
3. To compare the results of the proposed automatic analysis and measurement technique with other data mining and data processing methods.
4. To estimate the precision and reliability of the proposed automatic statistical post–processing based measurement technique by using metrology evaluation.

Scientific novelty

According to the literature review, there is no proposed method of enabling the possibility to process images of skin tumours that are captured by using different imaging technologies (ultrasound and digital dermatoscopy). In addition, there are no currently published research results that have been identified. A newly developed automatic algorithm based on the synergy of data captured by using two different

imaging technologies (ultrasound and digital dermatoscopy) is presented. A proposed new method is used for the analysis of clinical decision making of malignant skin tumours. As a result, the automatic post-processing statistical method can supplement well-known decision support tools in clinical practice and help to reduce the number of histological examinations and provide important information about the thickness of a skin tumour before planning any surgery.

Practical value of the work

The thickness of skin tumours measured by high frequency ultrasound strongly influences the forecasting and planning of medical treatment. The reliability of the ultrasonic thickness measurement of the skin tumour is completely covered by the high similarity to the histological thickness measurement and has a practical value in diagnosing skin melanoma. A newly developed and proposed statistical automatic ultrasonic B-scan and digital dermatoscopy images post-processing, characterising quantitave tissue parameters method, can be used for the classification of benign and malignant skin tumours and therefore used as a decision support tool in the field of dermatology. The newly proposed method does not depend on the experience of the dermatologist and due to the low price of the medical technique (ultrasound system and digital dermatoscope), it can additionally be used in smaller medical centres.

The results of the research were presented in the following projects

"Ultrasonic, optical and spectrophotometric data fusion technology for the diagnosis of superficial tissue lesions (ImageFusion)". Work sponsored by the Kaunas University of Technology and Lithuanian University of Health Sciences under a joint grant.

Statements under defence

- The evaluation of ultrasonic thickness measurements by applying a newly developed statistical method is completely covered by the high similarity to the histological thickness measurements, which are known as a golden standard in the field of dermatology. The proposed technique is appropriate to use for the classification of skin tumours.
- The classification of skin tumours based on the assessment of synergy of two different imaging technologies (ultrasound and digital dermatoscopy) was improved by 9%. This means that the proposed automatic statistical post–processing method could be used as a decision support tool in the field of dermatology in order to identify a malignant tumour and benign nevus. The reliability of classification is proved by the estimated area under the ROC curve of 0,908.
- The newly developed automatic statistical post–processing method has shown similar uncertainty results when compared with non-invasive ultrasound examination (made by dermatologist) and proved that the proposed fully automatic method is constructed under the necessary requirements and can be used for the estimation of the thickness of skin tumours.

Approbation

The results of the research are presented in 6 published articles: 2 papers are published in the periodic journals (Journals of the Master List of Thomson Reuters Web of Science, with impact factor), two in reviewed proceedings of international scientific conferences and two in reviewed proceedings of national scientific conferences. The results have also been presented at 5 scientific conferences, 2 of them at international scientific conferences held in Valmiera, Latvia and Druskininkai, Lithuania and 3 have been presented in national scientific conferences held in Kaunas, Lithuania.

Structure and contents of the thesis

The dissertation consists of an introduction, 5 general chapters, general conclusions, a list of the references, list of publications of the author and an appendix. The sequence of presentment of the doctoral thesis is defined below:

1. An overview of the main features, characteristics, structure and classification of lesions of human skin tissue is presented in chapter 1. Chapter 1 also includes a review and comparison of the morbidity and mortality rates among Lithuanians. The comparison of the expansion level of skin tumour diseases between Lithuanians and Europe citizens; Lithuanian and World statistics is also introduced in chapter 1.

2. The main characteristics and specification of ultrasound wave are presented in chapter 2. Chapter 2 also includes a theory of ultrasound imaging, methods used in digital dermatoscopy and the basics of spectrophotometric intracutaneous analysis. The comparison of the three different techniques mentioned above is also presented in chapter 2.

3. Assessment and comparison of likely density distributions in the cases of the thickness measurement of skin tumours by ultrasound examination and histological analysis are presented in chapter 3. As the assesment is based on the kernel density estimator, methods and analysis of estimation accuracy are presented in chapter 3. Chapter 3 also includes an application of goodness of fit test in order to prove that the reliability of the ultrasonic thickness measurement of the skin tumour is completely covered by a high similarity to the histological thickness measurement, which is known as a “golden standard” in the field of dermatology.

4. Theory of parametric and nonparametric methods used in the estimation of the parameters of human tissue are presented in chapter 4. As the discriminant analysis and logistic regression were the models used in research, a comparison of these two models is also presented in chapter 4. Gaussian smoothing, and expectation maximisation adopted to the thresholding procedure and used for skin tumour segmentation from ultrasonic and digital dermatoscopy images are defined in chapter 4. The selection of parameters of skin tumours, including estimation of significant and not significant parameters used in automatic classification, are presented in chapter 4.

Results of the automatic classification run by the two models defined above are shown in chapter 4. Diagnostic accuracy, sensitivity and specificity rates, as well as ROC analysis are also presented in chapter 4.

5. Chapter 5 includes the metrology evaluation of the skin tumours measurements. Uncertainty due to the measurements of thickness, as well as combined and expanded uncertainties, are presented in chapter 5.

6. General conclusions are presented in the 6 chapter.

The overall dissertation volume is 150 pages, including 29 figures, 34 tables, 58 formulas and 314 bibliographic references.

1. REVIEW OF SKIN STRUCTURE AND FACTS OF CANCER RATES

Human skin is an external body layer that is responsible for the protection of deeper layers and helps to interact with harmful environmental rakes. Unfortunately, unprotected skin can cause serious damage, which can lead to skin cancer. This is why people should also take as many preventative measures as possible. The collection of statistics of skin cancer rates is an important aspect of data collection, helping to monitor the pervasion and other phenomena of malignant tumours.

This chapter introduces a review of the structure of human superficial tissue (skin) and facts of cancer rates. Structure and classification of lesions of human skin tissue are presented in section 1.1. A review and comparison of the morbidity and mortality rates based on international and national levels are presented in section 1.2. Section 1.3. introduces the summarized outcomes of chapter 1.

1.1. Structure and classification of lesions of human skin tissue

Skin is the largest organ of the human body and approximately accounts for up to 10 percent of the body mass [28]. Skin is one of the human organs that allows people to interact with the environment and has many important other functions, such as prevention from the changes of temperature and other natural physical phenomenon, as wind, cold, rain and etc. In addition, skin also helps to protect deeper human body organs from environmental dangers, such as chemicals, bacteria's, allergies, radiation and etc. Skin is also a sensor that enables people to feel heat, cold, pain, micro-organisms' bites and etc. Skin also helps to control heat, blood pressure and production of excretory. Skin is an organ that is in a continual state of regeneration and repair. Skin is also responsible for a lot of chemical reactions, such as melanin absorption and etc. [29].

Skin consists of epithelial and mesenchymal tissues, which has a structure of multi-layered stratified epidermis, adnexal structures such as hair follicles, sweat glands and sebaceous glands, in addition to dermis containing collagen and elastic fibres and underlying subcutaneous fat [30].

Skin consists of three main layers called the dermis, epidermis and hypodermis (also known as subcutaneous tissue). The structure of human body skin is presented in Fig. 1.

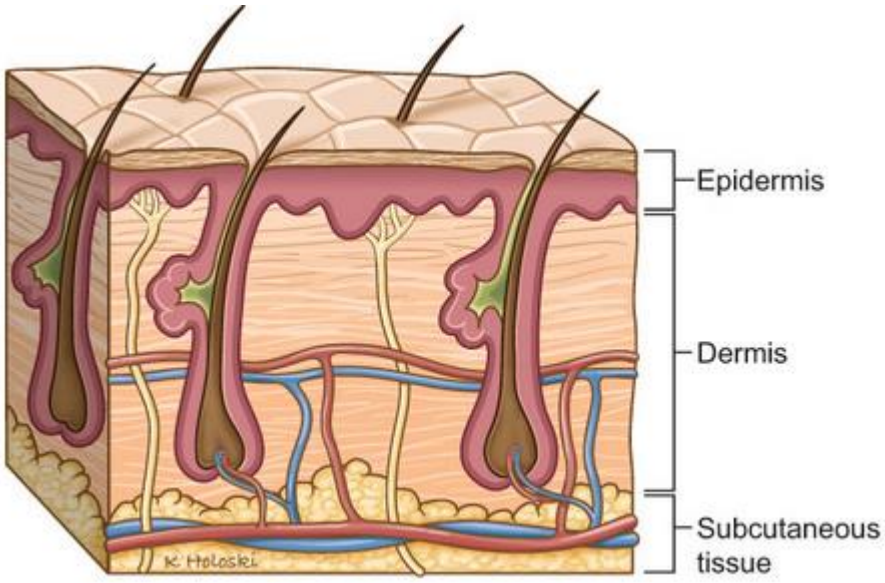

Fig. 1. Structure of human skin [30]

Consequently, skin also has a lot of different cell types, which can easily become cancerous cells. The epidermis is the external skin tissue that has a lot of layers and many more cell types, such as keratinocytes and melanocytes, Merkel cells and Langerhans cells [31]. The structure of the epidermis is presented in Fig. 2. Keratinocytes are the main part of the epidermis layer and are responsible of the formation of the barrier of the body. In the deeper layer of the epidermis, keratinocytes are called basal cells, which can also become cancerous and as a result, a human can get sick off basal cell carcinoma cancer. Melanocytes are the cells responsible of the protein called melanin. Melanin influences the colour of the skin, i.e. it means the more melanin the darker the skin is. Melanin also helps to prevent other skin cells from the harmful ultraviolet sun rays. Merkel cells are known as neuroendocrine cells and have some features of hormone cells. Langerhans cells are partly responsible for the immune system and can also be found in other skin layers, such as the dermis, lymph nodes and etc.

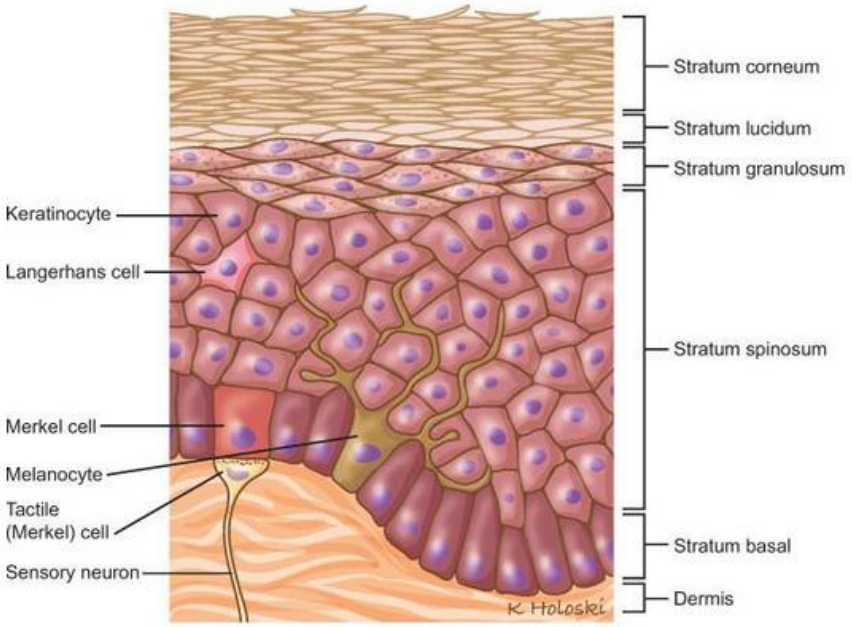

Fig. 2. Structure of the epidermis [30]

The dermis is the thickest layer of the skin and consists of blood vessels, hair follicles, sweat glands, lymph, oil glands, nerves ending etc. The dermis has two main layers, called the papillary are reticular dermis. Structure of the dermis is shown in Fig. 3.

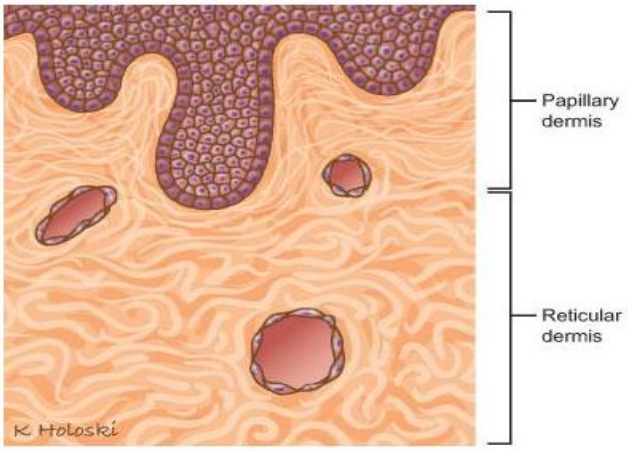

Fig. 3. Structure of the dermis [30]

The third skin layer is a subcutaneous layer, which consists of fat cells, as well as collagen cells and larger blood vessels.

1.2. Review of the morbidity and mortality rates compared to international and national levels

Analysing data of the overall morbidity of skin cancer in Lithuania, it is clear that the sickness rate during the period 1978 – 2009 has increased more than 3.5 times. Meanwhile, sickness of melanoma has increased more than 4 times [32]. The trend line of morbidity rate is presented in Fig. 4.

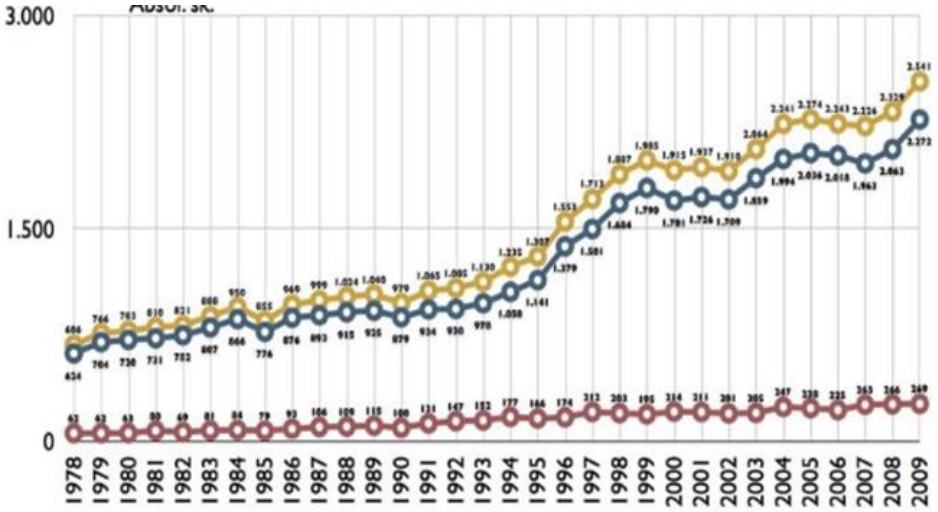

Fig. 4. Morbidity rates of skin cancer in Lithuania during the period of 1978 – 2009 years. Blue circles show an overall number of non-melanoma cancer, yellow circles show an overall number of skin cancer, red circles show an overall number of melanoma [32]

During the period 1978 – 2009 in Lithuania, the largest sickness rate of melanoma is diagnosed in women. The morbidity rate for men is 1.5 times less. The sickness rate of melanoma between genders is presented in Fig. 5.

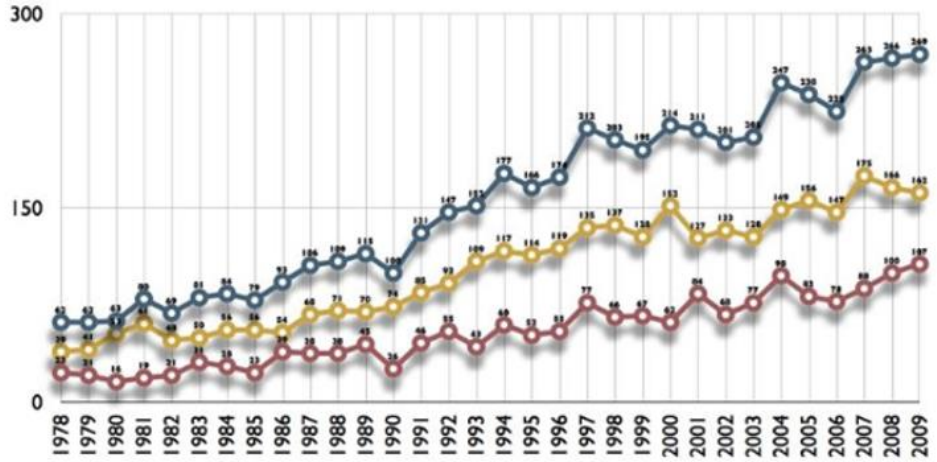

Fig. 5. Morbidity rates of skin cancer between genders in Lithuania, during the period of 1978 – 2009 years. Blue circles show an overall number of melanoma, yellow circles show a number of melanoma diagnosed in women, red circles show a number of melanoma diagnosed in men [32]

The latest study of skin cancer in Lithuania has shown that in 2011 there were 351 melanoma cases diagnosed, from them; 121 were diagnosed in men and the remaining 230 cases in women. Other types of malignant skin cancer have reached 2484 cases, where 65% of skin cancers were diagnosed in women. Comparing these results with the standards of melanoma rates in Europe and the rest of the world, Lithuania has exceeded the European standard by 30% and the world standard by around 75%. Analysing the results of other malignant skin cancer rates, Lithuanian has exceeded the European standard by 45% and the world standard more than 2 times. Another important observation is the differences of morbidity rates between genders. Women in Lithuanian, who are diseased by melanoma, have exceeded the European standards more than 35% and the world standard around 85%. Meanwhile, men in Lithuanian who are diseased by melanoma, have only exceeded the European standards by approximately 15% and the world standard by around 60%. The results of other malignant skin cancer rates have shown that Lithuanian women have exceeded the European standard by 60% and the world standard more than 2 times, while men have only exceeded the European standard by 15% and the world standard by 75%. Analysing 2011 the statistics of the stages of men's skin melanoma and other malignant skin cancer types, it is obvious that the most melanoma skin cancer was diagnosed in stage II (39.7%) and in stage I (37%). Other types of skin cancer were mostly diagnosed in stage I, i.e. more than 70%, which leads to a faster diagnosis of the early stage and a higher rate of morbidity. Comparing data of diseased women, the highest number of cases of melanoma was diagnosed in the early stage (41.7%),

as well as the highest number of cases of other types of skin cancer being diagnosed in the early stage (73.9%) [33,34].

1.3. Conclusions of 1st chapter

1. Skin is one of the most important human body parts that protects our deeper organs from a negative environment impact and also helps to monitor a lot of vital processes, such as control of temperature and renewal of old or damaged cells.
2. Skin consists of three main layers, called the dermis, epidermis and subcutaneous tissue. All these layers consist of various cells, which are responsible for the normal human body condition, such an immunity, balance of hormones, production of proteins.
3. Analysing data of morbidity and mortality statistics during the period 1978 – 2009, it has shown that Lithuania has exceeded the European standard by more than 35% and the world standard by more than 85% when comparing rates of skin melanoma from around the world. This means that Lithuanians are classed as an exposed nation.
4. Analysis also shows that women are the more vulnerable group when compared with the results of the statistical male group. In fact, there is no proven reason why the non-aligned existence between the two groups is so large, however prevention and a proper cure is required.
5. Modern developed diagnostic medical equipment strongly influences the higher number of diagnosed diseases and helps identify more malignant tumours in the early stages, which leads to more saved lives.
6. Social media is also a prevention tool, which motivates people to visit a dermatologist regularly in order to get a prophylactic examination and to preclude any skin cancer.

2. ULTRASOUND, DIGITAL DERMATOSCOPY AND SPECTROPHOTOMETRIC TECHNIQUES

These days', dermatology can offer various techniques to be used in order to improve the accuracy of diagnosing diseases. The most popular techniques are ultrasound, digital dermatoscopy and spectrophotometric intracutaneous analysis. All these non-invasive techniques allow dermatologist to look into the deepest skin lesions and get an accurate estimation of the skin diseases and also helps to select an appropriate treatment if needed.

This chapter presents a review and main features of the different techniques used in dermatology for the purposes of accurate identification of skin cancer at an early stage. A review of ultrasound and the main ultrasound characteristics are presented in section 2.1. Review of the ultrasound imaging in dermatology that is a popular technique between researchers is presented in section 2.2. Section 2.3. and section 2.4. introduce the basics and methods used for the analysis of digital dermatoscopy and spectrophotometric intracutaneous. Section 2.5. introduces the summarized outcomes of chapter 2.

2.1. Ultrasound and main ultrasound characteristics

Ultrasound is a sound wave, which has a frequency higher than the frequency of human hearing and can reach 20 kHz. Ultrasound cannot identify objects that are smaller than the length of an ultrasound wave. This means that the higher the frequency of the ultrasound, the higher the resolution of images. On the other hand, the higher frequency of ultrasound emits shorter length waves, which can easily be absorbed. This strongly affects the high frequency ultrasound that is used to scan lesions that are near the surface of the human body and the low frequency ultrasound that is used to scan deeper body parts. An ultrasound wave is mostly shown as a sinusoid wave, where the peaks and nadirs show a compression and a rarefaction [35 - 37]. A wavelength that is denoted as λ, is showing the distance between the two nearest peaks or troughs of the periodic waves and this also is a length unit. In medical ultrasound, it is acceptable to use a 0.1 – 1 mm scale [38]. The wavelength can be defined as:

$$\lambda = 2\pi/k; \tag{1}$$

Here k is the space frequency of wave.

Due to medical examinations, the ultrasound wave frequency, which is denoted as *f*, varies between 1 and 50 MHz, therefore it is acceptable to use a frequency which varies between 1 - 15 MHz [38, 39]. If the periodical structure propagates, therefore a rate where the peak reaches a fixed point – number of peaks passing per second – is named a frequency of wave. Frequency can be defined as:

$$f = \frac{1}{T}; \tag{2}$$

Here *T* is period of time.

Circular or corner frequency, which is denote as ω, and is the number of radians per second, can be expressed as follows:

$$\omega = 2\pi f. \tag{3}$$

Space frequency of the wave is denoted as k and is defined as $k = 2\pi/\lambda$. The measurement unit of frequency is the number of radians per meter, i.e. *rad/m* [38].

There are two types of ultrasound waves, transversal and longitudinal and the speed depends on the properties of density of the environment and tension.

The speed of sound in various materials are defined as:

$$c = \sqrt{\frac{\kappa}{\rho}}. \tag{4}$$

The speed of ultrasound in soft tissues of the human body varies between 1445 - 1600 m/s, while in water it is approximately equal to 1500 m/s [40].

The comparison of ultrasound speed between different materials is presented in Table 1.

Table 1. The comparison of ultrasound speed [40]

Material	Speed of ultrasound wave
Fat	1470 m/s
Muscles	1500 m/s
Heart	1570 m/s
Kidneys stones	1400-2200 m/s
Cornea	1640 m/s
Bones	3370 m/s

Characteristic acoustic impedance is a feature of the environment where a wave is moving. Acoustic impedance is very important in order to calculate the coefficients of reflection and transmission in the limit of two environments and to estimate an absorption of ultrasound.

Impedance can be in form as follows [41]:

$$Z_{el} = \frac{\tilde{V}}{\tilde{I}}, \tag{5}$$

$$Z_{ak} = \rho c. \tag{6}$$

Fig. 6. presents a scheme of the interactions within the materials affected by ultrasound [42].

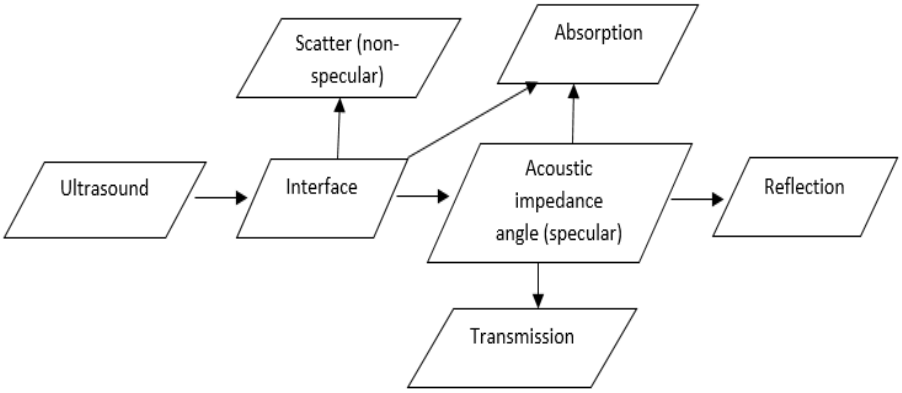

Fig. 6. A scheme of the interactions within the materials affected by ultrasound [42]

Coefficients of reflection and transmission

When the acoustic pressure wave with the amplitude of p_i is moving through the interface, therefore a wave with the amplitude p_r will be reflected, and another wave with the amplitude p_t will be transmitted. The coefficients *R* and *T* of these waves can be expressed as [36]:

$$R = \frac{p_r}{p_i} \qquad (7)$$
$$T = \frac{p_t}{p_i}.$$

The coefficient of reflection of moving pressure can be defined as follows [36]:

$$R = \frac{\rho_2 c_2 - \rho_1 c_1}{\rho_2 c_2 + \rho_1 c_1} = \frac{Z_2 - Z_1}{Z_2 + Z_1}. \qquad (8)$$

Therefore, the coefficient of transmission under the equality of *1+R=T,* can be expressed as [36]:

$$T = \frac{2\rho_2 c_2}{\rho_2 c_2 + \rho_1 c_1} + \frac{2Z_2}{Z_2 + Z_1}. \quad (9)$$

Coefficients of reflection and transmission by angle can be expressed as a function of movement by angle [36]:

$$R = \frac{\rho_2 c_2 \cos(\theta_i) - \rho_1 c_1 \cos(\theta_t)}{\rho_2 c_2 \cos(\theta_i) + \rho_1 c_1 \cos(\theta_t)}, \quad (10)$$

$$T = \frac{2\rho_2 c_2 \cos(\theta_i)}{\rho_2 c_2 \cos(\theta_i) + \rho_1 c_1 \cos(\theta_t)}. \quad (11)$$

The coefficients of the intensity reflection and transmission

Coefficient of reflection [36]:

$$R_t = \frac{W_{at}}{W_{kr}} = \frac{J_{at}}{J_{kr}} = (\frac{Z_2 - Z_1}{Z_2 + Z_1})^2; \quad (12)$$

where W_{kr} – energy of moving wave, W_{at} – energy of the reflected wave, J_{kr} - intensity of moving wave, J_{at} – intensity of reflected wave, Z_1 – acoustic impedance of the first environment, Z_2 – acoustic impedance of the second environment.

Therefore, the coefficient of transmission will be equal to [36]:

$$T_t = \frac{W_{pr}}{W_{kr}} = \frac{J_{pr}}{J_{kr}} = \frac{4Z_1 Z_2}{(Z_2 + Z_1)^2}; \quad (13)$$

where W_{pr} – energy of transmitted wave, W_{kr} – energy of the moving wave, J_{pr} - intensity of transmitted wave, J_{kr} – intensity of moving wave, Z_1 – acoustic impedance of the first environment, Z_2 – acoustic impedance of the second environment.

Refraction

Refraction is a phenomenon that allows a distorted stick view to be seen in water. This occurs because of the changed direction of light speed differences when it comes through the boundary of water and air [36].

Scattering and Diffraction

Scattering is a non-linear phenomenon, when a wave which is spread from one scatter can be spread from another scatter and again from the first and so on. Sometimes it is useful in order to scatter the whole pressure field to a self-moving field. i.e. a component made of waves, which were scattered one time, two times and so on. Scattering and diffraction are related and also overlapping incidences, but having different definitions. Scattering depends on the reflection of the speed from the surfaces or on the heterogeneity of the environment [43].

In analysing tissues, a backscatter coefficient is a parameter that shows an efficiency that is used in the scattering of ultrasound energy [43]:

$$\eta(w) = \frac{\langle |V_s(r\epsilon V,w)|^2 \rangle}{\left|V_{ref}(2z_{ref},w)\right|^2} * \frac{\left|D_{ref}(2z_{ref},w)\right|^2}{l*\overline{D_s}(r\epsilon V,w)}; \quad (14)$$

here V_{ref} is the voltage output due to the reflective wave at the transducer, V_s is the received voltage signal from the scattering volume, D_{ref} is the acoustic coupling function from the transducer surface to the reference plane and back to the transducer surface, D_s is the mean diffraction correction coefficient for backscattering, z_{ref} is an acoustic axis [43].

Analysing lesions of human skin tissue, ultrasound backscattering helps to identify the lesions and to classify various skin damage. An addiction of the frequency from ultrasound backscattering can be used in order to improve the resolution of B-scan images. The ultrasound backscattering technique is used to identify the differences of the parameters of microstructure of biological tissues.

Diffraction is mostly used in order to define a leak of sound to areas of shadows. Diffraction allows hearing a sound from another room, even though we cannot see the people who are speaking. Sound waves "wrap" the corner more than light waves.

Acoustic absorption

All moving ultrasound waves are partly absorbed, i.e. some energy is transformed to heat, and therefore an amplitude becomes higher. Absorption depends on the transformation of acoustic energy to heat [44]. Therefore, Stokes-Kirchhoff classical absorption coefficient can be expressed as follows [45]:

$$\alpha = \frac{w^2}{2\rho_0 v^3}\left(\frac{4}{3}\eta_s + \eta_B + \frac{\gamma-1}{C_p}K\right); \quad (15)$$

Here *w* is an angular frequency, η_s is the coefficient of shear viscosity and η_B is the coefficient of bulk viscosity, γ is the ratio of specific heats, C_p is the heat capacity and B is the thermal conductivity.

2.2. Ultrasound imaging in dermatology

An application of ultrasonography was first described in 1979, by Alexander and Miller [46]. The idea was that a high frequency wave propagated by a transducer pulsates into the human skin and detects returned echoes by a backscattering technique in an appropriate time delay. This method identified a lot of different advantages, such as determination of an incident signal, depth and thicknesses of the skin object, scatter properties, as well as the absorption characteristics of the lesion [47]. Echoes are also useful for capturing information about absorption and reflection of the lesion in the human skin tissue.

For example, Harland et al. used 20-MHz ultrasound B-scan imaging, including acoustic shadowing and entry echo line enhancement, in order to classify melanomas and basal cell papilloma. Researchers have found that the sensitivity to classify melanomas and basal cell papilloma is equal to 100%, while a specificity is equal to 79% [48]. ROC analysis has also shown reliable results of classification, i.e. coefficient in the case of quantitative estimation of shadowing areas was equal to 0,93 and for semi-quantitative estimation was equal to 0,97 [48].

In 2011, Machet et al. presented an overview of high resolution ultrasound imaging of pigmented skin damage, such as melanoma, nevi and basal cell carcinoma [49]. The group of researchers used a prototype based on the technique presented by Berson et al. in 1992s. This proposed solid ultrasonic tool was processing at 17 MHz and had an easy to use probe with an acoustic window that was covered by a thin membrane. This enabled the separation of the skin tumours on the epidermis of the face, where they are founded more frequent than on other parts of the human body [50]. The main focus of the research made by Machet et. al was to identify melanoma that is less than 0,5 mm thick and remove it before it becomes malignant. In previous research it was shown that a high-resolution ultrasound technique is able to determine melanoma and non-melanoma from ultrasound thickness and allow the patient to be operated on in a single operation in nearly 75% of cases. [51]. High resolution ultrasound imaging may also help in diagnosing the other most common skin cancer, i.e. basal cell carcinoma, which is a consequence of extreme sunbathing [52,53].

In 2010, Wortsman and Wortsman presented a study on an application of ultrasound imaging in order to identify different skin damage, such as melanoma, basal cell carcinoma, skin cyst and nail damage [54]. However, one of the disadvantages of the used technique was the lack of sensitivity to detect epidermis lesions that are around 0,1 mm of thickness. Even though all the diagnoses were confirmed independently by a single observer, it was stated that the ultrasound can affect the accuracy during the diagnostic stages by up to 17% [54]. As a result, the percent of correct classification of the lesions was equal to 73%, while sensitivity was equal to 99%, specificity - 100%, and statistical diagnostic certainty was 99% [54].

Rallan et al. presented a paper of the classification of benign nevus, melanoma and SKs by using a three-dimensional high-resolution ultrasound in order to capture images using a reflex transfer [55]. An ambient skin was used as a test, therefore digital ultrasonography parameters have been captured for all the significant

measurements of lesions of total sound attenuation, intra-lesion sound reflection, surface sound reflectance and the relative uniformity of each parameter across the tumour [55]. As a result, reliable differences between benign and malignant parameters of tumours were identified in order to reduce the accuracy of classification of benign tumours by 65% without missing melanoma [55].

Ultrasound technique allows the capture of a lot of different and significant parameters of malignant skin damage when compared with invasive methods. This includes significant anatomical data on the extension, exact location, vascularity, activity, and severity of common cutaneous abnormalities [56]. Information like this can help to manage the planning of surgeries, prevent a relapsing of the same disease and clearly determine the origin of lesions and endogenous or exogenous components. An additional stated fact is that sonography can be used as a way of saving the environment, without the use of contrast fluid, radiation and can be done in isolated areas [57 - 59]. These arguments should also be aligned to the fact that patients are seeking to get the best cosmetic results during the treatment stages [56]. More applications of ultrasonography in medicine can be found in research conducted by Kreitz,: Rallan and Harland; and Kleinerman et al. [60 - 62].

2.3. Digital dermatoscopy

Dermoscopy is one of the non-invasive clinical methods that is based on the evaluation of the morphological features of lesions of skin tissue. Digital dermoscopy uses an optical magnification in order to estimate the properties of skin lesions in situ. This method allows a detailed observation analysis of the pigmented and non–pigmented structures of the epidermis, dermo-epidermal junction and, to a lesser extent, the dermis. Digital dermoscopy is a widely used technique for analysis of features of those skin lesion tissues that cannot be clearly seen by the naked eye [63 – 73].

Typical dermoscopic features of melanoma are presented in Table 2 and for a visualization perspective in Fig. 7. These features can also be found for benign nevus [74 - 82].

Table 2. Dermoscopic features of melanoma [74 - 82]

Feature
Atypical network – 1
Dots - 2,5
Globules - 3,7
Blue – white veil – 4
Regression area – 6
Linear irregular vessels – 8
Blotch – 9
Streaks – 10

Fig. 7. Dermoscopic melanoma view [74 - 82]

Typical dermoscopic features of pigmented BCC are presented in Table 3. and for visualization purpose in Fig. 8.

Table 3. Dermoscopic features of pigmented BCC [83]

Feature
Maple leaf – like pattern – 1
Large grey – blue ovoid nests – 2
Arborizing telangiectasia – 3
Spoke wheel – 4

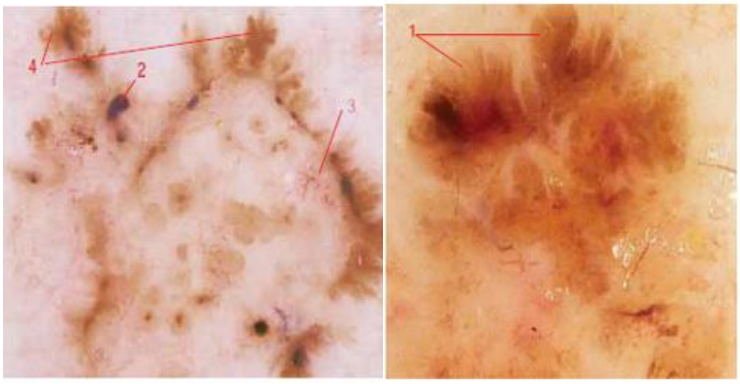

Fig. 8. Dermoscopic pigmented basal cell carcinoma views [83]

One of the most common methods for monitoring changes of benign and malignant tumours is the ABCD rule. The ABCD rule method was first proposed by Stolz et al. and can be easily applied in the analysis of skin damage changes. It is proven that this method is very reliable and can be used in cases for the diagnosis of melanoma [84].

ABCD rule method is based on the scoring process by using a formula [84]:

$$Total\ score = A\ score \cdot 1.3 + B\ score \cdot 0.1 + C\ score \cdot 0.5 + D\ score \cdot 0.5. \quad (16)$$

Ranges of total score are defined as:

$$\begin{cases} if\ total\ score < 4.75, then\ benign\ nevus \\ if\ total\ score\ is\ between\ 4.75\ and\ 5.45, then\ questionable\ diagnosis \\ if\ total\ score > 5.45, then\ very\ suspect\ lesion\ requesting\ deeper\ examination \end{cases}$$

Definitions and scores of ABCD rule features are presented in Table 4 [84].

Table 4. Features, definitions and scores of ABCD rule

Feature	Definition	Score
A – skewness	Need to look at the 0, 1 or 2 perpendicular axes.	0 – 2
B – borders	Estimation of ending of the pigmented lesion.	0 – 8
C – colour	Colour variation – white, red, light brown, dark brown, grey – blue, black	1 – 6
D – dermoscopic structure	View of the globules, dots, network, structure (homogeneous), branched streaks.	1 – 5

In 2000, Menzies et al. presented a simple dermoscopy technique in order to diagnose pigmented basal cell carcinoma disease [85]. This method has showed reliable results, where sensitivity for diagnosing of basal cell carcinomas was equal to 93%, specificity in comparing with melanoma was equal to 89% and comparing with benign lesion was equal to 92%. Details of the principle of using the Menzies methods are presented in Table 5 [85].

Menzies method depends on the counting of negative and positive features of a skin lesion. In the case of melanoma, no negative features should be satisfied and at least one of the positive features should be satisfied [85].

Table 5. Negative and positive features for identification of melanoma [85]

Negative feature	Positive feature
Symmetry of lesion along all the axes	Blue – white veil
Colour of lesion does not include white colour	Multiple brown dots
	Pseudopods
	Radial steaming
	Scar – like depigmentation
	Peripheral black dots or globules
	Multiple colours (more than 5)
	Multiple blue or grey dots
	Broadened network

A new method named as the 7 point's check list method was presented in 1998 by Argenziano et al. [86]. This method depends on the evaluation of the overall score of dermoscopic features. If the score is higher than 3, there is a high risk of melanoma disease and if the score is less than 3, then the tissue is not malignant. The evaluated features are presented in Table 6.

Table 6. Features and score used in 7 point's check list method [86]

Feature	Score
Atypical pigment network	2
Blue whitish veil	2
Atypical vascular pattern	2
Irregular streaks	1
Irregular dots/ globules	1
Irregular blotches	1
Regression structures	1

One other method to check the infusion of skin cancer is the methodology of Clark levels [87]. This system was developed by Wallace H. Clark Jr. in the 1960's and is widely used among dermatologists. The levels and definitions are presented in Table 7 and shown in Fig. 9.

Table 7. Clark's levels definitions [87]

Level	Definition
I	Skin cancer is placed in epidermis.
II	Skin cancer is placed in epidermis and started to spread into papillary dermis.
III	Skin cancer is full placed in papillary dermis, but does not reach the reticular dermis.
IV	Skin cancer is placed in reticular dermis.
V	Skin cancer is placed in subcutaneous tissue.

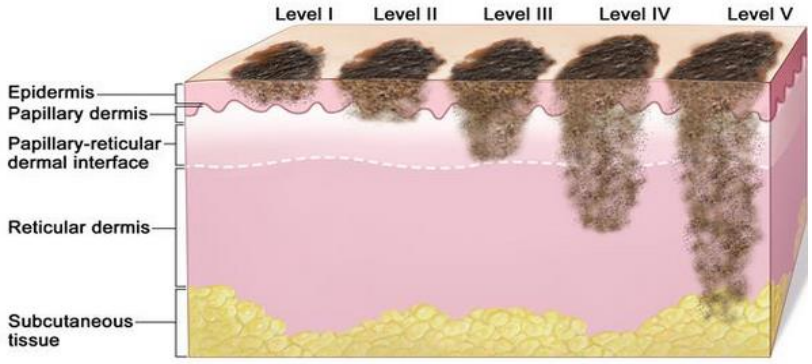

Fig. 9. Skin cancer infusion by Clark levels [88]

2.4. Spectrophotometric intracutaneous analysis

Spectrophotometric intracutaneous analysis, also known as SIA, is a new method to identify pigmented skin lesions and to diagnose various skin diseases. SIA allows the capture of different layers of pigmented skin lesions as collagen, dermal melanin, melanin and blood, which leads to faster and more reliable diagnosis. The establishment of these features depends on the translation of the colourful view of dermatoscopic images. Therefore, it depends on the reflection and absorption by chromophores within the superficial skin according to their depth and concentration and also upon the wavelength of incident light interacting with them [89 - 91].

The mainly used SIAscope features are presented in Table 8. Examples of melanoma SIAscope views are presented in the Fig. 10 [92].

Table 8. Determination of SIAscope features [92]

Feature	SIAscope view
Melanin globules	Total melanin
Blood globules	Blood
Blood displacement	Blood
Erythematous blush	Blood
Dermal melanin	Dermal melanin
Dermal melanin globules	Dermal melanin

Collagen holes	Collagen
Biaxial symmetry	Total melanin
Skewness	Total melanin

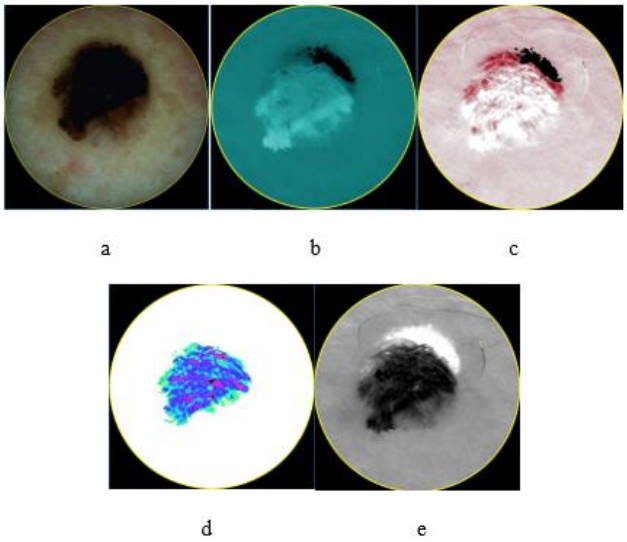

Fig. 10. Example of melanoma SIAscope views. (a) image presents an optical view of the melanoma disease. This tumour is 1.22 mm thickness and belongs to II stage by Breslow depth's scale. (b) image presents collagen of the tissue. Collagen is shown as a white colour and is placed in the centre and above the centre of the image, while clearly collagen holes are placed above the centre of image. (c) image presents blood displacement of the melanoma. Blood displacement is widely spread in the centre of the image and presented in a white colour. Images (d) and (e) present dermal melanin and total melanin. Dermal melanin, which is shown in a blue colour, allows to separate pigmented and non-pigmented lesions. Total melanin is shown in a black colour and allows to evaluate the symmetry of the tumour, which in this case seems to be skewness for melanoma disease.

The SIA algorithm first utilizes the infrared wavebands to ascertain the quantity of collagen within the papillary dermis for every point over the skin lesion. This affects a necessary transformation on the wavebands, allowing accurate extraction of total melanin and blood. The impact of these chromophores on the wavebands is then eliminate, allowing to identify the existence of melanin below the dermoepidermal junction, which provides the most significant diagnostic information. This is likely because of the spectral remittance of melanin depends on the position in the superficial anatomical layers of the skin, which are named as epidermis and papillary dermis [92].

In 2002, SIA was used by Moncrief et al. and has shown very significant results, i.e. specificity was equal to 80,1% and sensitivity was equal to 82,7% for melanoma [92]. As a conclusion, this study proved that SIA can be used as an extra tool in the case of melanoma disease.

SIA is also used as a valuable tool in the case of non - melanoma skin cancer. In 2006, Tehrani et al. presented a paper and showed incredible results of the analysis. Authors have found that the sensitivity of the mode is equal to 98,0% and specificity is equal to of 95,7%, while overall accuracy of the model is equal to 98,2% [93]. To construct a predictive model for non-melanoma skin cancer diagnosis, a logistic regression model was used. For the estimation of overall accuracy, receiver operator characteristic curves were used. In this case, the authors proposed that to use the SIAscope is a useful adjunct in the diagnosis of non-melanoma skin cancer.

For non – melanoma skin cancer, features strongly related to the traceable features in histopathology can be extracted. These features are presented in Table 9 [93].

Table 9. SIA features of non – melanoma skin cancer [93]

Histopathology	SIA features	SIAscope view
Microcirculatory changes: angiogenesis	Branched vessels - Wide, branched vessels coursing towards/into the lesion	Blood
Microcirculatory changes: ischaemia or tumour regression	Paleness - Large focal area of absent blood within the lesion	Blood
Microcirculatory changes: Angiogenesis, inflammation.	Flare - Uniform dark red appearance throughout at least 2/3 of the lesion	Blood
Collagen disturbance, possible invasion through basement membrane	Collagen disturbance - Paler or darker collagen areas where invasion is occurring	Collagen

Example of basal cell carcinoma (BBC) SIAscope views are presented in Fig. 11.

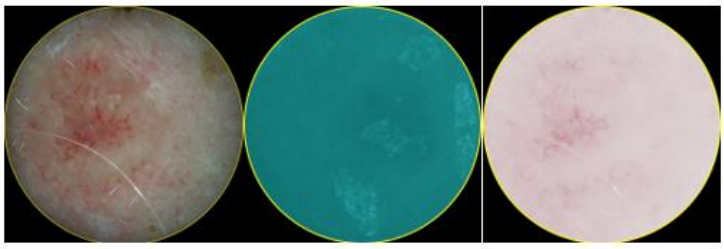

Fig. 11. Example of non – melanoma (BCC) skin cancer SIAscope views. (a) image presents an optical view of basal cell carcinoma which is in a bright colour and has a net of branched vessels. (b) image presents a collagen disturbance. (c) image shows a vascular flare.

Reviewing the types of possibly skin tumours, there is one more important area in analysing pigmented non – melanoma skin cancer. A pigmented basal cell

carcinoma is also an aggressive skin tumour the same as melanoma and is hard to identify whether it is a nevus or not. In 2007, Terstappen et al. stated that SIAscope has no advantages over dermoscopy when diagnosing pigmented basal cell carcinoma [94]. It was stated based on the facts that pigmented basal cell carcinomas have mostly the same characteristics as the melanomas, as they are both pigmented tumours invading the dermis with pigmented tumour masses, giving findings of dermal melanin, and sometimes erythematous blush with blood displacement and collagen holes [92]. Pigmented BCCs are included in the different methods of diagnosing invasive melanoma, due to the growth patterns and skewness of pigmentation keeping in mind that they can be confused with other benign pigmented skin lesions [94].

Example of pigmented basal cell carcinoma (BBC) SIAscope views are presented in the Fig. 12.

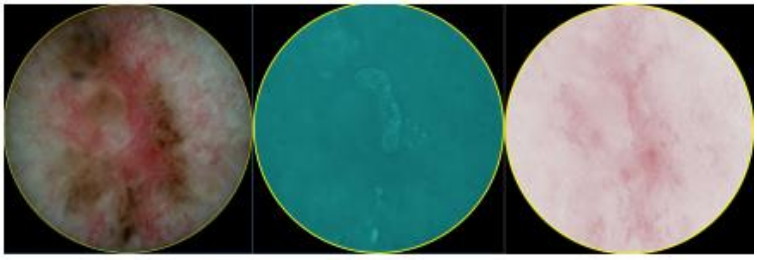

Fig. 12. Example of pigmented basal cell carcinoma SIAscope views. (a) image shows an optical view of the basal cell carcinoma (BCC). It is clearly seen that the tumour is pigmented and has a maple leaf like form and a net of branched vessels, which are one of the BCC common features. (b) image represents collagen disturbance of lesion. Paler areas are visible and show the area where invasion is occurring. (c) image represents a vascular flare.

2.5. Conclusions of 2nd chapter

1. Ultrasound is high frequency sound waves that can reach the skin lesions near the surface and scan deeper parts of the body, such as bones and soft lesions. Ultrasound can be defined by a lot of positive characteristics, such as refraction, scattering, absorption. In this way, ultrasound is a flexible technique allowing to scan in various positions by different exploratory objects. Due to the advantages, the ultrasound technique used in skin image processing helps to capture a lot of parameters of the investigative object and to identify the level and malignancy of skin damage. The relevance of ultrasound technique can be proved based on the published research results which are defined above.

2. Another widely used technique is digital dermatoscopy, which allows the smallest skin surface properties and damage to be seen that cannot be seen by the naked eye. Digital dermatoscopy can help to monitor the changes of the pigmented and non-pigmented skin lesions damage. Digital dermatoscopy analysis can be assessed by different methods, such as the ABCD rule, 7 point's check list and others.

3. The third proposed technique is a spectrophotometric intracutaneous analysis (SIA), which is also a non-invasive technique allowing the analysis of skin damage by different aspects, such blood, melanin, collagen, dermal melanin. As the SIA technique captures different layers of the pigmented and non-pigmented skin lesions it can be used in order to identify benign and malignant nevus.

4. Ultrasound, digital dermatoscopy and spectrophotometric intracutaneous analysis can be used as decision support tools that seek to identify skin damage from small benign nevus to basal cell carcinoma and to malignant skin tumours.

3. ASSESSMENT AND COMPARISON OF LIKELY DENSITY DISTRIBUTIONS IN THE CASES OF THICKNESS MEASUREMENT OF SKIN TUMOURS BY ULTRASOUND EXAMINATION AND HISTOLOGICAL ANALYSIS

A comparison of compatibility of likely density to prove that the reliability of the ultrasonic thickness of skin tumours measured by a newly developed and proposed automatic algorithm is completely covered by a high similarity to the histological thickness measurement is presented. Histological thickness is known as a "golden standard" in the field of dermatology but is invinsible. To prove this statement, the measurements of 43 tumours under a non-invasive ultrasound examination and invasive histological analysis was undertaken. The comparison of histological and non-invasive histological examination measurements is made by using kernel density functions and a hypothesis allowing to estimate the deviation between the density functions of different types of measurements.

This chapter presents an assessment and comparison of likely density distributions in the cases of the thickness measurement of skin tumours by ultrasound examination and histological analysis. Section 3.1. and section 3.2. introduce how to construct a kernel density estimator and how to select an optimal bandwith used for analysis, with estimation accuracy presented in section 3.3. Results of estimation of kernel densities are presented in section 3.4. An application of goodness-fit of test for the set of real clinical data is presented in section 3.5. Section 3.6. introduces the summarized outcomes of chapter 3.

3.1. Kernel density estimator

A *d*-dimensional random vector $X \epsilon R^d$ satisfies a mixture model if its distribution density function *f(x)* is given by equality:

$$f(x) = \sum_{k=1}^{q} p_k f_k(x) = f(x, Q). \quad (17)$$

The parameter q is the number of components in the mixture. The component weights p_k are called a priori probabilities and satisfy the conditions:

$$p_k > 0, \sum_{k=1}^{q} p_k = 1. \quad (18)$$

Function $f_k(x)$ is the distribution density function of the k^{th} component and p_k is the vector of parameters of the mixture model. Assuming that a sample X= (X(1), …, X(n)) of size n from X is known, therefore the evaluation of the

distribution density of a defined random vector is one of the common statistical objects [18].

A histogram is one of the oldest and most popular density estimators. Histogram and its representation were first introduced in 1891 by Karl Pearson [95]. For the approximation of density *f(x)*, the number of observations *X(t)* falling within the range of *Ω* is calculated and divided by *n* and the volume of area *Ω*. The histogram is based on a step function. Derivatives, which can be equal to zero or not defined, strongly affects the futher histogram analysis. For eaxmple, it can cause problems when trying to maximize a likelihood function which is defined in terms of the densities of the distributions [95].

It is imporatant to mention that the histogram was kept as the only nonparametric density estimator until the 1950's, while substantial and simultaneous progress was made in density and spectral density evaluations. Later in 1951, Fix and Hodges, in a little-known publication, presented the basics algorithm of nonparametric density evaluation [96]. This previously not published technical report was formally presented to the public only in 1989, as a review made by Silverman and Jones [97]. Researchers have focussed on the problem of statistical discrimination and did their investigations when the parametric form of the sampling density was not originally known. Later, several common algorithms and alternatives in theoretical modeling were introduced by Rosenblatt in 1956 [98], Parzen in 1962 [99], and Cencov in 1962 [100]. Then followed the second wave of important and primarily theoretical papers by Watson and Leadbetter in 1963 [101], Loftsgaarden and Quesenberry in 1965 [102], Schwartz in 1967 [103], Epanechnikov in 1969 [104], Tarter and Kronmal in 1970 [105] and Kimeldorf and Wahba in 1971 [106]. The natural multivariate generalization was introduced by Cacoullos in 1966 [107]. Finally, in the 1970's the first papers focusing on the practical application of these methods were published by Scott et al. in 1978 [108] and Silverman in 1978 [109]. These and later multivariate applications awaited the computing revolution.

The basic kernel estimator $\hat{f}(x)$ with a kernel function *K* and a fixed (global) bandwidth *h* for multivariate data $X \epsilon R^d$ may be written compactly as [18]:

$$f(x) = \frac{1}{nh^d} \sum_{t=1}^{n} K\left(\frac{x - X(t)}{h}\right). \tag{19}$$

The kernel function *K(u)* should satisfy the condition:

$$\int_{-\infty}^{+\infty} K(u)\, du = 1. \tag{20}$$

Usually, but not always, *K(u)* will be a symmetric probability density function $K(u) = K(-u)$ for all values of *u* [18].

At first, the data is usually prescaled in order to avoid large differences in data spread. A new application by Fukunaga was presented in 1972 [110]. The logic of this approach is first to standardize the data by using a linear transformation providing data with unit variance and zero mean. As a result, equation (3) is applied to the standardized data. Let *Z* denote the sphered values of

$$Z = S^{\frac{-1}{2}} * (X - \bar{X}); \tag{21}$$

where $\bar{X}$ means the empirical mean, and $S \epsilon R^{d \times d}$ means the empirical covariance matrix. Invoking the kernel density estimator to the standardized data *Z = (Z(1), ..., Z(n))* obtains an estimator of density function *f(x)* [110]:

$$f_z(z) = \frac{1}{nh^d} \sum_{t=1}^{n} K\left(\frac{z - Z(t)}{h}\right), \tag{22}$$

$$f(x) = \frac{(\det S)^{\frac{-1}{2}}}{nh^d} \sum_{t=1}^{n} K\left(S^{\frac{-1}{2}} \frac{x - X(t)}{h}\right). \tag{23}$$

A comparative analysis of estimation accuracy was made for four different types of kernels. The first three kernels are classical, whereas the last one is new.

The Gaussian kernel is consistent with the distribution of normal *φ(x)* (see Gasser et al., 1985 [111], Marron and Nolan, 1988 [112]) selection:

$$K_G(x) = \varphi(x) = \frac{1}{(2\pi)^{\frac{d}{2}}} e\left(\frac{-x^T x}{2}\right). \tag{24}$$

The Epanechnikov kernel is the second order polynomial, corrected to satisfy the properties of the density function (see Epanechnikov, 1969 [104], Sacks and Ylvisaker, 1981 [113]):

$$K_E(x) = \frac{d+2}{2V_d}(1 - x^T x)\mathbf{1}_{\{|x^T x \leq 1|\}}; \tag{25}$$

where $V_d = \frac{\pi^{d/2}}{\Gamma(\frac{d}{2}+1)}$ is the volume of the *d*-dimensional unit sphere, and $\Gamma(u) = \int_0^\infty y^{u-i}\, e^{-y} dy$.

The Triweight kernel proposed by Tapia and Thompson in 1978 [114] has better smoothness properties and finite support. It was investigated in detail by Hall in 1985 [115]:

$$K_T(x) = \frac{(d+4)(d+6)}{24}\frac{(d+2)}{2V_d}(1 - x^T x)^3 \mathbf{1}_{\{|x^T x \leq 1|\}}. \quad (26)$$

The new kernel K_{New} has lighter tails than the Gaussian distribution density and was introduced by the authors of this article [116]:

$$K_{New}(x) = \varphi(|u|^{\frac{1}{\alpha}})\frac{1}{\alpha^d}(\left|\prod_{i=1}^{d} x_i\right|^{1/d})^{1-\alpha}. \quad (27)$$

This kernel function depends on parameter α. In simulations, the chosen values of the parameter were 0.25, 0.5, and 0.75. The first two values produce the worse accuracy results in comparison with the value of 0.75. Therefore, only the results obtained for $\alpha = 0.75$ are reported here [116].

3.2. Optimal bandwidth selection

The main three parameters in a kernel density estimator are: the kernel function $K(\cdot)$, the sample size n, and the bandwidth h. The sample size is quite a tricky parameter and is not easily adaptable, but there is little that can be done about it. This research task is to get the most significant results by selecting a suitable bandwidth and an appropriate kernel for analysis. The selection of an optimal bandwith is the most decisive step in order to get a good evaluation [117] On the other hand, the selection of an optimal bandwith is one the greatest problems in kernel density estimation and a finite technique of how to acheive it does not exist. It can look surprising that the most effectual method of kernel bandwidth selection is a visual assesment and relies on the researcher. Usually, the researcher compares different density evaluations, which have a variety of bandwidths and then the bandwdith that corresponds to the optimal assesment is choosen. It is important to note, that the above bandwidths selection method will give different badwidths in the selection made by two diffrenets researchers. This method is also a time consuming method.

The application based on mathematical analysis is to figure out the inadequacy between the assesment and the target density by an estiated error criterion. In this case, an optimal bandwidth will then be the bandwidth value that minimizes the error measured by the error criterion. A method like this is objective and can be time-effective, as computers can now solve it numerically.

A global measure of precision is the asymptotic mean integrated squared error (AMISE) [117]:

$$AMISE\left(\hat{f}(x)\right) = \frac{K_v^2(K)}{(v!)^2} R(\nabla^v f) h^{2v} + \frac{R(K)^d}{nh^d}; \quad (28)$$

where $\nabla^v f(x) = \sum_{k=1}^{d} \frac{\partial^v}{\partial x_k^v} f(x)$ and $R(g) = \int_{-\infty}^{\infty} g(u)^2 du$ is the roughness of a function. The order of a kernel, *v*, is defined as the order of the first non-zero moment $\kappa_j(K) = \int_{-\infty}^{\infty} u^j K(u) du$. For example, if $\kappa_1(K) = 0$ and $\kappa_2(K) > 0$ then *K* is a second-order kernel and *v* = 2. If $\kappa_1(K) = \kappa_2(K) = \kappa_3(K) = 0$ but $\kappa_4(K) > 0$ then *K* is a fourth-order kernel and *v* = 4.The order of a symmetric kernel is always even. Symmetric non-negative kernels are second-order kernels. A kernel is a higher-order kernel if *v* > 2. These kernels will have negative parts and are not probability densities.

The optimal bandwidth is [117]:

$$h_0 = \left(\frac{(v!)^2 d R(K)^d}{2v K_v^2(K) R(\nabla^v f)}\right)^{1/(2v+d)} n^{-1/(2v+d)}. \quad (29)$$

The optimal bandwidth depends on the unknown quantity $R(\nabla^{(v)} f)$. For a rule-of-thumb bandwidth, Silverman proposed that it is possible to try the bandwidth computed by replacing *f* in the optimal formula by $g_{0,}$ where g_0 is a reference density – a plausible candidate for f, and $\hat{\sigma}$ is the sample standard deviation (see Bruce E. Hansen, 2009 [118]). The standard choice is a multivariate normal density. The optimal bandwidth depends on the normality of the true density, i.e. if the true density is close to the normal distribution, so then the bandwidth will be close to optimal. Calculation of this is proceeded according to

$$R(\nabla^v \varphi) = \frac{d}{\pi^{\frac{d}{2}} 2^{d+v}} \left((2v-1)!! + (d-1)\left((v-1)!!\right)^2\right); \quad (30)$$

where the double factorial means (2s + 1)!! = (2s + 1) (2s – 1) ... 5 · 3 · 1. Making this substitution, the following is obtained

$$h_0 = C_v(K, d) n^{-1/(2v+d)}; \quad (31)$$

where $C_\nu(K,d) = \left(\frac{\pi^{\frac{d}{2}} 2^{d+\nu-1}(\nu!)^2 R(K)^d}{\nu K_\nu^2(K)\left((2\nu-1)!!+(d-1)\left((\nu-1)!!\right)^2\right)}\right)^{1/(2\nu+d)}$. and this assumed that variance is equal to 1. Rescaling the bandwidths by the standard deviation of each variable, the rule-of-thumb bandwidth for the i^{th} variable is obtained

$$h_i = \hat{\sigma}_i \, C_\nu(K,d) n^{-\frac{1}{2\nu+d}}. \tag{32}$$

Table 10 provides the normal reference rule-of-thumb constants ($C_\nu(K,d)$ in (Eq. 50)) for the second-order *d*-variate kernel density estimator. First, in the general setting of a second order kernel, where $\nu = 2$, the rule-of-thumb constants decrease as *d* increases. In 1992, Scott noted that it reaches a minimum when $d = 11$ [95]. The $\nu = 2$ case is the only one Scott has considered. When $\nu > 2$, it is possible to prove that the rule-of-thumb constants increase in the dimensionality of the problem. The main focus behind it is that the higher-order kernels reduce bias, larger bandwidths are needed to minimize AMISE. However, note that the increase is not uniform over ν [95].

Table 10. Normal reference rule-of-thumb constants $(C_\nu(K,d))$ for the multivariate second-order kernel density estimator [116]

Kernel	$d = 1$	$d = 2$	$d = 3$	$d = 4$	$d = 5$	$d = 6$	$d = 7$	$d = 8$	$d = 9$	$d = 10$
Gaussian	1.059	1.000	0.969	0.951	0.9340	0.933	0.929	0.927	0.925	0.925
Epanechnikov	2.345	2.191	2.120	2.073	2.044	2.025	2.012	2.004	1.998	1.995
Triweight	3.155	2.964	2.861	2.800	2.762	2.738	2.723	2.712	2.706	2.702
New	1.142	1.079	1.045	1.025	1.014	1.007	1.002	1.000	0.998	0.998

3.3. The analysis of estimation accuracy

A comprehensive simulation study was conducted with the aim to compare the kernel functions described before. The main attention is paid to the case where the density of independent *d*-dimensional observations are Gausian mixture models (GMM) [17]:

$$f(x) = \sum_{i=1}^{q} p_i \, \varphi_i(x) = f(x,Q), x \epsilon R^d; \tag{33}$$

where $Q = (p_i, M_i, R_i, i=1, 2, \ldots, q)$. Univariate, bi-variate, and quinta-variate GMMs, from a suggested collection was used in a comparative analysis as the benchmark densities:

1) Gaussian

$p_1 = 1$, $M_1 = (0, \ldots, 0)$, $R_1 = I = \text{diag}([1, \ldots, 1])$

2) skewed unimodal

$p_1 = 1/5$, $M_1 = (0, \ldots, 0)$, $R_1 = I = \text{diag}([1, \ldots, 1])$

$p_2 = 1/5$, $M_2 = (1/2, 0, \ldots, 0)$, $R_2 = \text{diag}([(2/3)^2, \ldots, (2/3)^2])$

$p_3 = 3/5$, $M_3 = (13/12, 0, \ldots, 0)$, $R_3 = \text{diag}([(5/9)^2, \ldots, (5/9)^2])$

3) strongly skewed

$p_n = 1/8$, $M_n = (3((2/3)^n-1), 0, \ldots, 0)$, $R_n = \text{diag}([(2/3)^{2n}, \ldots, (2/3)^{2n}])$, $n = 0,\ldots, 7$

4) kurtotic unimodal

$p_1 = 2/3$, $M_1 = (0, \ldots, 0)$, $R_1 = I = \text{diag}([1, \ldots, 1])$

$p_2 = 1/3$, $M_2 = (0, \ldots, 0)$, $R_2 = \text{diag}([(1/10)^2, \ldots, (1/10)^2])$

5) outlier

$p_1 = 1/10$, $M_1 = (0, \ldots, 0)$, $R_1 = I = \text{diag}([1, \ldots, 1])$

$p_2 = 9/10$, $M_2 = (0, \ldots, 0)$, $R_2 = \text{diag}([(1/10)^2, \ldots, (1/10)^2])$

6) bimodal

$p_1 = 1/2$, $M_1 = (-1, 0, \ldots, 0)$, $R_1 = \text{diag}([(2/3)^2, \ldots, (2/3)^2])$

$p_2 = 1/2$, $M_2 = (1, 0, \ldots, 0)$, $R_2 = \text{diag}([(2/3)^2, \ldots, (2/3)^2])$

7) separated bimodal

$p_1 = 1/2$, $M_1 = (-3/2, 0, \ldots, 0)$, $R_1 = \text{diag}([(1/2)^2, \ldots, (1/2)^2])$

$p_2 = 1/2$, $M_2 = (3/2, 0, \ldots, 0)$, $R_2 = \text{diag}([(1/2)^2, \ldots, (1/2)^2])$

8) skewed bimodal

$p_1 = 3/4$, $M_1 = (0, \ldots, 0)$, $R_1 = I = \text{diag}([1, \ldots, 1])$

$p_2 = 1/4$, $M_2 = (3/2, 0, \ldots, 0)$, $R_2 = \text{diag}([(1/3)^2, \ldots, (1/3)^2])$

9) trimodal

$p_1 = 9/20$, $M_1 = (-6/5, 0, \ldots, 0)$, $R_1 = \text{diag}([(3/5)^2, \ldots, (3/5)^2])$

$p_2 = 9/20$, $M_2 = (6/5, 0, \ldots, 0)$, $R_2 = \text{diag}([(3/5)^2, \ldots, (3/5)^2])$

$p_3 = 1/10$, $M_3 = (0, \ldots, 0)$, $R_3 = \text{diag}([(1/4)^2, \ldots, (1/4)^2])$

10) claw

$p_1 = 1/2$, $M_1 = (0, \ldots, 0)$, $R_1 = I = \text{diag}([1, \ldots, 1])$

$p_n = 1/10$, $M_n = (n/2-1, 0, \ldots, 0)$, $R_n = \text{diag}([(1/10)^2, \ldots, (1/10)^2])$, $n = 0, \ldots, 4$

11) double claw

$p_1 = 49/100$, $M_1 = (-1, 0, \ldots, 0)$, $R_1 = \text{diag}([(2/3)^2, \ldots, (2/3)^2])$

$p_2 = 49/100$, $M_2 = (1, 0, \ldots, 0)$, $R_2 = \text{diag}([(2/3)^2, \ldots, (2/3)^2])$

$p_n = 1/350$, $M_n = ((n-3)/2, 0, \ldots, 0)$, $R_n = \text{diag}([(1/100)^2, \ldots, (1/100)^2])$, $n = 0, \ldots, 6$

12) asymmetric claw

$p_1 = 1/2$, $M_1 = (0, \ldots, 0)$, $R_1 = I = \text{diag}([1, \ldots, 1])$

$p_n = 2^{1-n}/31$, $M_n = (n+1/2, 0, \ldots, 0)$, $R_n = \text{diag}([(2^{-n}/10)^2, \ldots, (2^{-n}/10)^2])$, $n = -2, \ldots, 2$

13) asymmetric double claw

$p_j = 46/100$, $M_j = (2j-1, 0, \ldots, 0)$, $R_j = \text{diag}([(2/3)^2, \ldots, (2/3)^2])$, $j = 0, 1$

$p_n = 1/100$, $M_n = (-n/2, 0, \ldots, 0)$, $R_n = \text{diag}([(1/100)^2, \ldots, (1/100)^2])$, $n = 1, 2, 3$

$p_k = 1/100$, $M_k = (k/2, 0, \ldots, 0)$, $R_k = \text{diag}([(1/100)^2, \ldots, (1/100)^2])$, $k = 1, 2, 3$

14) smooth comb

$p_n = 2^{5-n}/63$, $M_n = (65\text{-}96(1/2)^n/21, 0, \ldots, 0)$, $R_n = \text{diag}([(32/63)/2^{2n}, \ldots,(32/63)/2^{2n}])$, n= 0, …, 5

15) discrete comb

$p_n = 2/7$, $M_n = ((12n\text{-}15)/7, 0, \ldots, 0)$, $R_n = \text{diag}([(2/7)^2, \ldots,(2/7)^2])$, n = 0, 1, 2

$p_k = 1/21$, $M_k = (2k/7, 0, \ldots, 0)$, $R_k = \text{diag}([(1/21)^2, \ldots,(1/21)^2])$, k = 8, 9, 10

The above densities have been selected because they introduce a large amount of different types of challenges to curve estimators. The first five densities introduce different types of problems that can appear for unimodal densities. All other densities are multimodal. Densities from six to nine are mildly multimodal and can be estimated by using a data set of a moderate volume.

The remaining densities are strongly multimodal and consequnetly for moderate sizes it is difficult to recover even their shape. Yet, they are well worth studying because the issue of just how many of them can be recovered is an important factor. The claw density, number 10, is of special interest; as this is where the surprising result of local minimum in the mean of an integrated square error is occuring. The double claw density, noted as 11, is essentially the same as sixth, except that approximately 2% of the probability mass is appearing in the spikes. The asymmetric claw and double claw densities, numbered as 12 and 13, are modifications of the 10^{th} and 11^{th} , respectively. The smooth and discrete comb densities, numbered as 14 and 15, are enhancements of the basic idea of the separated bimodal mixture model numbered as 7. Both of these are shown because they have many different Fourier transform properties, since 14 has essentially no periodic tendencies, while 15 has two strong periodic components.

Note that the univariate case of this set of models is similar to the collection suggested by Marron and Wand in 1992 [17].

In the simulation study, low-size and moderate-size samples (16, 32, 64, 128, 256, 512, 1024) were used [116]. 10000 replications were generated in each case. The conclusions presented below are based on the analysis of these medians and minimums. The estimation accuracy is measured by the mean absolute percentage error (MAPE) [119]:

$$MAPE = \frac{1}{n}\sum_{t=1}^{n}\left|\frac{f(X(t))-\hat{f}(X(t))}{f(X(t))}\right| \cong \int\left|f(x)-\hat{f}(x)\right|dx. \qquad (34)$$

3.4. Results of estimations of kernel densities

The results of the univariate kernel density estimation are examined in detail by Ruzgas and Drulyte, 2013 [6]. The experimental research showed that some of the kernel density functions used with multiple distributions mixtures lead to particularly good results. For example, the Triweight kernel density function is characterized as one of the most effective when the study is done by using “Discrete comb“ mixture

with a sample size larger than 256, and dimension equal to 2. The results obtained with the Epanechnikov kernel density function have shown that this function is appropriate to be used when the calculations are carried out with the average sample size by using “Bimodal”, “Separated bimodal” and “Smooth comb” mixtures with dimension equal to 2. In addition, the new kernel density function proposed by the authors of this research has also shown unexpected results. The smallest median errors for all sample sizes when the dimension is equal to 2, are obtained by using the mean average percentage error (MAPE), even at five different mixtures: “Gaussian”, “Skewed unimodal”, “Strongly skewed”, “Kurtotic unimodal” and “Outlier”. Meanwhile, when the sample size is less or equal to 256, the smallest median errors are obtained with “Bimodal”, “Separated bimodal”, “Smooth comb” and “Discrete comb” mixtures [116]. Another important point is that the new kernel density function gives the smallest median errors with all mixtures of Gaussian distribution and all sample sizes when the dimension is equal to five. The second effective function is Gaussian kernel density function.

The results of errors dependence on sample size and selected dimension by using the “Skewed bimodal” mixture and different dimensions are shown in Fig. 13. Here, the Gaussian, Epanechnikov, Triweight and new kernel density functions are marked as G, E, T and N show the results of estimation accuracy [116]. Medians and minimums of mean average percentage errors are marked by solid and dashed lines. The results of errors dependence on the sample size results acheived by using “Skewed bimodal” mixture and different dimensions are shown below in Fig. 13 [116].

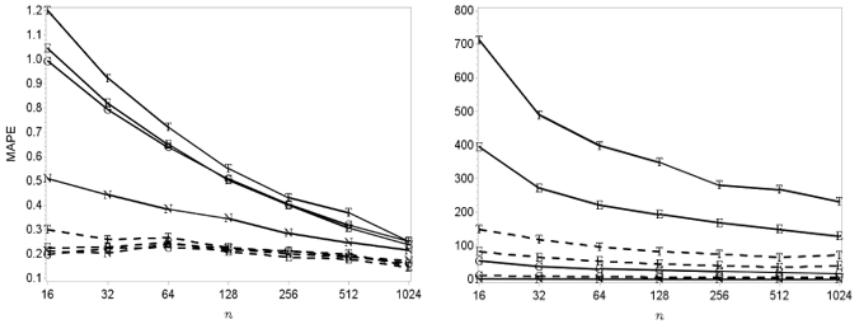

Fig. 13. Estimation accuracy based on MAPE for skewed bimodal bi-variate and quinta-variate densities (here MAPE means the mean absolute percentage error; *n* is the sample size; the Gaussian, Epanechnikov, Triweight and new kernel bi-variate density functions are marked as G, E, T and N in dashed lines, quinta-variate density functions for the same kernels are marked as G, E, T and N in solid lines) [116].

When the dimension is increasing, the smallest errors are acheived by using the new kernel density function [116]. Meanwhile, the Gaussian kernel density function is respectively appropriate to be used when the dimension is smaller or equal to 4 and

smaller than 3 in the case of the Epanechnikov and Triweight functions. The effectiveness of the Gaussian kernel density function is shown in Fig. 14.

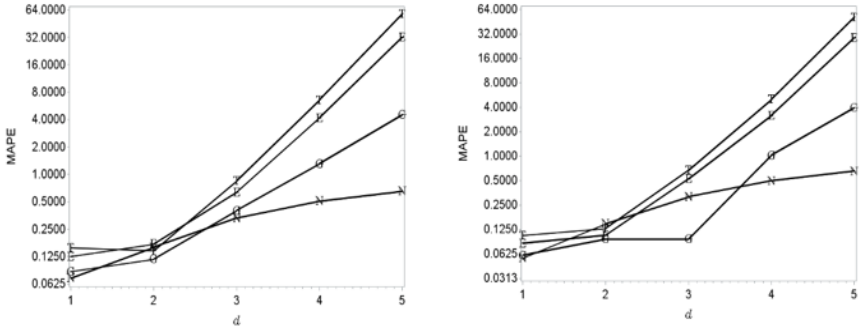

Fig. 14. The relationship between number of dimension and MAPE (Gaussian densities with sample sizes 512 on the left picture and 1024 on the right picture). Here MAPE means the mean absolute percentage error; *d* is the dimension; the Gaussian, Epanechnikov, Triweight and new kernel density functions are marked as G, E, T and N in solid lines [116].

3.5. The application of goodness fit of test

During the non-invasive ultrasonic measurements of human skin DUB-USB ultrasound system ("Taberna pro medicum")of 22 MHz's was used for transmission and reception of ultrasonic waves. The immersion experimental set-up with a mechanically scanned ultrasonic transducer was employed. The transducer was focused at the surface of the skin. In addition, the system was used for acquisition, digitization and transfer to a personal computer and received A-scan ultrasonic signals. The set of acquired A-scan signals were used for reconstruction of the B-scan image. Finally, the maximal thickness of the skin lesion was manually evaluated by a well-experienced dermatologist, measuring the distance between the lower edge of the entry echo and the deepest point of the posterior margin of the hypoechoic zone. During the evaluation of thickness, the value of ultrasound velocity was assumed to be 1580 m/s.

The principle of investigation of human skin lesions using an ultrasonic pulse-echo technique is presented in Fig. 15 [120].

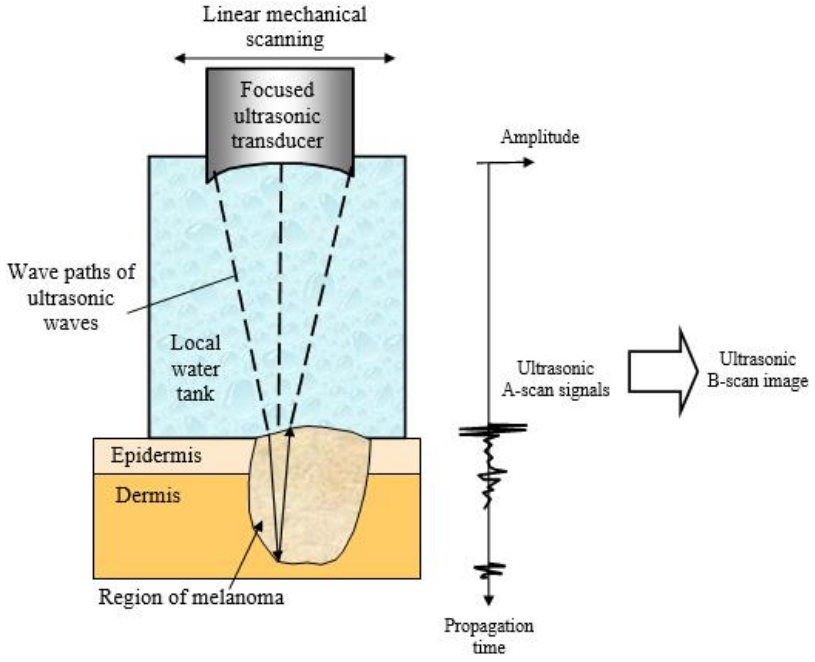

Fig. 15. The principle of investigation of human skin lesions using ultrasonic pulse-echo technique [120]

The set of real clinical data presented in Fig. 16 was used as an empirical example [116]. Within this section, a set of values (the sample size was equal to 52 observations) of the skin lesions previously used for clinical decision support by non-invasive ultrasonic measurements in vivo and the histological evaluation ex vivo of their thickness and malignancy after surgical excision has been obtained and compared. The analysis was performed retrospectively in an empirical context in order to estimate the goodness of fit tests.

Histological and ultrasonic data has been collected at the Department of Skin and Venereal Diseases at the Lithuanian University of Health Sciences (LUHS). The study was approved by the regional ethics committee; the collection of all data was approved by the institutional review board after the patients' informed consent was obtained in accordance with the Declaration of Helsinki Protocols. The data sets used in the empirical example were acquired on 52 suspicious melanocytic skin tumours (MST), which included 46 melanocytic nevi and 6 melanomas. Inclusion criteria of the study covered the size of the tumour up to 1 cm in diameter and histological thickness of $\leq$1.5 mm.

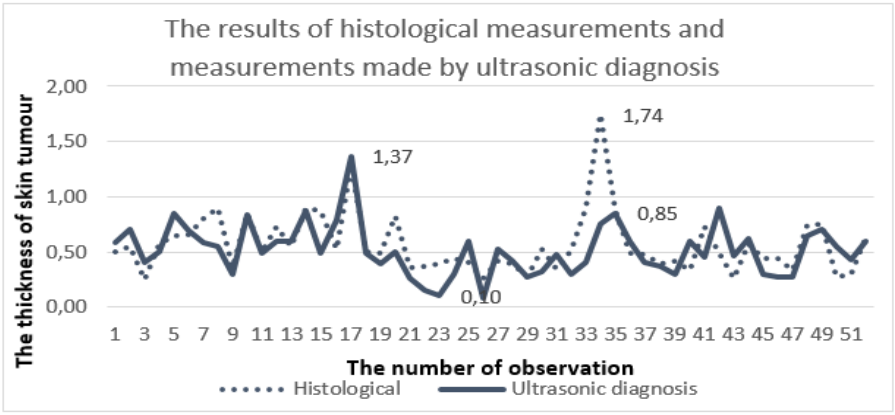

Fig. 16. The results of histological measurements and measurements made by ultrasonic diagnosis [116]

After a surgical excision and during the routine histopathology, the vertical distance from the uppermost level of the stratum granulosum in the epidermis to the lowest point of the lesion without infiltrate (histological tumour thickness, Breslow index) was independently evaluated by two pathologists and averaged.

More details about ultrasonic examinations in dermatology and comparison with histological data are provided by Jasaitiene et al. in 2011 [121] and Kučinskienė et al. in 2014 [122].

For the goodness of fit test, this research is using tests based on kernel density estimators described above. Let $X_1, \dots, X_n$ be a sample of independent observations of a random variable X with unknown probability density function $f(x), x \in R$. For the given sample, it is required to test the hypothesis mentioned in the publication made by Rudzkis and Bakshaev in 2013 [123]:

$$H_0: f(x) = f_0(x), \text{ against alternative } H_1: f(x) = (1-\epsilon)f_0(x) + \epsilon g(x).$$

Here $f_0(x)$ is a given probability density function, ϵ is negligible and $\epsilon g(x)$ is an arbitrary distribution, where ${\sigma^2}_g \leq {\sigma^2}_{f_0}$ *a*nd ${\sigma^2}_f$ is a variance of distribution *f*.

In this study, five tests of goodness of fit have been evaluated: Pearson's chi-squared test, Rudzkis-Bakshaev's test, Kolmogorov–Smirnov test, Cramer von Mises test and Kuiper's test for four different kernel functions. One of the steps leading to the main result was to check the goodness of fit between the density of ultrasonic thicknesses distribution and density of histological thicknesses distribution of the skin tumours. The next step was to compare the compatibility of likely density of histological thicknesses distribution of the skin tumours and Normal distribution density. If two mentioned checked conditions are satisfied, as a result it is clear that the density of ultrasonic thicknesses distribution and Normal distribution density are interconnected [116]. All results of the goodness of fit between the density of ultrasonic thicknesses distribution and density of histological thicknesses distribution of the skin tumours (denoted as U H) and the goodness of fit between the density of

histological thicknesses distribution and Normal distribution density (denoted as H and N) are shown in Table 11.

Table 11. The results of goodness fit of test based on kernel functions [116]

Goodness of Fit Test		Kernel Function			
		Normal	**Epanechnikov**	**Triweight**	**New proposed**
Pearson's chi-squared χ^2	U H	~1	~1	~1	~1
	H N	0.447	0.006	0.122	0.009
Rudzkis-Bakshaev	U H	0.993	0.997	0.997	0.990
	H N	0.973	0.967	0.978	0.899
Kolmogorov–Smirnov	H N	0.883	0.925	0.908	0.912
	H N	0.999	0.999	0.999	0.999
Cramer von Mises	U H	0.685	0.725	0.704	0.719
	H N	0.897	0.891	0.898	0.886
Kuiper's	U H	0.999	0.999	0.999	0.999
	H N	~1	~1	~1	~1

3.6. Conclusions of 3rd chapter

1. Within the performed study, a check of the goodness of fit test for thicknesses of the skin tumours measured in two different ways was conducted (non-invasive ultrasound examination and invasive histological analysis).

2. The performed simulation study leads to the kernel *K* which has shown a better performance for Gaussian mixtures with considerably overlapping components and multiple peaks (double claw distribution). In addition, its accuracy decreases more slowly than the other kernels, when the random vector dimension increases.

3. The empirical study has shown that Pearson's chi-squared test is the most sensitive of all used tests. The main reason is the differences between empirical and theoretical distributions due to heavy tails of the empirical distributions. Subsequently, Kuiper's test has the lowest sensitivity criteria and was the most powerful in the performed comparative analysis.

4. The obtained results have shown that the density of ultrasonic thicknesses distribution is similar to the Normal distribution density by more than 90 percent. Hence, the reliability of ultrasonic thickness measurement of the skin tumour is completely covered by a high similarity to the histological thickness measurement, which is known as a "golden standard" in the field of dermatology.

5. The application of goodness fit of test has shown that *p*-value of all criteria's with all kernel functions are approximately 2 times greater than Pearson's chi-squared test. Therefore, it proves that the application of a non-invasive ultrasonic technique (at least of 22 MHz) for thickness estimation of the melanocytic skin lesions (tumours

and nevus) possesses high reliability and is suitable to be used in daily clinical practise.

4. THE NONPARAMETRIC APPROACH IN ORDER TO ESTIMATE THE PARAMETERS OF LESIONS OF THE HUMAN TISSUE

Nowadays, accurate measurements are very important for the early diagnosis of skin cancer and can help to prevent skin cancer and increase survival rate. A newly developed and proposed automatic algorithm based on the synergy of digital dermatoscopy and ultrasonic B-scan images that is used to estimate the parameters of lesions of human tissue and can improve the accuracy are further discussed. The experimental study has been conducted with 31 ultrasonic and 31 digital dermatoscopy images.

This chapter presents a nonparametric approach in order to estimate the parameters of lesions of human tissue. Sections 4.1. – 4.4. consist of a review and comparison of two different classification models (discriminant analysis and logistic regression). The procedure of segmentation of ultrasonic and digital dermatoscopy medical images is presented in section 4.5. The results of automatic classification of melanoma and benign melanocytic nevi, analysing ultrasonic B-scan images and in combination with the analysis of digital dermatoscopy images are described in section 4.6. Section 4.6 also includes the diagnostic accuracy, as well as sensitivity and specificity rates of the proposed automated statistical method. The analysis of the separation significant and not relevant parameters in order to increase the classification accuracy of ultrasonic and digital dermatoscopy images is presented in section 4.7. Section 4.8. includes an overview of results of the different techniques used in the field of dermatology and results of a newly developed and proposed automated algorithm. Section 4.9. contains the summarized outcomes of chapter 4.

4.1. Discriminant analysis

The discriminant analysis method is simple and one of the most widely used methods in different research areas. It has been used for a long time in order to estimate the differences between observations. For example, in 1968, Peter A. Lachenbruch et al. presented a number of new methods in order to minimize the error rates and to improve the classification [124]. After 9 years, Peter A. Lachenbruch et al. were involved and analysed problems such as robustness, nonparametric rules, contamination, density estimation and mixture of variable, which leads to a more reliable result of classification tasks [125]. Later, in 1999, Jerome H. Friedman showed that the proposed method of regulation can increase the impact of discriminant analysis when the sample volume is small, and the quantity of measurement variables is high [126]. More research from 20^{th} century can be found here [127 – 134].

Reviewing the last decade, discriminant analysis is still one of the popular methods that helps to achieve reliable results in the case of differentiation purposes between groups. It has been used in various fields, such as medicine, gene science,

agriculture, veterinary, food science, human physics, electrical engineering, remote sensing, neuro science, finance and many others. In 2011, some of the authors have used discriminant analysis for face recognition and achieved results that clearly show the superiority of the proposed stochastic discriminant analysis (SDA) over state-of-the-art methods [135]. Meisam Khalil Arjmandi et al. have published a paper that presents an algorithm based on discriminant analysis and used in the identification of different voice disorders, with their origin in the vocal folds [136]. R. Romo Vazquez et al. have shown that the discriminant analysis application is one of the best approaches, using it for artefact removal and noise elimination from scalp electroencephalogram recordings (EEG) [137]. In addition, a number of Indian researchers shared their experience of using the discriminant analysis for brain tumour magnetic resonance image (MRI) classification, with feature selection and extraction [138]. In 2012, Ahmet Alkan et. al also used discriminant analysis (DA) for the identification of electromyography (EMG) signals [139]. Discriminant analysis is also used in the classification of glioma grading tasks and as Rishi Awasthi et. al stated, 'a non-invasive DCE-MRI can be used in order to separate high-grade and low-grade brain tumours and can help to prepare a plan of treatment, as well as control the progress of the disease' [140]. In 2010, research was presented regarding applying discriminant analysis in schizophrenia and healthy subjects, which showed significant results and could be applied to differentiate patients with schizophrenia from healthy subjects [141]. In 2011, as a remedy, Benjamin Blankertz et al. proposed an idea to use an estimation based on shrinkage and showed that the proper regulation of linear discriminant analysis (LDA) by shrinkage is providing incredible results on the classification of a single-trial ERP of brain images and is more preeminent than a well-known LDA classification [142]. K.J. Deluzio et al. have done research in the case of knee osteoarthritis (OA) and focused on three features, such as the knee flexion angle, flexion moment, and adduction moment; stating that "The discriminant analysis was able to rank these features from the gait measures in terms of their power to separate normal and OA gait patterns" [143]. In 2009, Yun-Chi Yeh et al. presented a method for Cardiac arrhythmia diagnosis, which showed incredible accuracy with regards to the correct diagnosis [144]. Another field where discriminant analysis was used also showed good results in the case of persons who have dementia [145]. In addition, discriminant analysis has been proven as being helpful when it is used in classifying and identifying brain tumours [135] and for automated differentiation of pre-diagnosis Huntington's disease [146]. Furthermore, DA has been used in gene science and also gave significant results in the case of the identification of clusters and graphical representation of between-group structures, which allow to unravel complex population structures by analysing microsatellite polymorphism in worldwide human populations and hemagglutinin gene sequence variation in seasonal influenza [147]. In 2015, Ivashchenko O.V. et al. presented a paper related to the human physics, where it used a discriminant analysis in order to determinate the classification model of senior forms' pupils' motor and functional fitness [134].

Suppose that the prior probabilities of group observations are labelled and the group-specific densities at x are easily assessed, therefore the probability

of *x* belonging to group *t*, in the case of discriminant analysis can be calculated by using Bayes' theorem:

$$p(t|x) = \frac{q_t f_t(x)}{f(x)}. \quad (35)$$

The discriminant analysis method allows to divide the *p-dim* vector space into regions R_t, where the particular region R_t is the subspace including all *p-dim* vectors *y* so that $p(t|y)$ is the largest of all groups. If observation is in the region R_t then it can be classified as coming from group *t* [148].

4.1.1. Parametric Methods

To have ideal conditions and assuming that all of samples have a multivariate normal distribution, means that they are distributed by a Gaussian curve. In this case, discriminant analysis is generating a classification criteria or discriminant function by applying a computation of generalized squared distance. The classification criterion is based on the individual within-group covariance matrices or pooled covariance matrix with respect to the prior probabilities of the classes. All observations are placed in the class depending on the smallest generalized squared distance [148]. The generalized squared distance from *x* to group *t* can be defined as the form below [148]:

$$D_t^2(x) = d_t^2(x) + g_1(t) + g_2(t);$$

where

$$g_1(t) = \begin{cases} ln|S_t| \; if \; the \; within - group \; covariance \; matrices \; are \; used \\ 0 \; it \; the \; pooled \; covariance \; matrix \; is \; used \end{cases}$$

and

$$g_2(t) = \begin{cases} -2\ln(q_t) \; if \; the \; prior \; probabilities \; are \; not \; all \; equal \\ 0 \; it \; the \; prior \; probabilities \; are \; all \; equal \end{cases}$$

Another important aspect is that discriminant analysis can be used in order to estimate the posterior probability of an observation belonging to each class of samples and has a form as detailed below [148]:

$$p(t|x) = \frac{\exp(-0.5D_t^2(x))}{\sum_u exp(-0.5D_u^2(x))}; \quad (36)$$

here $-0.5D_u^2(x)$ shows scores of discriminants. An observation is classified into group u if setting $t = u$ produces the largest value of $p(t|x)$ or the smallest value of $D_t^2(x)$.

4.1.2. Nonparametric Methods

Nonparametric methods are well known methodology used by many researchers between different research fields. For example, nonparametric methods are used in medicine, gene science, agriculture, veterinary, food science, human physics, electrical engineering, remote sensing, neuro science, finance and many others.

Lifeng Shang et al. [149] and N.M. Khan et al. [150] have presented how to use a nonparametric discriminant approach and apply it to facial expression recognition. Xiaodan Xie et al. have prepared research to show how the nonparametric methods can be useful in satellite imaging and aerial reconnaissance areas [151]. In addition, Tanvir Islam [152] et al. used it in the remote sensing area. In 2011, another publication was published about the nonparametric method application to amyotrophic lateral sclerosis, which showed excellent classification results (i.e. the area under the ROC curve reached more than 85%) [153]. In 2012, Allan R. Brasier M.D. showed how the nonparametric method can help in developing a biomarker for Dengue Hemorrhagic Fever [154]. In 2014, Loredana Murino et al. [155] published high accuracy results of classifying the multispectral brain MR images. Nonparametric models are also used in toxicology and pharmacology [156, 157, 158], as well as for the detection of rheumatic arthritis [159], clinical immunology [160] and in the field of chemometrics [161]. In 2013, Yan Cui et al. presented a paper that includes a nonparametric application to gene science [162, 163]. William G. Finn et al. showed in 2009 that the nonparametric approach can give significant results in Clinical flow cytometry [164]. Katie M. Hallahan [165] et al. used the nonparametric approach in research about the eye disease, named as Keratoconus and achieved high accuracy results, which reached over 96 percent. In 2008, Lukas Käll et al. also used the non-parametric approach for the estimation of posterior error probabilities associated with peptides [166]. In 2013 an application was presented in the field of agriculture [167] for the detection of immature peach fruits, which can help growers to create yield maps for adjusting management practices during the fruit maturing stages. More applications of nonparametric methods can be found in [168, 169, 170, 171, 172, 173, 174].

One of the methods is a nonparametric discriminant method, which is based on nonparametric estimates of group-specific probability densities. The estimation of nonparametric density is generated by using a kernel method or, for example the *k*-nearest-neighbour method and could be used to define classification criteria. There are various kernels that can be used in order to estimate densities, for example Gaussian, Epanechnikov, uniform, biweight, triweight and many others.

The classification of observations depends on the group of specific densities, which are computed by using a training set. After the assessment of the group densities, the posterior probabilities of group membership at *x* are also evaluated. Therefore, the sample *x* is included to group *u* if $t = u$ provides the largest value of $p(t|x)$ [148].

For the computation of density to group *t* for observations vector x, a fixed radius *r* and a specified kernel K_t are used. Suppose, that *z* is a *p*-dimensional vector, therefore a volume of a *p*-dimensional unit sphere bounded by $z'z = 1$ can be defined as [148]:

$$v_0 = \frac{\pi^{p/2}}{\Gamma(\frac{p}{2}+1)}. \quad (37)$$

Gamma function is represented by Γ.

In group *t*, the volume of a *p*-dimensional ellipsoid bounded by $\{z|z'V_t^{-1}z = r^2\}$ can be expressed as:

$$v_r(t) = r^p|V_t|^{1/2}v_0. \quad (38)$$

In this research, Normal kernel with mean zero and variance r^2V_t was used. Normal kernel, also known as Gaussian kernel, and has the form [148]:

$$K_t(z) = \frac{1}{c_0(t)}e^{(-\frac{1}{2r^2}z'V_t^{-1}z)}; \quad (39)$$

here $c_0(t) = (2\pi)^{p/2}r^p|V_t|^{1/2}$.

The density of group *t* at *x* was estimated by using [148]:

$$f_t(x) = \frac{1}{n_t}\sum_y K_t(x-y) \quad (40)$$

The above depends on the summation of all observations and the chosen kernel function K_t. Therefore, the calculation of posterior probability of membership in group *t* is calculated by using a form:

$$p(t|x) = \frac{q_t f_{t(x)}}{f(x)} \quad (41)$$

and depends on the estimated unconditional density that can be described as the function, $f(x) = \sum_u q_u f_u(x)$.

In the case of a fixed kernel shape, the smoothing parameter *s* is chosen by plotting the estimated densities with different values of *s* and selecting the estimate depending on the prior information about the density.

Another method of selecting the smoothing parameter *s* is to find an optimal value for a given criterion. The optimal value strongly depends on the group

probability density function. Assuming that the kernel has a symmetry form of probability density function and the unknown density has bounded and continuous second derivatives. One of the goals is to minimize an approximate mean integrated square error of the estimated density [148]. Optimal value of smoothing parameter, *s* is based on the kernel and its density function. Optimizing criteria with the presumption of normal group *t* distribution together with the covariance matrix V_t allows choosing the optimal smoothing parameter *r*.

Therefore, the smoothing parameter *s* in group *t*, can be described as [148]:

$$s = \left(\frac{A(K_t)}{n_t}\right)^{1/(p+4)}; \tag{42}$$

here an optimal constant $A(K_t)$ depends on the kernel K_t [104]. In this research, a constant $A(K_t)$ for a Gaussian kernel is expressed as:

$$A(K_t) = \frac{4}{2p+1}, with\ a\ normal\ kernel. \tag{43}$$

As a rule, there is no singular method that is the best when compared with other methods used in classification. The parametric discriminant technique is the oldest method for classification, firstly presented by Fisher in 1936 with the purpose to solve the problems arising from the biological measurements, and became widely used due to the simplicity and robustness, but linear discriminant analysis is not able to cope with highly collinear data [175]. The discussion about the advantages and disadvantages of the parametric and nonparametric models started long time ago. In 1984, E. Francis Cook et al. distinguished that it may depend on the sample size and the ability to construct an appropriate parametric model. If the size is small, then the nonparametric model is able to perform a few initial partitions, but may fail to identify other predictive factors. It has also been stated that the nonparametric model should be considered to assist in the identification of interaction terms that may then be used in the construction of a parametric model [176].

For example, in 2005, Zhifeng Li et al. stated that even the linear discriminant analysis is a popular face recognition technique, but a problem arises because of the parametric nature where in each group distribution of the sample should be normal and this causes issues when the distribution is non-normal. Due to the problem stated before, a nonparametric approach was used and showed the effectiveness of the used technique with extremely high accuracy (99.7%) [177]. Xipeng Qiu et al. have noticed that the results of face recognition research also depend on the volume of observations,

which is increasing for the case of high dimensional image data. It cannot be guaranteeing to get the best directions when the density is not a Gaussian density, so the nonparametric approach was used and outperformed the linear discriminant method [178]. Bor-Chen Kuo et al. have also noticed that there are two main advantages of using the nonparametric approach in order to solve problems related to face recognition. In this case, nonparametric scatter matrices provide the ability to select the exact number of features needed for the investigation and to reduce the effect of the singularity problem. Meanwhile, a parametric discriminant analysis, can only usually extract a number of classes minus one feature. Another advantage is that the nonparametric nature of scatter matrices reduces the effects of outliers and works well, even for non-normal data sets. As a result, this method strongly affects the accuracy of classification [179]. Many authors who are interested in the application of face recognition have shown that the nonparametric models are more effective than well-known parametric models. This statement is also proved by Zhifeng Li et al. [180], where the accuracy of classification is higher than 10 percent when comparing nonparametric and parametric results.

In 2010, Jinn-Min Yang et al. proved that the nonparametric methods are more useful than the parametric in regards with features extraction. In addition, they are much more suitable for data that is not distributed by Gaussian distribution [181]. As per M. Bressan et al. publication, it has been stated that the nonparametric models allow to extract the features that preserve relevant structures for classification which strongly affects the classification results [182].

In 2012, Nicolas Garcia-Pedrajas et al. separated two main disadvantages of parametric methods. The first one is the Gaussian presumption over the group distribution of the data samples, and secondly; the dimensionality of the subspaces depends on the number of analysed classes, mostly *L-1* dimensions for a dataset with *L* classes. In this case, a nonparametric discriminant analysis is the best choice [183]. It is obvious that none of these methods is the best and should only be used in unique situations depending on the data. Discussing the disadvantages of nonparametric methods, there can also be excluded two main disadvantages. The first one arises when the values of parameters k and q are defined by the rules of thumb. This means that, for example, if k = 1 and q = 1 so then within-class scatter matrix in nonparametric discriminant analysis the form still is parametric, and the volume of the training set is not large enough. The second observation is that the nonparametric discriminant analysis still has a singularity problem [183].

On the other hand, Federico Marini [175] showed that the nonparametric methods also have disadvantages related with the noise reduction, irrelevant or wrongly scaled features, which can seriously affect its performances.

As stated above, nonparametric methods are used in many different research fields. Seyed Omid Sadjadi et al. have presented some of the results in the field of language recognition and stated that the nonparametric discriminant analysis is more effective when compared with the linear discriminant analysis. The main advantage of nonparametric discriminant analysis is that it is suitable for a limited number of speech applications because of the full rank [184].

4.2. Cross validation

Another important step is to choose the method that will be used for the selection of prognostic model. One of the greatest challenges in the case of correct classification is to assign the independently random observation to one of the selected groups. An important note is that all of the observations could be assigned just to one group. This means that it can be done by using predictable parameters or other factors that could describe those observations according to the attributes of each specified classification group. The other challenge is to minimize the rate of error probability as much as is possible. Also, after the classification procedure it should be a significant choice to estimate the proportion of correct prediction or wrong classification. Fisher has suggested finding a linear combination of observations that would maximize the difference between groups relative to the standard deviation within groups [185].

Assuming there are two samples X_1 and $X_2$from two different classes, where $X = X_1 \cup X_2$. Then Fisher's linear discriminant is:

$$J(w) = \frac{w^T S_B w}{w^T S_W w}. \tag{44}$$

and $S_B = (m_1 - m_2)(m_1 - m_2)^T$, $S_w = \sum_{i=1,2} \sum_{\infty \in X_i} (x - m_i)(x - m_i)^T$. Meanwhile, the matrix $m_i = \frac{1}{l_i} \sum_{j=1}^{l_1} x_j^i$.

The point of maximizing *J(w)* is to detect the method that maximizes the numerator (projected class mean) and minimizes the denominator (the classes variance in this vector).

Lachenbruch [186] presented a paper on error rate estimation for discriminant analysis. The techniques of error rates estimation could be separate from each other: firstly, where it is using a sample to evaluate a given discriminant function and secondly where it is using the properties of the normal distribution. The former may be considered empirical methods, while the latter are dependent on the normality of the distribution for their validity.

The refinement of this type of assessment that gives a cross-validation criterion appears to have been developed by Lachenbruch, following a suggestion in Mosteller and Wallace [187, 188].

Lachenbruch and Mickey [189] have popularized this method and noted that the estimates of the probabilities of misclassification are computed by summing the number of cases that were misclassified from each group and dividing by the number in each group. To use the *U* (identified as named; leave - one - out or Jackknife method) method, the value of the discriminant function based on *n - 1* observations for each observation should be found. This technique allows to eliminate most of the bias of the assumed error rate in a way of calculating the number of evaluations of training vectors of the discriminant functions, denoted by *n*, defined by leaving out

one training vector each time. These discriminant functions are used for classification of the training vectors left out. Therefore, an assessment is made by counting the number misclassified and dividing by the number of evaluations of trainings vectors.

Meanwhile, Allen [190] has shown that the reliability of prediction, called Prediction Sum of Squares, could be described as:

$$PRESS\ (D) = \sum_{j=1}^{n}(Y - \hat{Y}_{(i)})^2. \quad (45)$$

Where $\hat{Y}_{(i)}$ is the estimator of $E(Y_i)$ except *i*-th observation. In other words, $\hat{Y}_{(i)} = (X'X - x_i x_i' + D)^{-1}(X'Y - x_i Y_i)$.

The point is that each contemplation is envisaged by using the rest of the sample of *n*-1 contemplations. As a result, errors of prediction are squared and summed, then to the above form called of prediction sum of squares (PRESS). PRESS is referring because it imitates the prediction avoiding the use of an observation to contribute in the prediction of itself [190].

Stone [188] developed the method of cross - validatory choice of alpha (alpha used to form a predictive value) and the method of cross - validatory assessment of this choice as follows. This leads to the conclusion that the realistic priors should be separated from the unrealistic priors, because presumably a realistic prior is one that would not give its user any cross - validatory shocks [188]. Commenting on Stones, in 1966 Hills et al. described a conundrum of an appropriate evaluation of the error rates of a discriminant when the form of it is well-known and fully detailed. In literature, an application of cross-validation has a prescription of type *j (x; S)*, with no *a* to be chosen, and the evaluation is a computation of Hills [188]. More detailed information about the cross - validatory choice and cross - validatory assessment of this choice could be found in the paper presented by Stone [191]. In addition, these developed methods were based on leave-one-out cross validation in a regression context.

Meanwhile, Geisser presented the differences of cross – validation methods. This was based on the V-fold cross validation [192]. Comparing these two methods, the main difference is that Geisser developed a method for multiple observations, not even for the single, which leads to much greater flexibility and reliability of the prediction function.

Wahba has also applied the methodology of cross – validatory in his procedure of determining the degree of smoothing [193]. The cross validation mean square error technique is very significant in order to obtain an optimal degree of smoothing. Less value of the cross – validation mean square error corresponds to a model representation of the data where the model gives the best prediction.

In 1984, Picard talked about the random splitting of large sets of observations by using a cross – validation method in order to estimate the prediction function [194]. In the case of data splitting, it impacts that the selection of the model should be kept for the analysis of the evaluation data and that the validation data should be allocated exclusively for the estimation. He showed that data splitting could also be used in

regression procedures and brings the value back. It is said that the examination of competing regression models, with respect to how well they predict validation data, can aid in model selection.

The method of cross – validation determines the selection of the model with the best average predictive ability estimated by different methods of data splitting [195]. The sample of observation is split into training and validation sets. Let the n_t – be the training sample and n_v – the validation sample, where $n_t + n_v = n$. There are a lot of different ways of how to split the sample. The larger the *nv*, the more complex the selection of model. This explains why the previous research results published by other researchers were carried out by setting n_v = 1. In this case, an author has noticed that the linear model cross-validation with n_v =1 is asymptotically incorrect (inconsistent) and is too conservative in the sense that it tends to select an unnecessarily large model [195]. This problem could be solved by changing n_v = 1 to larger n_v, depending on how large the sample *n* is. However, this procedure requires to select *nv* as having the same rate of divergence to infinity as *n*, in other words:

$$\frac{n_v}{n} \to 1, as\ n\ \to \infty.$$

In 2008, Alain Celisse proved the optimality of leave - one - out among a cross – validation algorithm in the context of risk estimation [196]. She also confirmed the results in the regression framework of previous research done by Burman [197, 198].

However, the cross – validation optimality in the risk estimation context does not always mean that it is necessarily the best for model selection. The main aspects of model selection are the estimation and identification. The proof and further information can be found in Alain Celisse [196].

In order to decrease the variance in an error-count evaluation, a smoothed error-rate evaluation is proposed [199]. Avoiding totalizing those which are either zero or one as in the error-count evaluator, a smoothed evaluator that is based on a continuum of values in ranges of 0 and 1 are summarized. As a result, a proposed evaluator will have a lower variance compared with the error-count evaluate. The posterior probability of each assessed class depends on the posterior probabilities of the observations that are assigned to the same class. The evaluations of posterior probability impact the high value assessments of the error rate when they are precise. In the case of parametric classification criteria, linear and/or quadratic discriminant function, which is gained from a non-normal population, the evaluations of posterior probability error-rate might not be relevant [199].

Weighted average of the specific group error rate evaluations is used for the calculation of the overall error rate. In this case, weights are the prior probabilities. In order to decrease variance and bias of the evaluator, the estimation of posterior probability based on cross validation should be calculated [200]. As a result, using a posterior probability based on cross validation, lower variance and bias are derived. The procedure is based on the Monte Carlo method, applying it on two-group multivariate normal distributions and then cross validation posterior probability

evaluations are likened the with assessments such as, posterior probability and cross validation evaluators the apparent error rate. The conclusion of the application detailed above is that the posterior probability estimation based on cross validation has a lower MSE (mean squared error).

Obviously, there are other alternative methods for prognostic model selection. For instance, Akaike presented the Akaike information criterion (AIC) [201]. Meanwhile, Stone, presented acomparison method based on Akaike information criterion and cross – validation [202]. In 1973, Mallows proposed another method of model selection, named Cp [203]. Herzberg presented the Monte – Carlo methodology for model selection [204]. Efron proposed an improvement on cross – validation and presented bootstrap-type procedures as an alternative [205]. Rob Kohavi, after his research about the accuracy estimation of different procedures, recommended to use 10-folds cross – validation procedure instead of bootstrapping, due to a large bias of this method [206].

4.3. Logistic regression

Logistic regression is one of the most popular and well-known prognostic models, where the observations for binary response *(Y)* models of an experimental and/or an individual observation can gain one of two possible values. For example, $Y = 1$ if it is true and $Y = 0$ if it is false. Assume that *x* is a vector of explanatory variables and $\pi = \Pr(Y = 1|x)$ is the response probability that should be estimated. The linear logistic model could be described as follows and is used by many researches [207 - 212]:

$$logit(\pi) = \log\left(\frac{\pi}{1-\pi}\right) = \alpha + \beta' x; \quad (46)$$

here α represents the intercept parameter and $\beta = (\beta_1 \dots \beta_s)'$ is the vector of *s* slope parameters.

In cases where nominal response logistic models are being used, with the $k + 1$ maximum number of likely responses that have no natural ordering, then the logistic model can be expanded to a multinomial model following the below [213]:

$$\log\left(\frac{\Pr(Y = i|x)}{\Pr(Y = t + 1|x)}\right) = \alpha_i + \beta'_i x, i = 1, .., t; \quad (47)$$

where $\alpha_1 \dots \alpha_t$ are *k*intercept parameters, and the $\beta_1 \dots \beta_t$are *t* vectors of slope parameters. More about the discrete choice or conditional logic models could be found in McFadden [213].

4.4. Comparison of the discriminant analysis and logistic regression models

The reliability of the causal prognostic model usually depends on the selection of probabilities in the discriminant analysis. This means that the posterior distributions

expressed by the selection of probabilities and the prior distribution could be useful in the estimation of the selection of probability parameters, but this procedure does not lead to being robust due to the prior probability misspecification. Discussing the conjoint models, the selection of probabilities and posterior distribution could be a multiple–choice in the conjoint distribution described. One approach is to use a logit model, which determines that the actual responses are defined from the multinomial distributions with the selection probabilities that depend on the subsequent values of individual characteristics and attributes of alternatives. Meanwhile, discriminant analysis leads to the conclusion that the subsequent values of individual characteristics and attributes of alternatives are obtained from the posterior distributions that depend in actual responses. Additional information about the causal and conjoint models' comparison and application examples about the logit or the discriminant analysis models can be found in Daniel McFadden's publication [214].

Efron has raised the issue of why it is useful to use the logistic regression if it less efficient and more difficult to calculate than the normal discriminant analysis [215]. The answer depends on the robustness in both aspects, theoretically and practically in comparison with the discriminant analysis.

S. James Press and Sandra Wilson have also noticed that one of the advantages to using the logistic regression model instead of discriminant analysis is that it is relatively robust; i.e., many types of underlying assumptions lead to the same logistic formulation [216].

Another advantage of using logistic regression modelling is that it is closely related to the contingency table analysis and could be a good alternatively choice. For example, Gordon argued that logistic regression models are significantly more important in the case of medical and biological applications, because of the cross-classified tables that include large numbers of cells and logistic (log-linear) models that can be used as alternative by removing a need to use those original tables [217].

Reviewing the estimation in comparison of maximum likelihood estimation and linear discriminant function estimation (for a logistic regression), Halperin et al. have found that in terms of timings needed for execution and compilation of the modelling programs, the maximum likelihood method need much more time than the discriminant function method, approximately from 1.3 to 2 time. [218].

"Efron has shown that logistic regression estimators are between one-half and two-thirds as efficient as discriminant function estimators when the data is multivariate normal with equal covariance matrices." This means that while the data is strictly normal, and the covariance matrices are equal, the discriminant function estimator is more economical in time scales and cost, and also more efficient than the logistic regression [215].

However, there are more arguments, both for and against, of using the discriminant function and the logistic regression detailed in S. James Press and Sandra Wilson [216].

4.5. The segmentation of ultrasonic and digital dermatoscopy medical images

Whilst researching medical images, a lot of techniques that allow the capture of different biomedical images in different ways have been identified. The common techniques are such as magnetic resonance imaging, X-ray computed tomography, ultrasound imaging, X-ray projection radiography, digital dermatoscopy imaging and etc. All of these techniques can give valuable information, but one of the greatest challenges is to find a tool that will provide better outputs, such as high accuracy, precision and speed. Regarding the challenges stated above, a more accurate estimation can help achieve a faster diagnosis, dependable prediction of the illness, in addition to reducing the cost of possible treatment and to save as many lives as is feasible. Nowadays, many segmentation methods, which could be split into different categories, are widely used, for example: thresholding approaches, region growing approaches, classifiers, clustering approaches, Markov random field models, artificial neural networks, deformable models or atlas guided approaches [219]. In addition, image segmentation tools such as active contours and snakes, edge detection and clustering techniques based on thresholding were used [220]. The edge detection technique is not effective when applied on skin images, because of the additional details, such as hair. The active contours and snake's method [221] is less attractive due to the complex shape of the melanoma suspicious lesions. However, thresholding does not present any of these disadvantages [222] and it could be used in order to get more reliable results.

The thresholding approach is the most common procedure used in different applications. For example, in biomedical image analysis [223], handwritten character identification [224], automatic target recognition [225], change-detection applications [226 - 228], reconstruction of a map of interference fringes [229] and segmentation based on colour images [230]. Colour is one of the most significant low-level features that can be used to extract homogeneous regions, which most of the time are related to; objects or part of objects, multilevel thresholding technique approaches [231, 232, 233], thresholding approach in Otsu algorithm [234], threshold approach in segmentation of satellite images [235] and other applications [236, 237].

For example, the segmentation of ovarian cysts research is done under the thresholding process [208] concentrating the intensity and texture from ultrasound images. In 1997, A. Sebbahi et al. have shown good results of deformable models in order to classify echocardiograms images by applying ultrasound examination [210]. Deformable models were also used to estimate the contours of the fetus and the fetus head [207]. Furthermore, a later technique was also used in segmentation of breast cysts from ultrasound images [209].

Automatic thresholding techniques are mostly assigned to one of two main groups. Common groups are local methods and global methods. The group of local methods are mostly used when object classes and the background do not have stationary statistical properties of the different parts of image which is analysed. This can be explained by the property that allows the use of threshold values which are dynamically changing. Meanwhile, global methods are used for receiving fixed threshold values [238]. In this research, borders of melanocytic skin tumours in

ultrasonic and dermatoscopic images are identified by using Gaussian smoothing and a global thresholding technique. The Gaussian smoothing technique is based on a mathematical convolution operation of a two-dimensional Gaussian kernel function. Generally, this could be translated as a mean filter, however in this case the kernel clearly represents the shape of a Gaussian distribution. The degree of Gaussian smoothing is based on the standard deviation of the distribution [239]. In this research, the standard deviation is chosen to be wide enough and is equal to 5.

Gaussian smoothing - spatial filtering was implemented according to equation [239]:

$$G(x,y) = \frac{1}{2\pi\sigma^2} e^{\frac{-x^2+y^2}{2\sigma^2}}; \quad (48)$$

here μ is the mean and σ is the variance.

Meanwhile, thresholding:

$$g(x,y) = \begin{cases} 1 \; if \; f(x,y) \geq T \\ 0 \; otherwise \end{cases}; \quad (49)$$

here *T* is the global threshold.

The thresholding technique allows the arrangement of scalar images by creating a binary partitioning of the image intensities. The procedure of thresholding enables the defining of an intensity value, which is known as a threshold. A threshold is like a boundary that can exclude the desirable groups. The classification is based on grouping pixels that have higher intensity than the threshold into one group, and the other group of pixels that have a lower intensity than the threshold to another group. The thresholding technique is an effective application for images segmentation purposes, where different structures have contrasting intensities or other quantifiable features [240]. Values which are equal or below the applied threshold are named as a background and all the grey level values which are higher are named as an object [212].

An application of thresholding procedure, presented in this study, is done by using an expectation–maximization (EM) algorithm and depends on the maximum likelihood estimation which can be expressed as $O^* = \arg max_O L(O)$, where

$$L(O) = \prod_{t=1}^{n} f(X(t), O). \quad (50)$$

The methodology of the EM algorithm operation is based on random values computations. The procedure of values convergence takes from several to hundreds

of iterations, which means that the assessment of tumour contour is based on the initial values [241]. After this cycle, a skin tumour with the contour of the largest area is selected [212]. Many research studies are made by using this particular approach of EM algorithm and could be found in references [242 – 249].

Dermatoscopic, ultrasonic and histological, along with images have been collected at the Department of Skin and Venereal Diseases of the Lithuanian University of Health Sciences (LUHS). The study was approved by the regional ethics committee. The cases of 31 suspicious melanocytic skin tumours, which included 19 melanomas and 12 benign nevi, were analysed. Inclusion criteria of images within the study covered the size of the tumour (up to 1 cm in diameter) and a histological thickness of ≤ 2.5 mm [250].

Ultrasonic data was acquired during non-invasive examination of human skin using the DUB-USB ultrasound system ("Taberna pro medicum", Germany) with a mechanically scanned single element focused transducer with centre frequency of 22 MHz's. The received A-scan ultrasonic signals were digitized and transferred to a personal computer in order to reconstruct the B-scan image. Optical dermatoscopic images were acquired using a spectrophotometer SimSys© (MedX Health Corp., Canada) operating in dermatoscopy mode and transferred to a personal computer for further analysis. The radius of informative area of optical images was 11 mm. The principle of the set-up of non-invasive ultrasonic and digital dermatoscopy imaging systems is visualized in Fig. 17 [120].

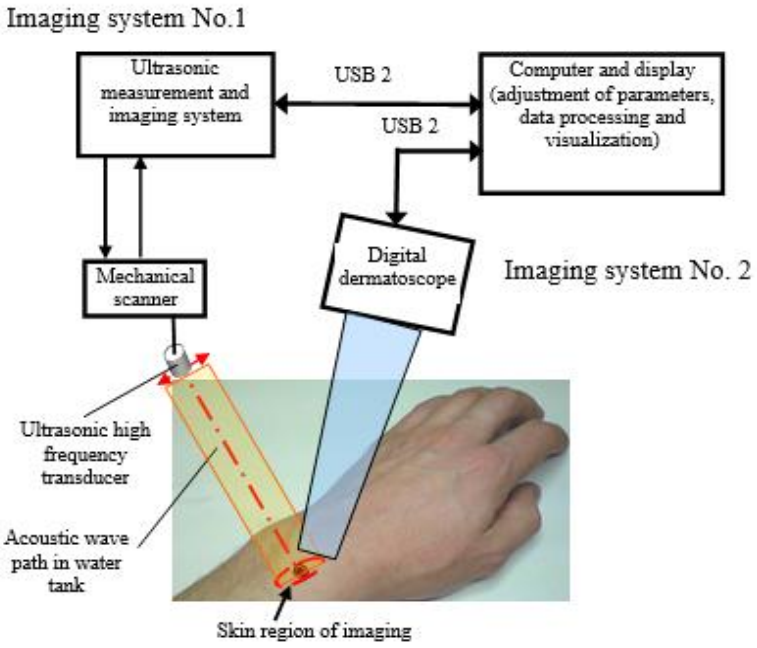

Fig. 17. The set-up of non-invasive ultrasonic and digital dermatoscopy imaging systems (No.1 and No.2) [120]

After surgical excision and during the routine histopathology, the diagnosis of skin lesions was confirmed [58]. The outcomes of the application of the thresholding procedure used for different types of skin tumour images are presented below [250]. Examples of primary ultrasonic raw B-scan images of malignant and benign skin tumours are presented in Fig. 18 a) and Fig. 20 a). The results of transformation of raw ultrasound B-scan and digital dermatoscopy example images to the binary images are shown in Fig. 18. – Fig. 21. This is made by using the procedure of equalization for all the values of matrix amplitude of every image. Equalization is based on the closest neighbours of that value which is not placed more than 40 pixels (steps, values). Bending, which is equal to 20 pixels for two sides, is made by using cross – validation. Smoothing of the images are made by using absolute magnitude amplitudes that are generated with the help of Gaussian kernel. Before the procedure of smoothing, all the absolute magnitude data of ultrasound images matrix was transformed using a logarithmic scale. Example images after transformation are presented in Fig. 18. b) – Fig. 21. b). After transforming the views, the Gaussian smoothing, and thresholding procedure defined above was applied in order to detect informative regions. Example images of detected informative regions are shown in Fig. 18. c)- Fig. 21. c) images.

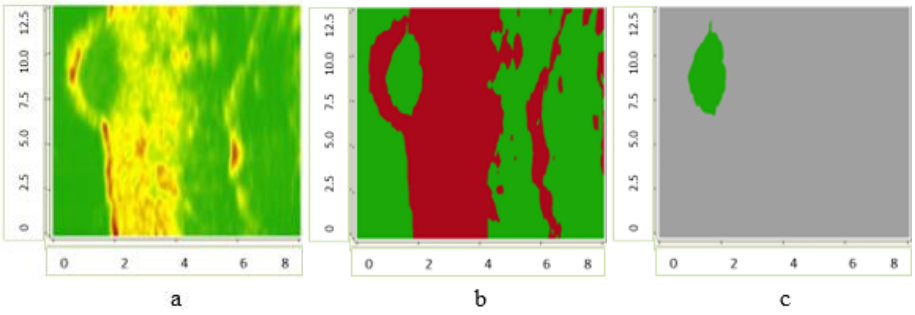

Fig. 18. Ultrasonic B-scan images (raw and processed) of skin melanoma, axes are in millimetres (1-pixel value for length is 0.033 mm, for depth – 0.0079 mm): a – ultrasonic raw B-scan image, b – binary B-scan image, c – detected informative region [250]

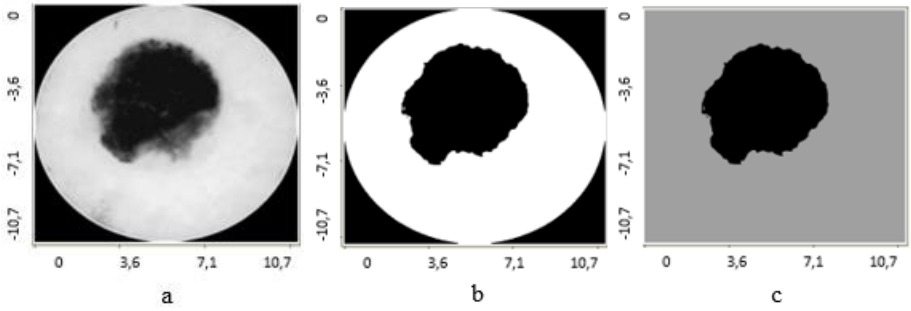

Fig. 19. Digital Dermatoscopy Images (raw and processed) of skin melanoma, axes are in millimetres (1-pixel value 0.0071 mm): a – raw optical image, b - binary optical image, c - detected informative region [250]

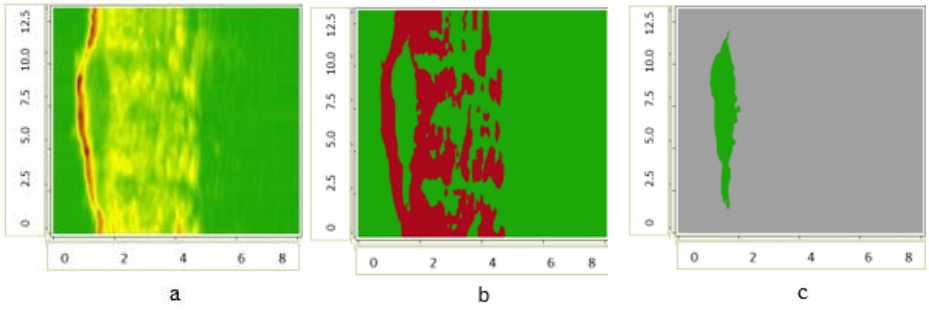

Fig. 20. Ultrasonic B-scan images (raw and processed) of benign nevus, axes are in millimetres (1-pixel value for length is 0.033 mm, for depth – 0.0079 mm): a – ultrasonic raw B-scan image, b – binary B-scan image, c – detected informative region [250]

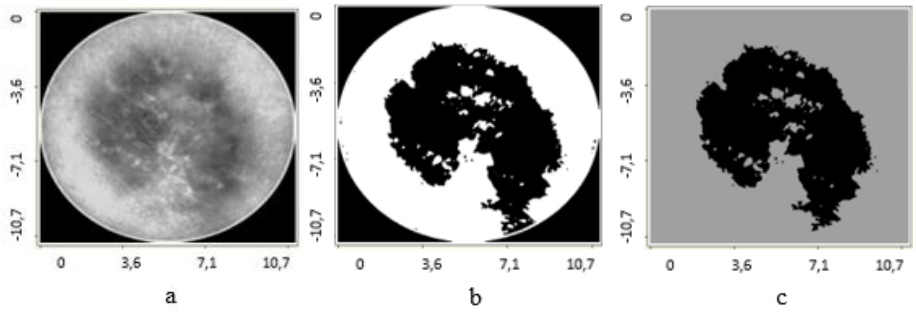

Fig. 21. Digital Dermatoscopy Images (raw and processed) of benign nevus, axes are in millimetres (1-pixel value 0.0071 mm): a – raw optical image, b - binary optical image, c - detected informative region [250]

All the examined 31 ultrasonic and 31 digital dermatoscopy raw and processed images are presented in Appendix 1. The first nineteen images present ultrasonic B-scan images of skin melanoma. In a sequence from 20 to 38 images, images of digital

dermatoscopy of skin melanoma are shown. The ultrasonic B-scan images for benign nevus are shown in a position starting from 39 to 50 images. The last twelve images present digital dermatoscopy images of benign nevus.

4.6. The estimation of diagnostic performance rate by applying ROC curve analysis

The diagnostic performance rate can be defined in terms of diagnostic accuracy, or the ability to classify subjects into clinically relevant groups. The accuracy of the estimation depends on the quality of the outcomes of the classification results and should be separated from the actual practical value or usefulness of the estimated data. A receiver operating characteristic (further - ROC) graph is a technique for visualizing, organizing and selecting classifiers based on their performance [251]. The ROC curve informs about the degree of accuracy by showing the limits of an ability to discriminate between alternative states of health over the disease possibility. ROC methodology is based on statistical decision theory and was developed in the context of electronic signal detection and problems of radar in the early 1950s, and has been used in experimental psychology and psychophysics [252]. In 1993, Mark H. Zweig and Gregory Campbell stated that the diagnostic accuracy is the most fundamental characteristic of the test itself as a classification device, because it can measure a test's ability to discriminate among alternative states of health [253]. It also involves distinguishing between health and disease, benign and malignant disease, responders and non-responders to therapy and etc. Therefore, the accuracy could be defined as the tool to separate two different groups of variables, when there are some clinically relevant reasons to do it. This also leads to the quality of the data concept of accuracy, which refers to the quality of the classification provided by the test and should be distinguished from the practical usefulness of the information. These two concepts are the key to the estimation of the diagnostic performance rate and affect the quality of patient care management [253]. The ROC graph is representing the ratio of sensitivity and specificity regarding the classification results of the malignant and benign skin tumours, where the receiver operating characteristics (ROC) curve introduces the connections between the false - positive fraction and true - positive fraction [254]. The false - positive fraction is the fraction of actually-negative cases incorrectly classified as positive, meanwhile true - positive fraction is a fraction of actually-positive cases correctly classified as positive. Sensitivity is the probability of correctly detecting the condition of interest among subjects with the condition. Specificity is the probability of correctly ruling out the condition among subjects without the condition [255]. The application of the ROC curve is simple to graph and easy to understand the dependencies of tumours classifications, because there are no requirements for selection of a particular decision threshold due to the whole spectrum of possible decision thresholds is included. Also, there is no dependence on occurrence, which means that no care need be taken to obtain samples with the representative prevalence [253]. Otherwise, the equal number of observations for both groups is promoted. The ROC curve does not require that the data would be grouped

or binned, as the frequency histograms do. In addition, it is not required that the plot should be different if the scales differ, as frequency histograms and dot diagrams do. The main ROC curves characteristics, specificity and sensitivity can be easily captured when compared with frequency histograms and dot diagrams [253]. One of the most preferable ways to represent the accuracy of diagnostic is to define its performance by a single number, rather than express it by intervals etc. In 1982, Swets and Pickett proposed to use an index of accuracy associated with the ROC curve [256]. In this case, the area under the ROC curve is a widely used technique. The area under the receiver operating characteristics (ROC) curve indicates that the value of the probability of the variable, which is randomly selected for individual from the non-normal group and a randomly selected individual from the normal group, will be in positive true [257]. The area under the ROC curve could be represented with values varying from 0 to 1, which means that more of the performance rate is closer to 1, more of the classification is reliable and for the values which start from 0.5 and less that there is no separation between the two tested clinical groups. ROC curves are also popular to use in discriminant analysis and is advantageous because it provides the linear- or quadratic-discriminant function that defines the optimal decision rule and logistic regression models in order to estimate the accuracy of two different patient groups classification [253, 258].

The possibilities of using ROC curve analysis in medical decision-making tools was first suggested by Lusted [259 – 262]. After this, researchers started to use this method in medical diagnostic [263 – 276] and medical imaging [277 - 287] aspects, seeking to ensure faster diagnostic and save more lives. In the last two decades, ROC curve analysis has been widely used in the field of dermatology. Most of the research has been done with respect to identify skin tissue damages [288 - 297].

ROC curve analysis is a meaningful tool to use for the estimation of model accuracy. A plot of ROC curve presents the ratio of sensitivity and 1-specificity, which are a measure of the model fit. Depending on the above, a receiving operating characteristics curve was chosen to use for this research [250]. The ROC curve of the classification of melanoma and benign melanocytic nevi analysing ultrasonic B-scan images only by using discriminant analysis is shown Fig. 22. The ROC curve of discriminant analysis classification model based on the assessment of synergy of digital dermatoscopy and ultrasonic B-scan images is shown in Fig. 23. The ROC curve of the classification of melanoma and benign melanocytic nevi analysing ultrasonic B-scan images only by using logistic regression is shown in Fig. 24. The ROC curve of logistic regression classification model based on the assessment of synergy of digital dermatoscopy and ultrasonic medical images is shown in Fig. 25.

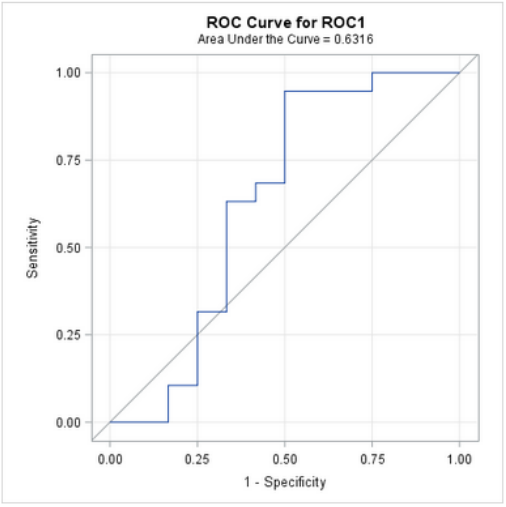

Fig. 22. ROC curve of the classification of melanoma and benign melanocytic nevus analysing ultrasonic B-scan images only by using discriminant analysis [250]

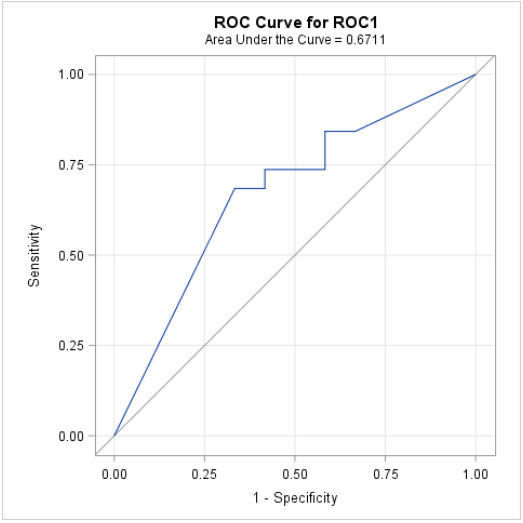

Fig. 23. ROC curve of discriminant analysis classification model based on the assessment of synergy of digital dermatoscopy and ultrasonic B-scan images [250]

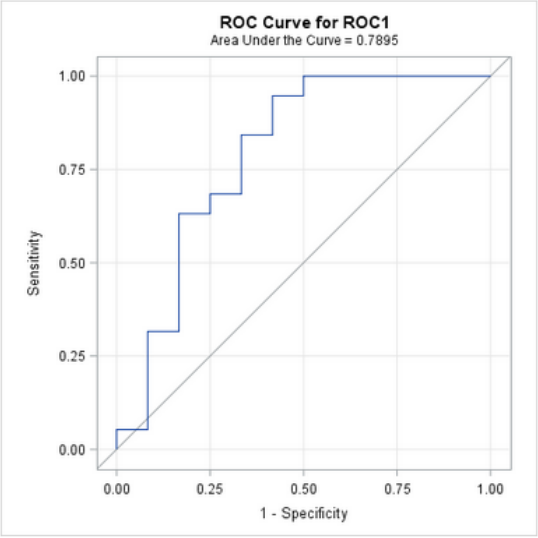

Fig. 24. ROC curve of the classification of melanoma and benign melanocytic nevi analysing ultrasonic B-scan images only by using logistic regression [250]

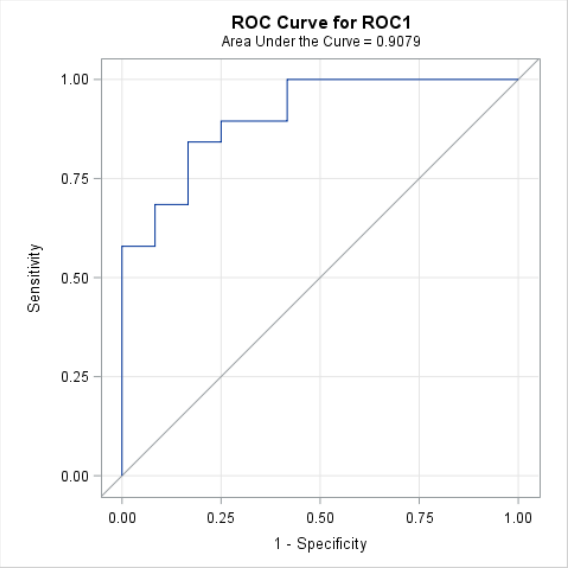

Fig. 25. ROC curve of logistic regression classification model based on the assessment of synergy of digital dermatoscopy and ultrasonic medical images [250]

Detailed results of the automatic classification are presented in Table 12 below.

Table 12. Results of the automated classification

True versus false prediction	Results of classification by discriminant analysis for ultrasonic B-scan images, %	Results of classification by discriminant analysis classification model based on the assessment of synergy of digital dermatoscopy and ultrasonic medical images, %	Results of classification by logistic regression for ultrasonic B-scan images, %	Results of classification by logistic regression classification model based on the assessment of synergy of digital dermatoscopy and ultrasonic medical images, %
True nevus	73.68	73.78	78.95	89.47
False nevus	26.32	26.32	21.05	10.53
True melanoma	50.00	50.00	33.33	25.00
False melanoma	50.00	50.00	66.67	75.00
Total true	**64.52**	**64.52**	**61.29**	**64.52**
Total false	**35.48**	**35.48**	**38.71**	**35.48**

After the classification of malignant and benign tumours by analysis of quantitative parameters extracted from ultrasonic and digital dermatoscopy images, the results based on receiver operating characteristics curve analysis are presented in the Table 13 below.

Table 13. The results of classification of melanoma and benign melanocytic nevi analysing ultrasonic B-scan images and in combination with analysis of digital dermatoscopy images based on receiver operating characteristics curve (ROC) analysis [250]

Classification model	The probability of correct prediction during the classification of ultrasonic images (parameters), % (ROC*)	The probability of correct prediction during the classification based on assessment of synergy of digital dermatoscopy and ultrasonic medical images(parameters), % (ROC*)	The classification improvement, %
discriminant analysis model (approximation by Normal distribution with cross - validation)	62 (0,632)	62(0,671)	0
logistic regression model (stepwise method with cross - validation)	73 (0,790)	82(0,908)	9

Assessing the results table, the probability of correct prediction during the classification of ultrasonic images by using a discriminant analysis classification model and significant parameters is equal to 62%. The probability of correct prediction during the classification based on assessment of synergy of digital dermatoscopy and ultrasonic medical images by using significant parameters is equal to 62%. The estimated area under the ROC curve is only 0.671, which means that the classification was not improved when comparing the results of the discriminant analysis classification models. Analysing the outcomes of an application of stepwise logistic regression, it is clear that the classification was improved by 9% and has reached 82% compared with the classification of ultrasonic B-scan analysis only. In addition, the area under the ROC curve is close to 1and therefore the prognostic features of the developed technique are accurate (in the case of <0.5 the obtained results are not reliable). In this case, an estimated area under the ROC curve is 0,908 [250].

For all the automated classification models presented above, sensitivity and specificity rates of automated classification of melanoma and benign melanocytic nevi analysing ultrasonic B-scan images in combination with analysis of digital dermatoscopy images were calculated and are detailed in Table 14.

Table 14. Sensitivity and specificity rates of automated classification of melanoma and benign melanocytic nevi analysing ultrasonic B-scan images in combination with analysis of digital dermatoscopy images

Classification model	Sensitivity, %	Specificity, %
Discriminant analysis classification model used for ultrasonic B-scan images	74	50
Discriminant analysis classification model based on assessment of synergy of digital dermatoscopy and ultrasonic medical images	74	50
Logistic regression model used for ultrasonic B-scan images	79	67
Logistic regression classification model based on assessment of synergy of digital dermatoscopy and ultrasonic medical images	89,5	75

Comparing the results of sensitivity and specificity, the discriminant analysis classification model used for ultrasonic B-scan images and discriminant analysis classification model based on assessment of synergy of digital dermatoscopy and ultrasonic medical images have shown the same results of sensitivity, which was equal to 74% and specificity which was equal to 50%. Comparing the results of the logistic regression model used for ultrasonic B-scan images and logistic regression classification model based on assessment of synergy of digital dermatoscopy and

ultrasonic medical images, sensitivity was 79% against 89,5% and specificity was 67% against 75%.

Diagnostic accuracy of automated classification of melanoma and benign melanocytic nevi analysing ultrasonic B-scan images in combination with analysis of digital dermatoscopy images for four presented classification models is shown in Table 15.

Table 15. Diagnostic accuracy (error count) of automated classification of melanoma and benign melanocytic nevi analysing ultrasonic B-scan images in combination with analysis of digital dermatoscopy images

Classification model	Diagnostic accuracy (error count)
Discriminant analysis classification model used for ultrasonic B-scan images	0.618 (0.382)
Discriminant analysis classification model based on assessment of synergy of digital dermatoscopy and ultrasonic medical images	0.618 (0.382)
Logistic regression model used for ultrasonic B-scan images	0.728 (0.272)
Logistic regression classification model based on assessment of synergy of digital dermatoscopy and ultrasonic medical images	0.822 (0.178)

The discriminant analysis classification model used for ultrasonic B-scan images and discriminant analysis classification model based on assessment of synergy of digital dermatoscopy and ultrasonic medical images have shown the same diagnostic accuracy. This means that the accuracy for a discriminant analysis model was not improved. Comparing the results of the logistic regression model used for ultrasonic B-scan images against the logistic regression classification model based on assessment of synergy of digital dermatoscopy and ultrasonic medical images, it is clear that the analysis based on synergy of two different technologies has improved the diagnostic accuracy. The proposed automatic classification algorithm based on data captured from two different technologies has shown better diagnostic accuracy than the other used models.

4.7. Estimation of group of quantitative parameters describing the informative regions of ultrasonic and dermatoscopy images

The purpose of this research part was to separate significant and not relevant parameters in order to increase the classification accuracy of ultrasonic and digital dermatoscopy images. For all B-scan ultrasonic and digital dermatoscopy images there were 46 parameters of tumour structure evaluated, i.e. 19 parameters of ultrasonic images and 27 parameters of digital dermatoscopy images [250].

After estimation of contours of informative regions (tumour or nevus) of ultrasonic and digital dermatoscopy images for all these detectable skin tumours, there were directly estimated quantitative statistic parameters, e.g. form features and values of various relative indexes [250]. The estimated parameters of ultrasonic and dermatoscopic images are presented in Table 16.

Table 16. Identified surface and form parameters of the ultrasonic B-scan and digital dermatoscopy images [250]

Identified surface and form parameters of the ultrasonic B-scan and digital dermatoscopy images	
Contour parameters of informative regions of ultrasonic B-scan images:	**Contour parameters of informative regions of digital dermatoscopy images:**
Maximum length Area Perimeter Average skewness (from 1000 directions) Maximum skewness The skewness of length projection Average kurtosis (from 1000 directions) Maximum kurtosis Minimum kurtosis The kurtosis of length projection	Maximum diameter Minimum diameter Area Perimeter Average skewness (from 1000 directions) Maximum skewness Average kurtosis (from 1000 directions) Maximum kurtosis Minimum kurtosis
Contour parameter(relative) of informative regions of ultrasonic B-scan images:	**Contour parameters (relative) of informative regions of digital dermatoscopy images:**
The ratio of average skewness (from 1000 directions) and maximum skewness The ratio of average skewness (from 1000 directions) and the skewness of length projection The ratio of maximum skewness and the skewness of length projection The ratio of average kurtosis (from 1000 directions) and maximum kurtosis The ratio of average kurtosis (from 1000 directions) and minimum kurtosis The ratio of average kurtosis (from 1000 directions) and the kurtosis of length projection The ratio of maximum kurtosis and the kurtosis of length projection The ratio of minimum kurtosis and the kurtosis of length projection The ratio of perimeter and area	The ratio of maximum diameter and average diameter The ratio of minimum diameter and average diameter The ratio of maximum diameter and minimum diameter The ratio of average skewness (from 1000 directions) and maximum skewness The ratio of average kurtosis (from 1000 directions) and maximum kurtosis The ratio of average kurtosis (from 1000 directions) and minimum kurtosis The ratio of perimeter and area

The values of mean and standard deviation of the parameters listed above are presented in Table 17 – Table 20. Table 17 and Table 18 represent the values of contour parameters of informative regions of ultrasonic B-scan images. Table 19 and Table 20 describe the values of contour parameters (relative) of informative regions of digital dermatoscopy images.

Table 17. Contour parameters of informative regions of ultrasonic B-scan images

Parameter	Mean of melanoma (n = 19)	Standard Deviation of melanoma (n = 19)	Mean of benign nevus (n = 12)	Standard Deviation of benign nevus (n = 12)
Maximum width	7.621	2.089	6.306	2.268
Area	3.997	1.844	2.845	2.111
Perimeter	18.761	5.773	15.318	7.385
Average skewness (from 1000 directions)	0.237	0.136	0.190	0.093
Maximum skewness	0.506	0.300	0.382	0.169
The skewness of length projection	0.254	0.188	0.182	0.119
Average kurtosis (from 1000 directions)	-0.822	0.212	-0.865	0.119
Maximum kurtosis	-0.256	0.730	-0.487	0.257
Minimum kurtosis	-1.066	0.131	-1.120	0.109
The kurtosis of length projection	-0.838	0.265	-0.848	0.157

Table 18. Contour parameters (relative) of informative regions of ultrasonic B-scan images

Parameter	Mean of melanoma (n = 19)	Standard Deviation of melanoma (n = 19)	Mean of benign nevus (n = 12)	Standard Deviation of benign nevus (n = 12)
The ratio of average skewness (from 1000 directions) and maximum skewness	0.495	0.174	0.506	0.178
The ratio of average skewness (from 1000	1.151	0.561	1.364	0.761

directions) and the skewness of length projection				
The ratio of maximum skewness and the skewness of length projection	3.254	4.080	3.310	2.509
The ratio of average kurtosis (from 1000 directions) and maximum kurtosis	1.711	3.562	6.463	11.962
The ratio of average kurtosis (from 1000 directions) and minimum kurtosis	0.774	0.184	0.776	0.113
The ratio of average kurtosis (from 1000 directions) and the kurtosis of length projection	1.011	0.115	1.030	0.078
The ratio of maximum kurtosis and the kurtosis of length projection	0.289	0.784	0.598	0.340
The ratio of minimum kurtosis and the kurtosis of length projection	1.470	0.821	1.359	0.252
The ratio of perimeter and area	5.290	1.962	7.670	4.048

Table 19. Contour parameters of informative regions of digital dermatoscopy images

Parameter	**Mean of melanoma (n = 19)**	**Standard Deviation of melanoma (n = 19)**	**Mean of benign nevus (n = 12)**	**Standard Deviation of benign nevus (n = 12)**
Maximum diameter	1182.300	283.108	1064.510	328.497
Average diameter	1074.410	273.421	902.885	284.260
Minimum diameter	932.058	260.188	695.872	275.939
Area	759201.740	388217.870	470307.330	412327.460

Perimeter	3017.170	1886.780	2283.890	1916.600
Average skewness (from 1000 directions)	0.092	0.074	0.240	0.492
Maximum skewness	0.176	0.153	0.452	0.941
Average kurtosis	-0.930	0.075	-0.157	2.435
Maximum kurtosis	-0.762	0.291	0.651	4.036
Minimum kurtosis	-1.069	0.081	-0.908	0.562

Table 20. Contour parameters (relative) of informative regions of digital dermatoscopy images

Parameter	**Mean of melanoma (n = 19)**	**Standard Deviation of melanoma (n = 19)**	**Mean of benign nevus (n = 12)**	**Standard Deviation of benign nevus (n = 12)**
The ratio of maximum diameter and average diameter	1.105	0.054	1.178	0.122
The ratio of minimum diameter and average diameter	0.865	0.057	0.771	0.124
The ratio of maximum diameter and minimum diameter	1.286	0.145	1.606	0.537
The ratio of average skewness (from 1000 directions) and maximum skewness	0.543	0.058	0.538	0.073
The ratio of average kurtosis (from 1000 directions) and maximum kurtosis	0.982	0.881	1.053	0.394
The ratio of average kurtosis (from 1000 directions) and minimum kurtosis	0.876	0.102	1.462	2.351
The ratio of perimeter and area	0.005	0.003	0.006	0.005

1st decile	9.158	5.833	18.083	9.258
2nd decile	10.632	7.515	21.333	10.228
3rd decile	12.368	9.215	24.583	10.933
4th decile	14.474	10.637	27.667	11.881
5th decile	17.789	11.583	31.333	13.096
6th decile	22.000	12.987	35.083	14.761
7th decile	27.000	14.079	39.833	16.563
8th decile	33.632	14.720	45.833	17.309
9th decile	42.789	15.109	54.583	16.412
10th decile	109.000	46.489	101.333	34.054

In this research, the *F* test was used in order to select significant parameters for discriminant analysis of malignant and benign skin tumours. The *F* test is closely related to the analysis of variance, named as ANOVA, which is well-known as a parametric statistical method for the evaluation of significances between more than one group [299]. In 1987, Parasurama showed that a univariate *F* test could be used to assess the significant differences between two variances [300]:

$$F = \frac{\text{variance between mean squares}}{\text{variance within mean squares}} \tag{51}$$

The results of the *F* test are based on the degrees of freedom, which correspond to the numerator and the denominator and on the level of significance. If the value of the *F* test is less than the critical value, then there are no relevant differences between variances and the null hypothesis should be returned or otherwise the model should refuse it. The Univariate *F*-ratio test is used in order to estimate the significance of the discriminating power of all of the common variables, taken separately, excluding among and between the various sets of groups [298].

In the case of discriminant analysis, Fisher ‘s test known as *F* test was applied, while for the logistic regression model Chi-squared test used in order to evaluate parameters of the 31 lesions of the human tissue, where 19 of them were melanoma and 12 were benign nevus. All these parameters were clustered to informative and not relevant groups of quantitative parameters.

The logistic regression model is a parametric model, because it has a finite set of parameters that are known as regression coefficients. Coefficients correspond to one for each predictor plus a constant. The Chi-Squared test, also known as Wald Chi-Squared test, is one of tools to check if the parameters in this model are meaningful or not. The Chi-Squared test can be used for a multitude of different models, including those with continuous variables or binary variables [301].

Before checking the null hypothesis, it is obvious that each parameter is equal to the relevant value. In the case of the null hypothesis is refused, it is acceptable that some of the variables can be eliminated, excluding meaningful impact to the model fit [301].

Wald test [301] is evaluated according to equation:

$$W_T = \frac{(\hat{O}-O_0)^2}{1/I_n(O)} = I_n(\hat{O})(\hat{O} - O_0)^2; \quad (52)$$

here $\hat{O}$ is a maximum likelihood estimator and O_0 is …., $I_n(\hat{O})$ is an expected Fisher information, evaluated at the MLE. W_T is distributed by asymptotic Chi-square distribution with the number of l degrees of freedom in order to grant a null hypothesis. Here l represents the rank of the parameter.

In the case of discriminant analysis, under the *F* test there were five informative parameters of ultrasonic images and 17 of digital dermatoscopy images that were selected. The Chi-squared test was used for the logistic regression model and as result two significant parameters of ultrasonic images and two of digital dermatoscopy images were identified [250]. The significant parameters of two different classification models are shown in the Table 21 below.

Table 21. Significant parameters evaluated from detected skin lesion region of ultrasonic and dermatoscopic images [250]

Discriminant Analysis Model (*Fisher 's test*)	
Significant parameters of ultrasonic images: (n=5/19)	**Significant parameters of digital dermatoscopy images: (n=17/27)**
maximum width, area, perimeter, the ratio of average kurtosis (from 1000 directions) and maximum kurtosis, the ratio of perimeter and area.	average diameter, minimum diameter, area, average kurtosis (from 1000 directions), maximum kurtosis, the ratio of maximum diameter and average diameter, the ratio of minimum diameter and average diameter, the ratio of maximum diameter and minimum diameter, 9 of 10 deciles.
Logistic Regression Model (*Chi-squared test*)	
Significant parameters of ultrasonic images: (n=2/19)	**Significant parameters of digital dermatoscopy images: (n=2/27)**
the ratio of average kurtosis (from 1000 directions) and maximum kurtosis, the ratio of perimeter and area.	the ratio of minimum diameter and average diameter, 2nd decile.

Detailed results of all measurements of selected contours and relative parameters for malignant and benign tumours are presented in Tables 22 - 29. The measurements of significant parameters of ultrasonic images and digital dermatoscopy images are marked in bold. Measurements of contour parameters of informative regions of melanoma ultrasonic B-scan images are presented in Table 22.

Measurements of contour parameters of informative regions of benign nevus ultrasonic B-scan presented in Table 23. Measurements of contour parameters (relative) of informative regions of melanoma ultrasonic B-scan images are shown in Table 24. Measurements of contour parameters (relative) of informative regions of benign nevus ultrasonic B-scan images are presented in Table 25. Measurements of contour parameters of informative regions of melanoma digital dermatoscopy images are detailed in Table 26. Measurements of contour parameters of informative regions of benign nevus digital dermatoscopy images are presented in Table 27. Measurements of contour parameters (relative) of informative regions of digital melanoma and benign nevus dermatoscopy images are shown in Table 28 and Table 29.

Table 22. Measurements of contour parameters of informative regions of melanoma ultrasonic B-scan images in millimetres

Maximum width	**Area**	**Perimeter**	Average skewness (from 1000 directions)	Maximum skewness	The skewness of length projection	Average kurtosis (from 1000 directions)	Maximum kurtosis	Minimum kurtosis	The kurtosis of length projection
5.28	**3.94**	**11.68**	0.11	0.18	0.13	-0.90	-0.82	-1.04	-0.82
6.93	**7.59**	**19.63**	0.24	0.46	0.17	-0.81	-0.57	-1.05	-0.89
5.02	**2.64**	**10.61**	0.10	0.25	0.06	-1.07	-0.63	-1.20	-1.19
11.98	**2.84**	**24.95**	0.13	0.46	0.09	-1.04	-0.64	-1.08	-1.06
10.82	**8.31**	**28.10**	0.43	0.76	0.47	-0.55	0.15	-1.21	-0.57
5.81	**2.01**	**11.89**	0.19	0.28	0.20	-0.96	-0.75	-1.01	-0.99
11.02	**4.24**	**23.85**	0.24	1.18	0.25	-1.01	2.05	-1.14	-1.10
9.14	**3.42**	**20.17**	0.43	0.58	0.49	-0.30	0.17	-1.06	-0.23
6.90	**4.74**	**16.70**	0.03	0.19	0.01	-1.01	-0.79	-1.11	-1.07
6.67	**5.08**	**18.45**	0.20	0.30	0.26	-0.76	-0.72	-0.95	-0.72
10.03	**6.68**	**28.87**	0.27	0.40	0.32	-0.64	-0.52	-1.02	-0.54
10.66	**2.98**	**22.61**	0.36	1.04	0.33	-0.81	1.28	-1.34	-0.92
8.84	**3.75**	**25.92**	0.50	1.07	0.66	-0.61	-0.18	-1.10	-0.54
5.68	**1.34**	**11.43**	0.17	0.47	0.12	-0.83	-0.64	-0.96	-0.84
5.61	**3.93**	**12.73**	0.11	0.15	0.13	-1.02	-0.73	-1.13	-1.11
7.29	**5.05**	**18.82**	0.49	0.68	0.68	-0.50	-0.03	-0.71	-0.43
8.18	**3.69**	**16.78**	0.19	0.34	0.20	-0.76	-0.58	-1.04	-0.71
6.60	**1.74**	**13.47**	0.14	0.43	0.11	-1.03	-0.35	-1.10	-1.09
6.14	**2.82**	**16.13**	0.20	0.44	0.16	-0.99	-0.42	-1.16	-1.08

Table 23. Measurements of contour parameters of informative regions of benign nevus ultrasonic B-scan images in millimetres

Maximum width	**Area**	**Perimeter**	Average skewness (from 1000 directions)	Maximum skewness	The skewness of length projection	Average kurtosis (from 1000 directions)	Maximum kurtosis	Minimum kurtosis	The kurtosis of length projection
4.55	**5.57**	**19.25**	0.14	0.21	0.21	-0.82	-0.54	-1.11	-0.67
7.95	**6.83**	**19.13**	0.14	0.32	0.05	-0.90	-0.76	-0.95	-0.91
3.23	**0.55**	**7.19**	0.15	0.26	0.14	-0.95	-0.27	-1.11	-1.00

5.25	**0.73**	**10.55**	0.19	0.30	0.20	-1.07	-0.60	-1.13	-1.09
10.53	**5.12**	**22.72**	0.33	0.39	0.39	-0.67	-0.60	-1.08	-0.62
3.50	**0.90**	**7.68**	0.05	0.17	0.03	-0.98	-0.73	-1.06	-1.00
8.75	**3.57**	**6.54**	0.17	0.61	0.13	-0.75	-0.02	-1.00	-0.72
6.63	**1.49**	**14.75**	0.28	0.61	0.29	-0.93	-0.05	-1.32	-0.95
9.41	**3.54**	**26.39**	0.23	0.62	0.17	-0.86	-0.34	-1.16	-0.89
7.79	**2.88**	**26.94**	0.35	0.56	0.36	-0.93	-0.67	-1.30	-0.89
5.91	**1.96**	**12.18**	0.08	0.23	0.03	-0.81	-0.62	-1.18	-0.78
5.21	**1.00**	**10.50**	0.18	0.31	0.19	-0.70	-0.64	-1.05	-0.65

Table 22 and Table 23 present measurements of contour parameters of informative regions of ultrasonic B-scan images for melanoma and benign nevus. The significant parameters are maximum width, area, perimeter and measurements of them marked in bold.

Table 24. Measurements of contour parameters (relative) of informative regions of melanoma ultrasonic B-scan images in millimetres

The ratio of average skewness (from 1000 directions) and maximum skewness	The ratio of average skewness (from 1000 directions) and the skewness of length projection	The ratio of maximum skewness and the skewness of length projection	**The ratio of average kurtosis (from 1000 directions) and maximum kurtosis**	The ratio of average kurtosis (from 1000 directions) and minimum kurtosis	The ratio of average kurtosis (from 1000 directions) and the kurtosis of length projection	The ratio of maximum kurtosis and the kurtosis of length projection	The ratio of minimum kurtosis and the kurtosis of length projection	**The ratio of perimeter and area**
0.59	0.81	1.38	**1.09**	0.87	1.09	1.00	1.26	**2.97**
0.54	1.42	2.65	**1.41**	0.77	0.91	0.65	1.18	**2.59**
0.41	1.59	3.89	**1.69**	0.89	0.90	0.53	1.01	**4.02**
0.28	1.39	4.95	**1.61**	0.96	0.98	0.61	1.02	**8.79**
0.57	0.92	1.63	**-3.59**	0.46	0.98	-0.27	2.13	**3.38**
0.67	0.92	1.39	**1.28**	0.95	0.97	0.76	1.02	**5.93**
0.20	0.96	4.72	**-0.49**	0.88	0.92	-1.86	1.04	**5.62**
0.75	0.88	1.18	**-1.81**	0.29	1.32	-0.73	4.61	**5.90**
0.17	3.27	19.73	**1.28**	0.91	0.95	0.74	1.04	**3.52**
0.65	0.75	1.15	**1.06**	0.80	1.06	1.00	1.32	**3.63**
0.67	0.85	1.26	**1.23**	0.63	1.19	0.97	1.88	**4.32**
0.34	1.08	3.16	**-0.64**	0.61	0.88	-1.39	1.46	**7.60**
0.47	0.75	1.61	**3.31**	0.55	1.13	0.34	2.05	**6.92**
0.36	1.38	3.80	**1.29**	0.86	0.99	0.77	1.14	**8.51**
0.68	0.79	1.15	**1.40**	0.90	0.92	0.66	1.02	**3.24**
0.72	0.73	1.00	**15.25**	0.70	1.15	0.08	1.63	**3.72**
0.56	0.98	1.75	**1.29**	0.73	1.06	0.82	1.46	**4.55**
0.33	1.28	3.86	**2.93**	0.94	0.95	0.32	1.01	**7.76**
0.46	1.25	2.69	**2.38**	0.85	0.92	0.38	1.07	**5.71**

Table 25. Measurements of contour parameters (relative) of informative regions of benign nevus ultrasonic B-scan images in millimetres

The ratio of average skewness (from 1000 directions) and maximum skewness	The ratio of average skewness (from 1000 directions) and the skewness of length projection	The ratio of maximum skewness and the skewness of length projection	**The ratio of average kurtosis (from 1000 directions) and maximum kurtosis**	The ratio of average kurtosis (from 1000 directions) and minimum kurtosis	The ratio of average kurtosis (from 1000 directions) and the kurtosis of length projection	The ratio of maximum kurtosis and the kurtosis of length projection	The ratio of minimum kurtosis and the kurtosis of length projection	**The ratio of perimeter and area**
0.65	0.66	1.01	**1.51**	0.74	1.23	0.81	1.67	**3.46**
0.44	3.02	6.90	**1.19**	0.95	1.00	0.84	1.05	**2.80**
0.56	1.03	1.82	**3.46**	0.86	0.94	0.27	1.10	**13.06**
0.65	0.95	1.48	**1.77**	0.94	0.98	0.55	1.03	**14.52**
0.86	0.86	1.00	**1.12**	0.63	1.10	0.98	1.75	**4.44**
0.28	1.56	5.68	**1.34**	0.93	0.98	0.73	1.06	**8.57**
0.28	1.28	4.58	**40.23**	0.75	1.03	0.03	1.38	**1.83**
0.46	0.97	2.12	**20.57**	0.71	0.98	0.05	1.38	**9.87**
0.37	1.32	3.54	**2.57**	0.74	0.96	0.38	1.30	**7.46**
0.63	0.97	1.55	**1.39**	0.72	1.05	0.76	1.46	**9.36**
0.33	2.80	8.38	**1.30**	0.69	1.04	0.80	1.50	**6.22**
0.57	0.95	1.65	**1.09**	0.66	1.07	0.99	1.61	**10.45**

Table 24 and Table 25 present measurements of contour parameters (relative) of informative regions of ultrasonic B-scan images for melanoma and benign nevus. The significant parameters are the ratio of average kurtosis (from 1000 directions) and maximum kurtosis, the ratio of perimeter and area and measurements of them marked in bold.

Table 26. Measurements of contour parameters of informative regions of melanoma digital dermatoscopy images in millimetres

Maximum diameter	**Average diameter**	**Minimum diameter**	**Area**	Perimeter	Average skewness (from 1000 directions)	Maximum skewness	**Average kurtosis**	**Maximum kurtosis**	Minimum kurtosis
842.45	**772.08**	**693.19**	**423223.00**	2778.56	0.07	0.13	**-0.97**	**-0.91**	-1.01
964.27	**809.20**	**670.49**	**397556.00**	3846.06	0.12	0.20	**-0.92**	**-0.88**	-0.98
968.82	**870.96**	**760.85**	**385450.00**	23.31	0.13	0.30	**-0.89**	**-0.48**	-1.16
1444.00	**1433.15**	**1357.42**	**1533583.00**	2801.17	0.05	0.09	**-0.99**	**-0.92**	-1.06
1435.64	**1158.86**	**917.61**	**820520.00**	4546.66	0.03	0.06	**-0.94**	**-0.80**	-1.10
979.10	**859.62**	**705.78**	**518490.00**	3247.32	0.06	0.10	**-0.99**	**-0.95**	-1.02

1398.13	**1294.31**	**1126.80**	**1144288.00**	5531.29	0.06	0.11	**-0.96**	**-0.88**	-1.03
585.44	**540.70**	**476.84**	**196687.00**	2139.06	0.06	0.12	**-0.96**	**-0.86**	-1.07
1338.08	**1241.20**	**1040.94**	**672284.00**	6426.97	0.18	0.36	**-0.80**	**-0.62**	-1.10
1443.98	**1350.47**	**1195.25**	**668781.00**	2379.91	0.35	0.71	**-0.75**	**0.29**	-1.35
1443.99	**1353.17**	**1151.50**	**1306833.00**	4367.75	0.08	0.14	**-0.97**	**-0.90**	-1.04
1443.99	**1330.16**	**1220.01**	**1186502.00**	356.48	0.06	0.13	**-0.95**	**-0.81**	-1.08
1327.53	**1260.47**	**1155.82**	**1027794.00**	139.15	0.04	0.07	**-0.99**	**-0.92**	-1.04
936.07	**843.64**	**713.00**	**468496.00**	3190.15	0.11	0.17	**-0.95**	**-0.85**	-1.04
1058.66	**897.87**	**656.84**	**485109.00**	3381.48	0.06	0.12	**-0.96**	**-0.83**	-1.07
1436.54	**1307.85**	**1182.93**	**1256586.00**	4672.21	0.07	0.13	**-0.98**	**-0.88**	-1.09
1349.43	**1248.56**	**1140.20**	**693971.00**	25.24	0.12	0.23	**-0.76**	**-0.48**	-0.98
1345.21	**1174.92**	**917.86**	**921524.00**	4905.63	0.06	0.11	**-0.96**	**-0.88**	-1.04
722.42	**666.67**	**625.76**	**317156.00**	2567.80	0.03	0.05	**-0.98**	**-0.91**	-1.05

Table 27. Measurements of contour parameters of informative regions of benign nevus digital dermatoscopy images in millimetres

Maximum diameter	**Average diameter**	**Minimum diameter**	**Area**	Perimeter	Average skewness (from 1000 directions)	Maximum skewness	**Average kurtosis**	**Maximum kurtosis**	Minimum kurtosis
1222.73	**918.61**	**589.28**	**22984.00**	34.14	1.78	3.41	**7.51**	**13.03**	0.85
646.58	**604.27**	**495.84**	**105715.00**	48.38	0.29	0.46	**0.09**	**2.80**	-0.87
399.71	**370.48**	**332.11**	**87239.00**	1587.37	0.03	0.07	**-0.94**	**-0.75**	-1.06
1108.49	**907.54**	**671.31**	**521003.00**	4593.43	0.02	0.05	**-0.97**	**-0.89**	-1.04
1301.18	**1119.79**	**929.95**	**694467.00**	3488.11	0.14	0.26	**-0.96**	**-0.67**	-1.25
1443.99	**1223.85**	**872.74**	**735826.00**	7.00	0.13	0.34	**-0.91**	**-0.61**	-1.24
1444.00	**1428.32**	**1362.83**	**1551867.00**	5201.68	0.04	0.07	**-0.99**	**-0.95**	-1.04
734.21	**646.99**	**536.73**	**252000.00**	2503.86	0.16	0.27	**-0.88**	**-0.69**	-1.09
1015.89	**893.05**	**708.74**	**519221.00**	3620.51	0.06	0.12	**-0.95**	**-0.81**	-1.07
1296.27	**882.99**	**417.43**	**257434.00**	2507.36	0.12	0.19	**-0.93**	**-0.85**	-1.05
1210.32	**1027.26**	**812.84**	**469566.00**	8.41	0.06	0.10	**-0.97**	**-0.90**	-1.01

950.71	**811.47**	**620.65**	**426366.00**	3806.46	0.04	0.07	**-0.98**	**-0.91**	-1.03

Table 26 and Table 27 present measurements of contour parameters of informative regions of digital dermatoscopy images for melanoma and benign nevus. The significant parameters are average diameter, minimum diameter, area, average kurtosis (from 1000 directions), maximum kurtosis and measurements of them marked in bold.

Table 28. Measurements of contour parameters (relative) of informative regions of melanoma digital dermatoscopy images in millimetres

The ratio of maximum diameter and average diameter	**The ratio of minimum diameter and average diameter**	**The ratio of maximum diameter and minimum diameter**	The ratio of average skewness (from 1000 directions) and maximum skewness	The ratio of average kurtosis (from 1000 directions) and maximum kurtosis	The ratio of average kurtosis (from 1000 directions) and minimum kurtosis	The ratio of perimeter and area
1.09	**0.90**	**1.22**	0.54	1.06	0.96	0.01
1.19	**0.83**	**1.44**	0.61	1.05	0.94	0.01
1.11	**0.87**	**1.27**	0.42	1.85	0.76	0.00
1.01	**0.95**	**1.06**	0.60	1.07	0.93	0.00
1.24	**0.79**	**1.56**	0.60	1.18	0.85	0.01
1.14	**0.82**	**1.39**	0.60	1.03	0.97	0.01
1.08	**0.87**	**1.24**	0.55	1.09	0.93	0.00
1.08	**0.88**	**1.23**	0.49	1.12	0.90	0.01
1.08	**0.84**	**1.29**	0.51	1.30	0.73	0.01
1.07	**0.89**	**1.21**	0.49	-2.56	0.56	0.00
1.07	**0.85**	**1.25**	0.58	1.07	0.93	0.00
1.09	**0.92**	**1.18**	0.43	1.17	0.88	0.00
1.05	**0.92**	**1.15**	0.60	1.07	0.95	0.00
1.11	**0.85**	**1.31**	0.62	1.11	0.91	0.01
1.18	**0.73**	**1.61**	0.51	1.17	0.91	0.01
1.10	**0.90**	**1.21**	0.51	1.12	0.90	0.00
1.08	**0.91**	**1.18**	0.55	1.58	0.78	0.00
1.14	**0.78**	**1.47**	0.57	1.09	0.93	0.01
1.08	**0.94**	**1.15**	0.55	1.07	0.93	0.01

Table 29. Measurements of contour parameters (relative) of informative regions of benign nevus digital dermatoscopy images in millimetres

The ratio of maximum diameter and average diameter	**The ratio of minimum diameter and average diameter**	**The ratio of maximum diameter and minimum diameter**	The ratio of average skewness (from 1000 directions) and maximum skewness	The ratio of average kurtosis (from 1000 directions) and maximum kurtosis	The ratio of average kurtosis (from 1000 directions) and minimum kurtosis	The ratio of perimeter and area
1.33	**0.64**	**2.07**	0.52	0.58	8.87	0.00
1.07	**0.82**	**1.30**	0.62	0.03	-0.11	0.00
1.08	**0.90**	**1.20**	0.45	1.25	0.89	0.02
1.22	**0.74**	**1.65**	0.45	1.09	0.94	0.01
1.16	**0.83**	**1.40**	0.54	1.44	0.77	0.01
1.18	**0.71**	**1.65**	0.39	1.48	0.74	0.00
1.01	**0.95**	**1.06**	0.58	1.05	0.96	0.00
1.13	**0.83**	**1.37**	0.58	1.28	0.81	0.01
1.14	**0.79**	**1.43**	0.52	1.17	0.89	0.01
1.47	**0.47**	**3.11**	0.60	1.09	0.88	0.01
1.18	**0.79**	**1.49**	0.59	1.08	0.96	0.00
1.17	**0.76**	**1.53**	0.60	1.08	0.95	0.01

Table 28 and Table 29 present measurements of contour parameters (relative) of informative regions of digital dermatoscopy images for melanoma and benign nevus. The significant parameters are the ratio of maximum diameter and average diameter, the ratio of minimum diameter and average diameter, the ratio of maximum diameter and minimum diameter and measurements of them marked in bold.

For the significant parameters and their measurements detailed above, the plots of distributions of significant parameters of ultrasonic and digital dermatoscopy images are presented in Appendix 2. Plots of significant parameters distributions are shown for benign and malignant tumours separately, based on the classification model and the data source of the captured images. The analysis of distributions are based on mean and standard deviation for each significant parameter of benign and malignant tumours depending on the imaging technique and classification model that was used. The description and values of mean and standard deviations for the significant parameters are listed under each of the plots provided in Appendix 2. The first five images represent the distributions of the significant parameters that are evaluated from the ultrasonic images by using the discriminant analysis model. Images starting from 6 to 22 represent the distributions of the significant parameters that are evaluated from the digital dermatoscopy images by using the discriminant analysis model. The 23rd and 24th images represent the distributions of the significant parameters that are evaluated from the ultrasonic images by using the logistic regression model. The last two images represent the distributions of the significant parameters that are evaluated from the digital dermatoscopy images by using the logistic regression model.

4.8. An overview of results of histopathology, digital dermatoscopy, ultrasound B-scan and a newly developed automatic statistical post-processing method, which is based on the assessment of synergy of digital dermatoscopy and ultrasound B-scan imaging

Nowadays, there are a lot of different techniques used in dermatology, such as histopathology; where the skin tumours are measured manually after a surgical intervention has been made. All these measurements are known as a "golden standard" in the field of dermatology and are used for decision making in order to identify malignant skin tumours. Another decision support technique is digital dermatoscopy, including spectrophotometric intracutaneous analysis technique, which is also a widely used tool in the field of dermatology. For example, in 2000, Menzies et al. presented a simple dermoscopy technique in order to diagnose pigmented basal cell carcinoma disease [85]. This method has shown reliable results, with sensitivity for diagnosing of basal cell carcinomas equal to 93%, specificity in comparison with melanoma equal to 89% and compared with the benign lesion was equal to 92%. Spectrophotometric intracutaneous analysis, known as SIA, is also used as a valuable tool in the case of identifying a skin cancer. In 2002, SIA was used by Moncrief et al. and showed very significant results, i.e. specificity was equal to 80,1% and sensitivity equal to 82,7% for melanomas [92]. SIA is also a relevant method to use for identifying a non-melanoma skin cancer. To construct a predictive model for non-melanoma skin cancer diagnosis a logistic regression model was used. In 2006, Tehrani et al. presented a paper and showed incredible results in the classification of basal cell carcinomas, melanocytic nevus and other non-melanoma tumours. For the estimation of overall accuracy, receiver operator characteristic curves were used. Authors found that the sensitivity of the mode is equal to 98,0% and a specificity equal to of 95,7%, while overall accuracy of the model was equal to 98,2% in the case of non-melanoma skin cancer classification [93]. The third well-known method is ultrasound B-scan images processing technique as an alternative method in diagnosing skin cancer. For example, Harland et al. used 20-MHz ultrasound B-scan imaging including acoustic shadowing and entry echo line enhancement in order to classify melanomas and basal cell papilloma. Researchers found that the sensitivity in order to classify melanomas and basal cell papilloma was equal to 100%, while specificity was equal to 79% [48]. ROC analysis has also shown reliable results in the classification of melanomas and basal cell papilloma, i.e. coefficient in the case of quantitative estimation of shadowing areas was equal to 0,93 and for semi-quantitative estimation was equal to 0,97 [48]. In 2010, Wortsman and Wortsman presented a study of an application of ultrasound imaging in order to identify different skin damage, such a melanoma, basal cell carcinoma, skin cyst and nail damage [54]. One of the disadvantage of the used technique was the lack of sensitivity to detect epidermis lesions that are around 0,1 mm of thickness. Although all the diagnoses

were confirmed independently by a single observer, it was stated that the ultrasound can affect accuracy during the diagnosing stages up to 17% [54]. As a result, the percent of correct classification of the lesions was equal to 73%, while sensitivity was equal to 99% and specificity - 100% [54]. Rallan et al. presented a paper on classification of benign nevus, melanoma and SKs by using a three-dimensional high-resolution ultrasound in order to capture images using a reflex transfer [55]. An ambient skin was used as the test, where digital ultrasonography parameters have been captured for all the significant measurements of lesions of total ultrasound attenuation, intra-lesion sound reflection, surface sound reflectance and the relative uniformity of each parameter across the tumour [55]. As a result, reliable differences were identified between benign and malignant parameters of tumours in order to reduce the accuracy of classification of benign tumours by 65% without missing melanomas [55]. A newly developed method proposes to use information captured from two different image processing techniques, such as ultrasonic B-scan and digital dermatoscopy tools. This novel technique is used for classification of melanomas and melanocytic nevus. Looking at the results of a newly developed automatic statistical post-processing method, which is based on assessment of synergy of digital dermatoscopy and ultrasound B-scan techniques, the probability of correct prediction during the classification of ultrasonic images by using a discriminant analysis classification model and significant parameters is equal to 62%. However, the probability of correct prediction during the classification based on assessment of synergy of digital dermatoscopy and ultrasonic medical images by using significant parameters is similar and equal to 62%, while sensitivity was equal to 74% and specificity equal to 50%. The estimated area under the ROC curve is 0.671, which means that the classification was not improved when comparing the results of the discriminant analysis classification models. Analysing the outcomes of application of the stepwise logistic regression, it is obvious that the automatic classification was improved by 9% and has reached 82% of correct prediction compared with the classification of ultrasonic B-scan analysis only. In this case, sensitivity was equal to 85,5% and specificity equal to 75%. The proposed automatic classification method is usable for automatic identification of melanoma and melanocytic nevus. An automatic algorithm based on data captured from two different technologies has shown high diagnostic accuracy compared with the methods that are not fully automated. As a conclusion, a newly developed automatic statistical post – processing method could be used as a decision support tool in the field of dermatology in order to identify the malignant tumour and benign nevus.

4.9. Conclusions of 4th chapter

1. The segmentation of ultrasonic and digital dermatoscopy medical images were made by using Gaussian smoothing and a thresholding procedure based on an expectation – maximization (EM) algorithm, which depends on calculations of

random values and a skin tumour where the contour of the largest area is then selected. 31 ultrasonic and 31 digital dermatoscopy images were selected, 19 melanomas and 12 benign nevi were analysed.

2. After the selection of contours, 46 parameters of tumour structure were evaluated, i.e. 19 parameters of ultrasonic images and 27 parameters of digital dermatoscopy images.

3. Fisher's and Chi-squared tests were used to separate significant and not relevant parameters. The classification of measurements was made by using discriminant analysis and logistic regression methods. The probability of correct prediction for the discriminant analysis model when analysing ultrasonic images was equal to 62%, which is the same as the probability of correct prediction during the classification based on the assessment of synergy of digital dermatoscopy and ultrasonic B-scan images. It means, that the classification was not improved. The probability of correct prediction for the logistic regression model when analysing ultrasonic images was equal to 73%, with the sensitivity of 79% and specificity of 67%. The probability of correct prediction during the classification based on the assessment of synergy of digital dermatoscopy and ultrasonic medical images was equal to 82%, with the sensitivity of 89,5% and specificity of 75%. The classification results were improved by 9%.

4. To prove the reliability of the proposed automatic statistical post-processing method, the area under ROC curve has been calculated. The results are closer to 1, therefore the method is reliable.

5. For this research, the area under the ROC was equal to 0.908, which means that the proposed method can be employed as an alternative to the well-known methods used in dermatology in order to improve the classification results.

5. METROLOGY EVALUATION OF THE SKIN TUMOURS THICKNESSES MEASUREMENTS

Estimation of measurement uncertainty includes a usage of the measurements of the proposed model in order to establish the uncertainty that is closest to the best assessment of the value of the quantity to be gauged and provide the best assessments of the values of all quantities that crucially impacts the relations between those evaluations and quantity as well as defined uncertainties [302]. There are a number of methods that could be used in the evaluation procedure of measurements uncertainty. The application of these methods strongly depends on the properties of the measurands. The Guide to the Expression of Uncertainty in Measurement (GUM) is one of widely used techniques, which recommends a standard approach in order to express the uncertainty of measurements and ensures that the method used in some kind of analysis is reliable [303]. The GUM uncertainty framework has been implemented in standards define procedures and in computer software programs. There are also some other tools, for example; the Monte Carlo method (MCM) or the Bayesian method. Picking up a reasonable methodology for the estimation of measurements uncertainties should be based on the confidence of estimation of physical reality it designates to reveal [302]. The GUM approach is one of the most suitable approaches to apply this methodology to different models with the linear distribution or mild non-linear. In addition, it is adequate in using Central Limit Theorem and the PDF, which have symmetric inputs [304].

This chapter presents a metrology evaluation of the skin tumours thicknesses measurements. Section 5.1. presents an uncertainty due to the measurements of thickness of skin tumours. Uncertainty due to the ultrasound velocity in skin tissue, time and the position of transducer is shown in section 5.2. Combined and expanded uncertainties are presented in section 5.3. Section 5.4. introduces summarized outcomes of chapter 5.

5.1. Uncertainty due to the measurements of thickness of skin tumours

This section represents the comparison of uncertainties due to the automatically and manually estimated ultrasonic B – scan measurements of thickness of skin tumours with the histological examination. In the field of dermatology, an invasive histological tool is known as a golden standard. It is acceptable that the measurement under the histological procedure is an etalon. On the other hand, the accuracy of histological examination strongly depends on the human factor, experience, lack of knowledge, in addition to the equipment which is using during the histological examination along other key factors. Due to this, it is assumed that the average of two pathologists' estimations will be more adequate in this case. All the measurements

were grouped into four ranges of thicknesses as shown in Table 30. Mean and standard deviation of differences between thicknesses measured by two methods. These ranges were selected assuming that the approximate number of values contained in each of these four groups is more adequate and impacts a more accurate result. Looking at the mean and standard deviation of measurement differences for both methods, proves that the selection of ranges of thicknesses is reliable and the observations in each group are not extremely spread compared with the mean of measurement differences. Additionally, the results have showed that the proposed automatic statistical post – processing method versus invasive histological analysis is more or less similar to manual non-invasive ultrasound examination (made by dermatologist) versus invasive histological analysis. This proves that the proposed fully automatic method is constructed under the requirements in order to estimate the thickness as accurate as it is possible.

Table 30. Mean and standard deviation of differences between thicknesses measured by two methods

Method	Ranges of thicknesses, mm	Mean of differences between thicknesses measured by two methods	Standard Deviation of differences between thicknesses measured by two methods
Proposed automatic statistical post – processing method vs Invasive histological analysis	0 < histological <= 0.3 0.3 < histological < 0.5 0.5 <= histological < 0.7 0.7 <= histological <=1	0.090 -0.067 -0.033 -0.375	0.146 0.184 0.192 0.158
Manual non-invasive ultrasound examination (made by dermatologist) vs Invasive histological analysis	0 < histological <= 0.3 0.3 < histological < 0.5 0.5 <= histological < 0.7 0.7 <= histological <=1	0.141 0.081 0.029 -0.265	0.081 0.204 0.187 0.239

As the thickness of skin measurements was directly estimated, it was included in evaluation of type A standard uncertainty. Type A standard uncertainty (regarding the differences of mean thicknesses) was measured in order to compare the proposed automatic statistical post – processing method versus invasive histological analysis method and manual non-invasive ultrasound examination (made by dermatologist) versus invasive histological analysis methods.

Type A standard uncertainty of the systematic error can be expressed as [305]:

$$u(\Delta d) = \sqrt{\frac{1}{n(n-1)}\sum_{p=1}^{n}(\Delta d_p - \overline{\Delta d})^2}\,; \tag{53}$$

here Δd_p means the difference between results of measurements of the two methods described above. n shows the size of the sample and is equal to 31 cases. $\overline{\Delta d}$ is the mean of the differences of the two methods and can be presented by the form:

$$\overline{\Delta d} = \frac{1}{n}\sum_{p=1}^{n} d_{1/2,p} - d_{3,p}; \quad (54)$$

here $d_{1,p}$ is the thickness of an application of the proposed automatic statistical post – processing method, $d_{2,p}$ is the thickness of non – invasive ultrasound examination (made by dermatologist) and $d_{3,p}$ is the thickness of invasive histological analysis examination.

As a result, the uncertainty for all the measurements of both methods differ by just 0.003 mm (Table 31. Type A standard uncertainty of ultrasonic measurements comparing two methods) and also proves that the proposed automatic method could be used in the estimation of skin tumours thicknesses from the ultrasonic images.

Table 31. Type A standard uncertainty of ultrasonic measurements comparing two methods

Method	Systematic error (bias), mm	Type A standard uncertainty (differences of mean thicknesses), mm
Proposed automatic statistical post – processing method vs invasive histological analysis	$\overline{\Delta d} = -0.070$	$u(\Delta d) = 0.225$
Non-invasive ultrasound examination (made by dermatologist) vs invasive histological analysis	$\overline{\Delta d} = 0.022$	$u(\Delta d) = 0.222$

Uncertainty of the thickness of the skin tumours measured by automatic and manual non-invasive ultrasonic images examination methods. Assume that all the measurements of automatic and manual methods are divided into four groups by the ranges of thicknesses presented in Table 31. Mean and standard deviation of ultrasonic measurements differences. Type A standard uncertainties of the proposed automatic statistical post – processing method and non-invasive ultrasound examination could be defined as:

$$u(d_i) = \sqrt{\frac{1}{n(n-1)}\sum_{p=1}^{n}(d_{i,p} - \overline{d_\iota})^2}. \quad (55)$$

Here *i* denotes the index of thickness group (in this case *i* = 1,2,3,4), *n* is the number of observations, which belong to one of 4 indexed groups, $\overline{d_\iota}$ is the average thickness of one of the 4 indexed groups and $d_{i,p}$ is the thickness of the invasive histological examination.

The results of this application are presented in Table 32. Comparison of type A standard uncertainty of two measurement methods.

Table 32. Comparison of type A standard uncertainty of two measurement methods

Method	Ranges of thicknesses, mm	Type A standard uncertainty, mm
Proposed automatic statistical post – processing method	0 < histological <= 0.3 0.3 < histological < 0.5 0.5 <= histological < 0.7 0.7 <= histological <=1	$u(d1) = 0.096$ $u(d2) = 0.184$ $u(d3) = 0.200$ $u(d4) = 0.151$
Non-invasive ultrasound examination (made by dermatologist)	0 < histological <= 0.3 0.3 < histological < 0.5 0.5 <= histological < 0.7 0.7 <= histological <=1	$u(d1) = 0.066$ $u(d2) = 0.200$ $u(d3) = 0.183$ $u(d4) = 0.248$

Fig. 26. and Fig. 27. represent the Least-Square (or L – S) means plots of the proposed automatic statistical post – processing method and non-invasive ultrasound examination in each of the four selected ranges of thicknesses detailed above with the level of confidence of 95%. Plumb lines propagating from the four-defined means are representing confidence interval of a level of 95%. Mean and standard deviation for each of the ranges are calculated by using pooled estimations of the variance. The length of the corresponding 95% confidence interval for their difference is based on the size of observations sample and magnitude of the variance of pooled grip [306]. Figures also shows that 95% confidence intervals of the L-S Means can overlap, (which may also be inferred from the considerable overlap of the data distributions) with more information about it found in the references [307].

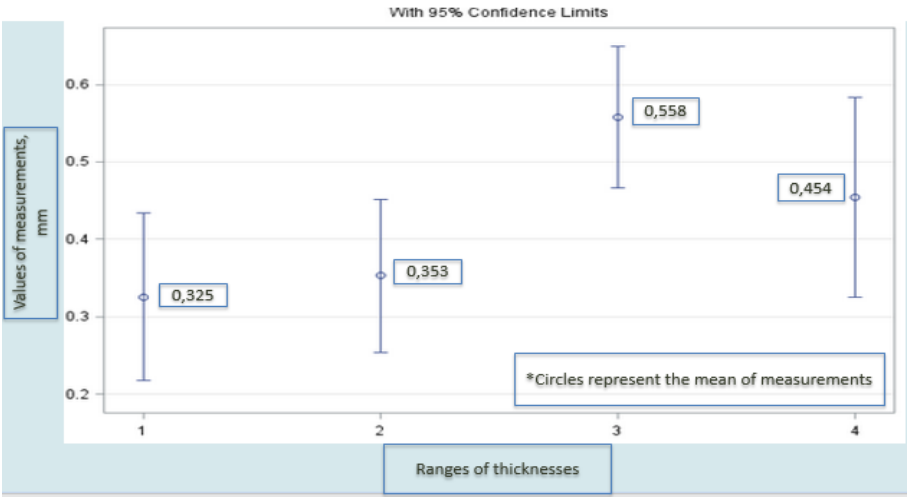

Fig. 26. L-S means graph of the proposed automatic statistical post – processing method regarding the ranges of thicknesses

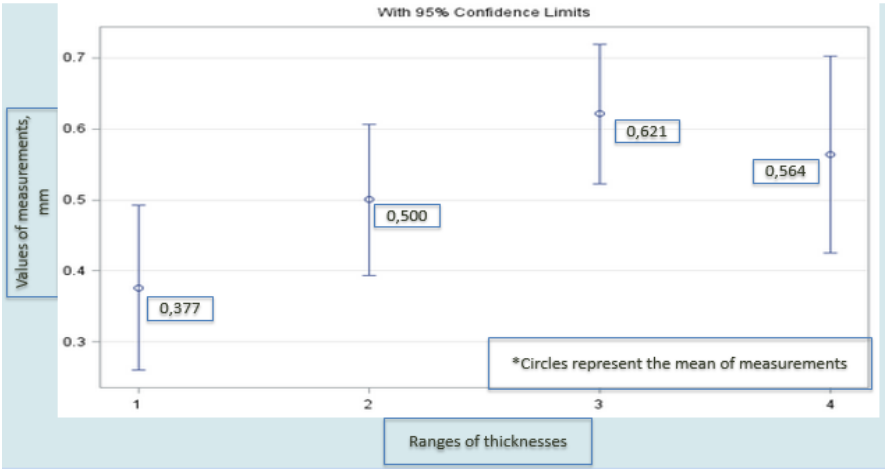

Fig. 27. L-S means graph of the non-invasive ultrasound examination (made by dermatologist) method regarding the ranges of thicknesses

The results of the measurements evaluated by the proposed automatic statistical post – processing method are shown in Fig. 28. The Bland-Altman plot of the proposed automatic statistical post – processing method. The plot is representing the systematic error, which is equal to -0,070 and the range of agreements (±1.96 SD), within which 95% of the differences between the proposed automatic method and thicknesses measured by invasive histological analysis are found.

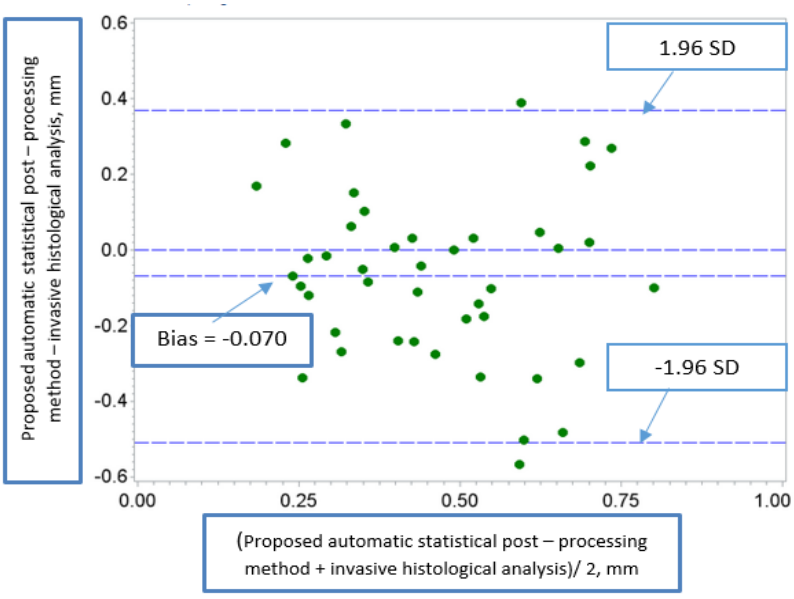

Fig. 28. The Bland-Altman plot of the proposed automatic statistical post – processing method and invasive histological analysis

In order to compare the proposed method with the non-invasive ultrasound examination, a Bland-Altman plot is presented in Fig. 29.

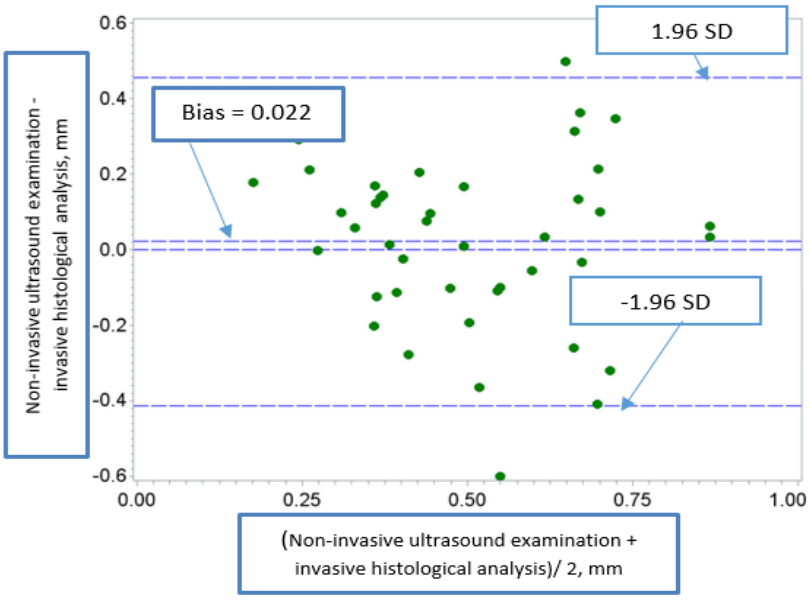

Fig. 29. The Bland-Altman plot of non-invasive ultrasound examination and invasive histological analysis

Comparing the results of the Bland-Altman plot of non-invasive ultrasound examination and invasive histological results against the Bland-Altman plot of the proposed automatic statistical post – processing method and invasive histological analysis; it is clear that the systematic errors differ. The larger the bias is, the larger the differences between the two methods measurements are. Following this note, it is obvious that measurements of non-invasive ultrasound examination are more closely associated to the measurements of invasive histological analysis (bias is equal to 0.022) than the measurements of the proposed automatic statistical method, because the bias is higher. This could be explained by the fact that the measurements of non-invasive ultrasound examination were made by experienced dermatologist.

Spearman Correlation is used for identifying the relationship between paired groups of measurements of lesions of the human skin tissue. In this case, the highest correlation is between the proposed automatic statistical post – processing method and the non-invasive ultrasound examination and is equal to 0.713 (see Table 33 below). Looking at the correlation of the invasive histological method and the other two non-invasive methods, it is clear that there is not enough relative, but the proposed automatic statistical post – processing method is more associated than the non-invasive ultrasound examination.

Table 33. Spearman's Correlation Coefficient (n = 43)

Methods	Proposed automatic statistical post – processing method	Invasive histological analysis	Non-invasive ultrasound examination
Proposed automatic statistical post – processing method	1.0	0.435	0.713
Invasive histological analysis	0.435	1.0	0.423
Non-invasive ultrasound examination	0.713	0.423	1.0

5.2. Uncertainty due to the ultrasound velocity in skin tissue, time and the position of transducer

Many authors of studies assumed that the general velocity of ultra-sonographic measurements in skin melanoma's is equal to 1580 m/s. This was based on data for the whole human skin, even the velocity differs in every tissue [308] and depends on the structure of human skin [309].

Weichenthal et al., presented an ultrasound velocity that was calculated from runtime differences of a 20 MHz ultrasound signal along a known distance, either through fluid alone or through thick specimens of primary melanoma. Although the most preferable for practical reasons is to set a velocity equal to 1580 m/s, in fact could be lower than normally assumed, thereby explaining a part of the overestimation usually found in sonographic measurement of melanoma invasion depth. As a result, authors have shown that the ultrasound velocities vary between 1553 m/s and 1588 m/s with a mean of 1564 m/s [310].

In this way, the type B standard uncertainty due to the difference of ultrasound velocity is assumed to be evaluated by a rectangular distribution and could be expressed as [311]:

$$u_{\Delta c} = \frac{\Delta c}{2\sqrt{3}}; \tag{56}$$

here Δc is the difference between the maximum and minimum ultrasound velocities, measured by Weichenthal et al. [311]. The differences of the ultrasound velocity in melanoma tissue for the B type standard uncertainty is equal to 10 m/s. Limits of the predicted errors in ultrasound velocity is equal to 6.4 μm for melanoma of 1 mm thickness. The uncertainty of constant ultrasound velocity is distributed by the function $u_{\Delta c}(d) = 0.02d$. Features, such as stiffness and density of human skin tissue strongly affect the speed and sound.

Time of flight, known as TOF, can be measured by different methods such as cross – correlation, threshold and by using other digital methods. Taking into account that the velocity is a constant, the measurement of TOF uncertainty depends on the sampling frequency. As the system with 100 MHz sampling frequency was used, a discretisation time interval was equal to Δt=0.01 μs, so then the uncertainty of time discretisation is equal $u_{\Delta t}(d) = 5\,ns$. Seeking to increase a resolution for TOF measurements, an interpolation can be used. In this case, the discretised time interval was interpolated twice up to 5 ns, therefore the uncertainty due to the time discretization is equal to 2μm [312].

Another important aspect is the uncertainty of the transducer position that is used by a dermatologist, moving it through the lesion in order to find the thickest cross-section of the tumour. The results of the examination strongly depend on the human factor, but the uncertainty of the transducer position is unavoidable and irregular, while the tumours have no regular shape.

5.3. Combined and expanded uncertainties

The proposed automatic statistical post – processing method has shown systematic error (bias) which is equal to -0.070 and a type A standard uncertainty equal to 0.225. Meanwhile, a non-invasive ultrasound examination (made by dermatologist) method has a systematic error equal to 0.022 and an uncertainty equal to 0.222. Results of the proposed automatic statistical post – processing method was therefore used in the calculation of combined and expanded uncertainties. All the above described components are not correlated, so combined and expanded uncertainties could be defined by using individual type A and type B standards uncertainties.

Expanded uncertainty can be expressed as follows:

$$u_{comb} = \sqrt{W_{\Delta d}^2 u_{\Delta d}^2 + W_{\Delta td}^2 u_{\Delta td}^2 + W_{\Delta c}^2 u_{\Delta c}^2}; \quad (57)$$

here $u_{\Delta td}$ is an uncertainty of ultrasonic signal sampling frequency.

Where W represents a sensitivity coefficient of the uncertainty part and is calculated by using partial derivatives. Here, in order of simplicity uncertainty the coefficient is set to be equal to 1. Combined uncertainty depends on the linearity of evaluated thickness and depends on the function $u_{comb}(d) = 0.222 + 0.02d$, where d means the value of measured thickness. An expanded uncertainty is calculated by multiplying a combined uncertainty by a coverage factor. Generally, this is set to be equal to 2 and up to 3 [313], as European Accreditation has recommended to use a coverage factor equal to 2 if the combined uncertainty has a normal distribution [314]. A definition of normal distribution means that at least three components of uncertainty should be distributed by normal or rectangular distributions. In this case, a coverage factor m is set to be equal to 2. Therefore, an expanded uncertainty is equal to a

function of $u_{expand}(d) = 0.44 + 0.04d$. Summary of the components and the above described uncertainties are presented in Table 34.

Table 34. Combined and expanded uncertainties relationship

Components	Distribution	Uncertainty (d – means the thickness of measurements, mm)
Systematic error (bias) due to the differences of measurement thickness	Normal	$0.225(A)$
Ultrasound velocity, $u_{\Delta c}(d)$ (constant)	Rectangular	$u_{\Delta c}(d) = 0.02d(B)$
Ultrasound sampling frequency, $u_{\Delta t}(d)$	Rectangular	$0.002(B)$
Combined uncertainty	Normal	$u_{comb}(d) = 0.22 + 0.02d$
Expanded uncertainty (coverage factor *m = 2)*	$u_{expand}(d) = 0.44 + 0.04d$	

5.4. Conclusions of 5th chapter

1. Uncertainty is a measure of the reliability of method accuracy. As the measurements results depend on various factors, different uncertainties were calculated.
2. Uncertainty due to the measurements of thickness of skin tumours when comparing results of the proposed automatic statistical post – processing method versus the invasive histological analysis with results of non-invasive ultrasound examination (made by dermatologist) versus invasive histological analysis has shown that the results are similar.
3. The uncertainty of non-invasive ultrasound examination measurements is less than per 0.003 mm of the proposed method and explained by the fact that the measurements were made by well trained and experienced dermatologist. Following the above, it can be stated that the proposed fully automatic method is constructed under the requirements and can be used as an accurate alternative method helping to identify skin cancer.
4. The Spearman Correlation test has shown that the results measured by dermatologist and by the automatic proposed statistical post-processing method are strongly related. The correlation is equal to 0.713.
5. The results of Spearman Correlation showed that not all the uncertainties factors are correlated. Combined and expanded uncertainties were calculated. Expanded uncertainty consists of type A standard systematic error uncertainty and type B uncertainties due to the ultrasound velocity and time is equal to $u_{expand}(d) = 0.44 + 0.04d$, where the coverage coefficient is *m = 2*.

6. GENERAL CONCLUSIONS

1. The results of the assessment of synergy between two different imaging technologies (ultrasound and digital dermatoscopy) identified the classification was improved by 9%. The reliability of classification is proven by the estimated area under the ROC curve of 0,908. This means that the newly developed and proposed automatic statistical post–processing method can be used as a decision support tool in the field of dermatology in order to identify malignant tumours and benign nevus.

2. To prove that the reliability of the ultrasonic thickness of skin tumours measured by the proposed automatic algorithm is completely covered by a high similarity to the histological thickness measurement, 43 measurements of tumours under a non-invasive ultrasound examination and invasive histological analysis were analysed. It showed that the density of the ultrasonic thicknesses distribution is similar to the Normal distribution density by more than 90 percent and a high similarity to the histological results was obtained.

3. Overall, 46 parameters of skin tumours were estimated by using the same proposed automatic algorithm, which has shown reliable results when comparing the thicknesses of skin tumours. Significant parameters were selected by using the Fisher's test and Chi-Square test. Additionally, 19 parameters of ultrasonic B-scan images and 27 parameters of digital dermatoscopy images were included in the classification models. In the case of the logistic regression model, the probability of correct prediction during the classification was equal to 82%, with a sensitivity of 89,5% and specificity of 75%.

4. To estimate the precision and reliability of the proposed automatic analysis and measurement technique; type A standard, combined and expanded uncertainties were calculated. The uncertainty due to the systematic error of the proposed automatic statistical post-processing method was equal to 0.225 mm and is just 0.003 mm higher than the uncertainty of measurements made by a dermatologist. The expanded uncertainty consisting of type A standard systematic error uncertainty and type B uncertainties due to the ultrasound velocity and time of flight measurement equal to $u_{expand}(d)$=0.44+0.04d, where k = 2.

REFERENCES

1. American Cancer Society. “Cancer Facts and Figure”. 2018.
2. Lens M. B., Dawes M. “Global perspectives of contemporary epidemiological trends of cutaneous malignant melanoma”, British Journal of Dermatology 2004, 150, pp. 179 – 185.
3. Markovic S. N. et al. “Malignant Melanoma in the 21st Century, Part 1: Epidemiology, Risk Factors, Screening, Prevention, and Diagnosis”, Mayo Clin Proc 2007, 82(3), pp. 364 - 380.
4. Parkin D. M., Mesher D., Sasieni P. “Cancers attributable to solar (ultraviolet) radiation exposure in the UK in 2010”. Br J Cancer, 2011, 105, pp. S66 - S69.
5. Spitz S. “Melanomas of childhood”. Am J Pathol, 1948, 24, pp. 591 - 609.
6. Ruzgas T., Drulytė I. Kernel density estimators for Gaussian mixture models. Lithuanian journal of statistics = Lietuvos statistikos darbai. Lithuanian Statistical Association, Vilnius, 2013, Vol. 52, No. 1, p. 14-21.
7. Report by the US Congress Office of Technology Assessment. Policy Implications of Medical Information Systems. http://digital.library.unt.edu/ark:/67531/metadc39374/, 1977.
8. Ministry of Health of the Republic of Lithuania, http://sam.lrv.lt/en/.
9. Esfandiari N., Babavalian M.R., Moghadam A.M., Tabar V.K. Knowledge discovery in medicine: Current issue and future trend. Expert Systems with Applications, Elsevier, 2014, Vol. 41, Iss. 9, p. 4434-4463.
10. Bellazzi R., Zupan B. Predictive data mining in clinical medicine: Current issues and guidelines. International journal of medical informatics, Elsevier, 2008, Vol.77, Iss. 2, p. 81-97.
11. Houston A.L., Chen H., Hubbard S.M., Schatz B.R., Ng T.D., Sewell R.R., Tolle K.M. Medical Data Mining on the Internet: Research on a Cancer Information System. Artificial Intelligence Review, Springer, 1999, Vol.13, Iss. 5 p. 437-466.
12. Silver M., Sakata T., Su H.C., Herman C., Dolins S.B., O’Shea M.J. Case Study: How to Apply Data Mining Techniques in a Healthcare Data Warehouse. Journal of healthcare information management, Wiley, 2001, Vol. 15, No. 2, p. 155-164.
13. Lalayants M., Epstein I., Auslander G.K., Chan W.C.H, Fouché C., Giles R., Joubert L., Rosenne H., Vertigan A. International Social Work, Sage Journals, 2013, Vol. 56, No. 6, p. 775-797.
14. Wasan S., Bhatnagar V., Kaur H. The impact of data mining techniques on medical diagnostics. Data Science Journal, Ubiquity Press, 2006, Vol. 5, p.119-126.
15. Cios K.J., Moore G.W. Uniqueness of medical data mining. Artificial Intelligence in Medicine, Elsevier, 2002, Vol. 26, Iss. 1-2, p.1-24.
16. Jones M.C., Marron J.S. and Sheather S.J. A Brief Survey of Bandwidth Selection for Density Estimation, Journal of the American Statistical Association, 1996, Vol. 91, p. 401–407.
17. Marron J.S., Wand M.P. Exact mean integrated squared error. Annals of Statistics, 1992, Vol. 20, p. 712–736.
18. Silverman B.W. Density Estimation for Statistics and Data Analysis. London, Chapman and Hall, 1986.
19. Bashtannyk D.M., Hyndman R.J. Bandwidth selection for kernel conditional density estimation. Technical report, Department of Econometrics and Business Statistics, Monash University, 1998.
20. Jones M.C. Potential for automatic bandwidth choice in variations of kernel density estimation. Statistics and Probability Letters, 1992, No. 13, p. 351–356.

21. Zhang X., King M.L. and Hyndman R.J. Bandwidth Selection for Multivariate Kernel Density Estimation Using MCMC. Computational Statistics and Data Analysis, 2004, Vol. 50, p. 3009–3031.
22. Smailyte G., Jasilionis D., Kaceniene A., Krilaviciute A., Ambrozaitiene D., Stankuniene V. Suicides among cancer patients in Lithuania: a population-based census-linked study, Cancer Epidemiology, Elsevier, 2013, Vol. 37, Iss. 5, p. 714–718.
23. Sant M., Allemani C., Santaquilani M., Knijn A., Marchesi F., Capocaccia R. EUROCARE–4. Survival of cancer patients diagnosed in 1995–1999. Results and commentary. European Journal of Cancer, Elsevier, 2009, Vol.45, p. 931–91.
24. Braun R.P., Saurat J.H., French L.E. Dermoscopy of pigmented lesions: a valuable tool in the diagnosis of melanoma. Swiss Medical Weekly, 2004, Vol. 134(7–8), p. 83–90.
25. Gershenwald J.E., Soong S.J., Balch C.M. 2010 TNM staging system for cutaneous melanoma and beyond. Annals of Surgical Oncology, Springer, 2010, Vol. 17, Iss. 6, p. 1475–1477.
26. Jasaitienė D., Valiukevičienė S., Linkevičiūtė G., Raišutis R., Jasiūnienė E., Kažys R.J. "Principles of high-frequency ultrasonography for investigation of skin pathology". Journal of the European Academy of Dermatology and Venereology. Malden: Wiley-Blackwell. ISSN 0926-9959. 2011, Vol. 25, iss. 4, pp. 375-382.
27. Kučinskienė V., Samulėnienė, D. G., Gineikienė A., Raišutis R., Kažys R. J., Valiukevičienė, S. "Preoperative assessment of skin tumour thickness and structure using 14-MHz ultrasound". Medicina. Amsterdam: Elsevier. ISSN 1010-660X. 2014, vol. 50, iss. 3, pp. 150-155.
28. Kim J. S. "Characteristics of Piezoelectric Ceramic Transducers Tapered with an Exponential Function". Journal of the Korean Physical Society, Vol. 55, No. 4, 2009, pp. 1440 - 1445.
29. Walters K.A. "Drugs and the Pharmaceutical Sciences" Series No. 119, Marcel Dekker, New York, NY, USA, 2002, pp. 1 – 41.
30. Lai-Cheong J. E., McGrath J. A. "Structure and function of skin, hair and nails". International Journal of Cosmetic Science, Volume 41, Issue 6, 2013, pp. 317 – 320.
31. Internet source: http://headandneckcancerguide.org/adults/introduction-to-head-and-neck-cancer/skin-cancer/anatomy/.
32. Internet source: http://www.odosnavikai.lt/index.asp?DL=L&EditionID=244&ParentID=10&TopicID=10&Code=.
33. Montvila A., Matulevičiūtė A., Žvinienė K. "Changes in radiological HCC diagnostics in Lithuanian university of health sciences hospital Kaunas clinics during a period of time from 2003 to 2014 years." Medicinos teorija ir praktika, 2015 - T. 21 (Nr. 4.1), pp. 553 – 558.
34. Internet source: http://www.manosveikata.lt/lt/aktualijos/naujienos/melanoma-dazniau-serga-moterys.
35. Internet source: http://www.genesis.net.au/~ajs/projects/medical_physics/ultrasound/.
36. Internet source: http://www.ucl.ac.uk/medphys/staff/people/bcox/USlecturenotes_Jan2013.pdf.
37. Chan V., Perlas A. "Basics of Ultrasound Imaging". Atlas of Ultrasound-Guided Procedures in Interventional Pain Management 2011, pp. 13 – 19 ISBN 978-1-4419-1679-2.
38. Internet source: http://courses.washington.edu/bioen508/Lecture6-US.pdf.
39. Internet source: http://www.shdmu.com/uploadfile/files/20120629063208.pdf.
40. Internet source: http://techno.su.lt/~lauruska/turinys1.html.

41. Bauer A. B. "Impedance Theory and Measurements on Porous Acoustic Liners". Journal of Aircraft, Vol. 14, No. 8, 1977, pp. 720-728, https://doi.org/10.2514/3.58844. 42. Hendee W. R., Ritenour E. R. “Medical Imaging Physics”, 2002, Wiley-Liss, ISBN: 0-471-38226-4.
43. Parker K. J. et al. “The Measurement of Backscatter Coefficient from a Broadband Pulse-Echo System: A New Formulation”. IEEE Transactions on ultrasonic ferroelectrics and frequency control, 1997, vol. 44, no. 2, pp. 515 – 525.
44. Internet source: http://www.brl.uiuc.edu/Publications/1969/Dunn-BookChap-205-1969.pdf
45. National bureau of standards. “Ultrasonic tissue characterization”. Internet source: https://nvlpubs.nist.gov/nistpubs/Legacy/SP/nbsspecialpublication453.pdf
46. Alexander H., Miller D.L. “Determining skin thickness with pulsed ultrasound.” J Invest Dermatol, 1979, pp. 17 – 9.
47. Kreitz G. “A- and B-scan techniques of conventional ultrasound units”. Ultrasound in Dermatology, Berlin: Springer Verlag, 1992, pp. 12 – 21.
48. Harland C. C., Kale S. G., Jackson P., Mortimer P. S., Bamber J. C. “Differentiation of common benign pigmented skin lesions from melanoma by high-resolution ultrasound.” British Journal of Dermatology, 2000, pp. 281 - 289.
49. Machet L. et.al. “High Resolution Ultrasound Imaging of Melanocytic and Other Pigmented Lesions of the Skin.” Ultrasound Imaging, 2011, pp. 139 – 151, ISBN 978-953-307-239-5.
50. Berson M., Vaillant L., Patat F., Pourcelot L. “High-resolution real-time ultrasonic Scanner”. Ultrasound Med Biol., 1992, pp. 471 - 478.
51. Machet L., Belot V., Naouri M., Boka M., Mourtada Y., Perrinaud A., Giraudeau B., Laure B., Machet M. C., Vaillant L. “Preoperative measurement of thickness of cutaneous melanoma using high-resolution 20 mhz ultrasound imaging: feasibility and pitfalls to predict surgical margins”. A prospective study of 31 cases and a systematic review of the literature. Ultrasound Med Biol, 2009, pp. 1411 - 1420.
52. Vaillant L., Grognard C., Machet L., Cochelin N., Callens A., Berson M., Aboumrad J., Patat F., Lorette G. “Imagerie ultrasonore haute résolution: utilité pour le traitement des carcinomes basocellulaires par cryochirurgie”. Ann Dermatol Venereol., 1998, pp. 500 - 504.
53. Uhara H., Hayashi K., Koga H., S Toshiaki. “Multiple hypersonographic spots in basal cell Carcinoma”. Dermatol Surg, 2007, pp. 1215 – 1219.
54. Wortsman X., Wortsman J. “Clinical usefulness of variable-frequency ultrasound in localized lesions of the skin”. J AM ACAD DERMATOL, 62, 2010, pp. 247 – 256.
55. Rallan D., Bush N. L., Bamber J. C., Harland C. C. “Quantitative Discrimination of Pigmented Lesions Using Three-Dimensional High-Resolution Ultrasound Reflex Transmission Imaging”. Journal of Investigative Dermatology, 2007, pp. 189 – 195. doi:10.1038/sj.jid.5700554; published online 26 October 2006.
56. Wortsman X. “Ultrasound in Dermatology: Why, How, and When?”. Semin Ultrasound CT MRI 34, 2013, pp. 177 – 195.
57. Wortsman X. “Common applications of dermatologic sonography”. J Ultrasound Med1 31, 2012, pp. 97 – 111.
58. Wortsman X., Wortsman J. “Clinical usefulness of variable-frequency ultrasound in localized lesions of the skin”. J Am Acad Dermatol 62, 2010, pp. 247 – 256.
59. Wortsman X. “Sonography of cutaneous and ungual lumps and bumps”. Ultrasound Clin, 2012. doi:http://dx.doi.org/10.1016/j.cult.2012.08.006.
60. Kreitz G. “A- and B-scan techniques of conventional ultrasound units”. Ultrasound in Dermatology. Berlin: Springer Verlag., 1992, pp. 12 – 21.

61. Rallan D., Harland C.C. “Ultrasound in dermatology – basic principles and applications”. Clin Exp Dermatol 28, 2003, pp. 632 – 638.
62. Kleinerman R., Whang T. B., Bard R. L., Marmur E. S. “Ultrasound in dermatology: Principles and Applications”. Am Acad Dermatol, 2012, pp. 478 - 487.
63. Krahn G., Gottlober P., Sander C., Peter R. U. “Dermatoscopy and high frequency sonography: two useful non-invasive methods to increase preoperative diagnostic accuracy in pigmented skin lesions”. Pigment Cell Res, 11, 1998, pp 151 – 154.
64. Steiner A., Pehamberger H., Wolff K. “In vivo epiluminescence microscopy of pigmented skin lesions. II. Diagnosis of small pigmented skin lesions and early detection of malignant melanoma”. J Am Acad Dermatol, 17, 1987, pp. 584 – 591.
65. Pehamberger H., Binder M., Steiner A., Wolff K.”In vivo epiluminescence microscopy: improvement of early diagnosis of melanoma”. J Invest Dermatol, 100, 1993, pp. 356 – 362.
66. Steiner A., Pehamberger H., Binder M., Wolff K. “Pigmented Spitz nevi: improvement of the diagnostic accuracy by epiluminescence microscopy”. J Am Acad Dermatol 1992, pp. 697 – 701.
67. Binder M., Schwarz M., Winkler A., Steiner A., Kaider A., Wolff K., Pehamberger H. “Epiluminescence microscopy: a useful tool for the diagnosis of pigmented skin lesions for formally trained dermatologists”. Arch Dermatol, 131, 1995, pp. 286 – 291.
68. Nachbar F., Stolz W., Merkle T., Cognetta A. B., Vogt T., Landthaler M., et al. “The ABCD rule of dermatoscopy: high prospective value in the diagnosis of doubtful melanocytic skin lesions”. J Am Acad Dermatol, 30, 1994, pp. 551 – 559.
69. Pazzini C., Pozzi M., Betti R, Vergani R., Crosti C. “Improvement of diagnostic accuracy in the clinical diagnosis of pigmented skin lesions by epiluminescence microscopy”. Skin Cancer, 11, 1996, pp. 159 – 161.
70. Binder M., Puespoeck-Schwarz M., Steiner., Kittler H., Muellner M., Wolff K., Pehamberger H. “Epiluminescence microscopy of small pigmented skin lesions: short-term formal training improves the diagnostic performance of dermatologists”. J Am Acad Dermatol, 36, 1997, pp. 197 – 202.
71. Carli P., De Giorgi V., Naldi L., Dosi G. “Reliability and inter-observer agreement of dermoscopic diagnosis of melanoma and melanocytic naevi”. Eur J Cancer Prev, 7, 1998, pp. 397 – 402.
72. Stanganelli I., Serafini M., Cainelli T., Cristofolini M., Baldassari L., Staffa M., Bucchi L. “Accuracy of epiluminescence microscopy among practical dermatologists: a study from the Emilia-Romagna region of Italy”. Tumouri, 1998, pp. 701 – 705.
73. Argenziano G., Soyer H. P., Chimenti S., Talamini R., Corona R., Sera F., et al. “Dermoscopy of pigmented skin lesions: results of a consensus meeting via the internet”. Journal of the American Academy of Dermatology, 48(5), 2003, pp. 679 - 693.
74. Massi D., V. De Giorgi, Soyer H.P. “Histopathologic correlates of dermoscopic Criteria”. Dermatol Clin, 2001. 19(2): p. 259 - 268.
75. Yadav S., et al. “Histopathologic correlates of structures seen on dermoscopy (epiluminescence microscopy)”. Am J Dermatopathol, 1993. 15(4): p. 297-305.
76. Argenziano G. S.H.P., De Giorgi V, Piccolo D, Carli P, Delfino M, Ferrari A, Hofmann-Wellenhof R, Massi D, Mazzocchetti G, Scalvenzi M, Wolf I.H, Dermoscopy - a tutorial. 2000, Milan: EDRA Medical Publishing & New Media.
77. Miyazaki A., et al. “Anatomical and histopathological correlates of the dermoscopic patterns seen in melanocytic nevi on the sole: a retrospective study”. J Am Acad Dermatol, 2005. 53(2): p. 230 – 236.

78. Ishihara Y., et al. “Early acral melanoma in situ: correlation between the parallel ridge pattern on dermoscopy and microscopic features”. Am J Dermatopathol, 2006. 28(1): p. 21 - 27.
79. Argenziano G., et al. “Proposal of a new classification system for melanocytic naevi”. Br J Dermatol, 2007. 157(2): p. 217- 227.
80. Bahmer F.A., et al. “Terminology in surface microscopy”. Consensus meeting of the Committee on Analytical Morphology of the Arbeitsgemeinschaft Dermatologische Forschung, Hamburg, Federal Republic of Germany, Nov. 17, 1989. J Am Acad Dermatol, 1990. 23(6 Pt 1): p. 1159 - 1162.
81. Rezze G.G., et al. “Structural correlations between dermoscopic features of cutaneous melanomas and histopathology using transverse sections”. Am J Dermatopathol, 2006. 28(1): p. 13-20.
82. Argenziano G., et al. “Dermatoscopic pitfalls in differentiating pigmented Spitz naevi from cutaneous melanomas”. Br J Dermatol, 1999. 141(5): p. 788 - 793.
83. Demirtasoglu M., et al. “Evaluation of dermoscopic and histopathologic features and their correlations in pigmented basal cell carcinomas”. J Eur Acad Dermatol Venereol, 2006. 20(8): pp. 916 - 920.
84. Stolz W., Riemann A., Cognetta A.B., et al. “ABCD rule of dermatoscopy: a new practical method for early recognition of malignant melanoma”. Eur J Dermatol, 4, 1994, pp. 521 - 527.
85. Menzies S. W., Westerhoff K., Rabinovitz H., Kopf A.W., McCarthy W. H., Katz B. “Surface microscopy of pigmented basal cell carcinoma”. Arch Dermatol, 136, 2000, pp. 1012 – 1016.
86. Argenziano G., Fabbrocini G., Carli P., Giorgi V. D., Sammarco E., Delfino M. “Comparison of the ABCD Rule of Dermatoscopy and a New 7-Point Checklist Based on Pattern Analysis”. Arch Dermatol, 1998, pp. 1563 - 1570.
87. Balch C. M., Soong S.J., Gershenwald J.E., Thompson J.F., Reintgen D.S., Cascinelli N., Urist M., McMasters K.M., et al. "Prognostic factors analysis of 17,600 melanoma patients: Validation of the American Joint Committee on Cancer melanoma staging system". Journal of Clinical Oncology, 19, 2001, pp. 3622 – 3634.
88. Internet source: https://www.cancer.gov/publications/dictionaries/cancer-terms/def/clark-level-iv-skin-cancer
89. Cotton S. “A Non-invasive Imaging System for Assisting in the Diagnosis of Malignant Melanoma” PhD Thesis. Faculty of Science, University of Birmingham, U.K. 1998.
90. Cotton S. D., Claridge E., Hall P. N. “Noninvasive Skin Imaging Information Processing in Medical Imaging”. Springer-Verlag, 1997, 501–7.
91. Cotton S. D., Claridge E. “Developing a predictive model of human skin colouring”. In: Proceedings of the SPIE Medical Imaging, 1996, 2708; pp. 814 – 825.
92. Moncrieff M., Cotton S., Claridge E., Hall P. “Clinical Investigations Spectrophotometric intracutaneous analysis: a new technique for imaging pigmented skin lesions”. British Journal of Dermatology, 146, 2002, pp. 448 – 457.
93. Tehrani H., Walls J., Price G., Cotton S., Sassoon E., Hall P. “A novel imaging technique as an adjunct to the in vivo diagnosis of nonmelanoma skin cancer”. British Journal of Dermatology, 155, 2006, pp. 1177 – 1183.
94. Terstappen K., Larkö O., Wennberg A-M. “Pigmented Basal Cell Carcinoma – Comparing the Diagnostic Methods of SIAscopy and Dermoscopy”. Acta Derm Venereol, 87, 2007, pp. 238 – 242.

95. Scott D.W. Multivariate Density Estimation: Theory, Practice and Visualization. New York, John Wiley, 1992.
96. ix E., Hodges J.L. Discriminatory analysis – nonparametric discrimination: consistency properties. Report no. 21-49-004, US Air Force School of Aviation Medicine, Random Field, Texas, 1951.
97. Silverman B.W., Jones M.C. E. Fix and J.L. Hodges (1951): an important contribution to nonparametric discriminant analysis and density estimation. International Statistical Review, 1989, Vol. 57 (3), p. 233–247.
98. Rosenblatt M. Remarks on some nonparametric estimates of a density function, The Annals of Mathematical Statistics, 1956, Vol. 27, p. 832–837.
99. Parzen E. On the estimation of probability density and mode. The Annals of Mathematical Statistics, 1962, Vol. 33, p. 1065–1076.
100. Cencov N.N. Estimation of unknown density function from observations. SSSR Academy of Sciences, 1962, Vol. 147, p. 45–48.
101. Watson G.S., Leadbetter M.R. On the estimation of the probability density II, The Annals of Mathematical Statistics, 1963, Vol. 34, p. 480–491.
102. Loftsgaarden D.O., Quesenberry C.P. A Nonparametric Estimate of a Multivariate Density Function. The Annals of Mathematical Statistics, 1965, Vol. 36 (3), p. 1049–1051.
103. Schwartz S.C. Estimation of Probability Density by an Orthogonal Series. The Annals of Mathematical Statistics, 1967, Vol. 38 (4), p. 1261–1265.
104. Epanechnikov V.A. Nonparametric estimates of a multivariate probability density. Theoretical Probability Applications, 1969, Vol. 14, p. 153–158.
105. Tarter M., Kronmal R. On Multivariate Density Estimates Based on Orthogonal Expansions. The Annals of Mathematical Statistics, 1970, Vol. 41 (2), p. 718–722.
106. Kimeldorf G., Wahba G. Some results on Tchebycheffian spline functions. Journal of Mathematical Analysis and Applications, 1971, Vol. 33, 82–95.
107. Cacoullos T. Estimation of a multivariate density, Annals of the Institute of Statistical Mathematics, 1966, Vol. 18 (1), p. 179–189.
108. Scott D.W., Tapia R.A., Thompson J.R. Multivariate Density Estimation by Discrete Maximum Penalized-Likelihood Methods. Graphical Representation of Multivariate Data, Peter C.C. Wang, Editor, Academic Press, New York, 1978.
109. Silverman B.W. Weak and strong uniform consistency of the kernel estimate of a density and its derivatives. The Annals of Statistics, 1978, Vol. 6, p. 177–184.
110. Fukunaga K. Introduction to Statistical Pattern Recognition. New York, Academic Press, 1972.
111. Gasser T., Müller, H.G., Mammitzsch V. Kernels for nonparametric curve estimation. Journal of the Royal Statistical Society, 1985, B, Vol. 47, p. 238–252.
112. Marron J.S., Nolan D. Canonical kernels for density estimations. Statistics and Probability Letters, 1988, Vol. 7 (3), p. 195–199.
113. Sacks J., Ylvisaker D. Asymptotically optimum kernels for density estimation at a point. The Annals of Statistics, 1981, Vol. 9, p 334–346.
114. Tapia R.A., Thompson J.R. Nonparametric Probability Density Estimation. Johns Hopkins Series in the Mathematical Sciences. Baltimore and London, Johns Hopkins University Press, 1978.
115. Hall P. Kernel Estimation of a distribution function. Communications in Statistics. Theory and Methods, 1985, Vol. 14, p. 605–620.
116. Drulytė I., Ruzgas T., Raišutis R., Valiukevičienė A. “Assessment and comparison of likely density distributions in the cases of thickness measurement of skin tumours by

ultrasound examination and histological analysis". Journal of vibroengineering, 2016, vol. 18, iss. 5, p. 3279 - 3291.
117. Wand M.P., Jones M.C. Kernel Smoothing. London: Chapman and Hall, 1995.
118. Hansen B.E. Lecture Notes on Nonparametrics. University of Wisconsin, 2009. http://www.ssc.wisc.edu/~bhansen/718/NonParametrics1.pdf
119. Makridakis S., Andersen A., Carbone R., Fildes R., Hibon M., Lewandowski R., et al. "The accuracy of extrapolation (time series) methods: Results of a forecasting competition". Journal of Forecasting. 1982;1(2), p. 111 – 153.
120. R. Raišutis, E. Jasiūnienė, D. Jasaitienė, S. Valiukevičienė. "Investigation of human skin using pulse-echo ultrasonic technique: review and development". Ultragarsas (Ultrasound), 2010, Vol. 65, No. 1, 37, ISSN 1392-2114.
121. Jasaitiene D., Valiukeviciene S., Linkeviciute G., Raisutis R., Jasiuniene E., Kazys R. Principles of high-frequency ultrasonography for investigation of skin pathology. Journal of the European Academy of Dermatology and Venereology, 2011, p. 375-382.
122. Kučinskienė V., Samulėnienė D., Gineikienė A., Raišutis R., Kažys R., Valiukevičienė S. Preoperative assessment of skin tumour thickness and structure using 14-MHz ultrasound. Medicina (B Aires), 2014, p. 150-155.
123. Rudzkis R., Bakshaev A. Goodness of fit tests based on kernel density estimators. IRFORMATICA, 2013, Vol. 24 (3), p. 447-460.
124. Lachenbruch P. A., Mickey M. R. "Estimation of Error Rates in Discriminant Analysis". Technometrics, Vol. 10, No. 1, 1968, pp. 1 - 11.
125. Lachenbruch P. A., Goldstein M. "Discriminant Analysis". Biometrics, Vol. 35, No. 1, Perspectives in Biometry, 1979, pp. 69 - 85.
126. Friedman J. H. "Regularized Discriminant Analysis", Journal of the American Statistical Association, Vol. 84, No. 405, 1989, pp. 165 - 175.
127. Mika S. et al. "Fisher discriminant analysis with kernels". IEEE, 07803-5673-X, 1999, pp. 41 – 48.
128. Lachenbruch P. A. "Robustness of discriminant functions" pp. 626 – 636.
129. Ahmed S., Lachenbruch P.A. "Discriminant Analysis When Scale Contamination is Present in The Initial Sample." In Classification and Clustering. New York: Academic Press, 1977.
130. Ashikaga T., Chang P. "Robustness of Fisher I s Linear Discriminant Function Under Two Compound Mixed Normal Models". II J Amer Stat Assoc 6, 1981, pp. 676 – 680.
131. Lachenbruch P.A. "Misclassification Effects Discriminant". 1979 pp. 129 - 132.
132. Lachenbruch P.A., Broffitt B. "On Classifying Observations When One Population is a Mixture of Normals." Biometric Journal 22, 1981, pp. 295 - 301.
133. Goldstein M., Dillon W.R. "Discrete Discriminant Analysis". New York: John Wiley and Sons, 1978.
134. Ivashchenko O.V., Yermakova T.S., Cieslicka M., Muszkieta R. "Discriminant analysis as method of pedagogic control of 9-11 forms girls' functional and motor fitness". Journal of Physical Education and Sport, 15(3), Art 86, 2015, pp.576 – 581.
135. Zhou Ch., Zhang Z., Yi D., Lei Z., Li S. Z. "Low-Resolution Face Recognition via Simultaneous Discriminant Analysis".
136. Arjmandi M. K., Pooyan M. "An optimum algorithm in pathological voice quality assessment using wavelet-packet-based features, linear discriminant analysis and support vector machine". Biomedical Signal Processing and Control 7, 2012, pp. 3 – 19.

137. Vizquez R. R., Vélez-Pérez H., Ranta R., Dorr V. L., Maquin D., Maillard L. “Blind source separation, wavelet denoising and discriminant analysis for EEG artefacts and noise cancelling”. Biomedical Signal Processing and Control 7, 2012, pp. 389 – 400.
138. Gladis V.P., Rathi P., Palani S. “Brain tumour MRI image classification with feature selection and extraction using linear discriminant analysis”.
139. Alkan A., Gunay M. “Identification of EMG signals using discriminant analysis and SVM classifier”. Expert Systems with Applications 39, 2012, pp. 44 – 47.
140. Awasthi R. et al. “Discriminant analysis to classify glioma grading using dynamic contrast-enhanced MRI and immunohistochemical markers”. Neuroradiology, 54, 2012, pp. 205 – 213.
141. Azechi M. et al. “Discriminant analysis in schizophrenia and healthy subjects using prefrontal activation during frontal lobe tasks: A near-infrared spectroscopy”. Schizophrenia Research 117, 2010, pp. 52 – 60.
142. Blankertz B., Lemm S., Treder M., Haufe S., Müller K. B. “Single-trial analysis and classification of ERP components — A tutorial”. NeuroImage 56, 2011, pp. 814 – 825.
143. Deluzio K. J., Astephen J. L. “Biomechanical features of gait waveform data associated with knee osteoarthritis: An application of principal component analysis”. Gait & Posture 25, 2007, pp. 86 – 93.
144. Yeh Y. Ch., Wang W. J., Chiou Ch. W. “Cardiac arrhythmia diagnosis method using linear discriminant analysis on ECG signals”. Measurement 42, 2009, pp. 778 – 789.
145. Maroco et al. “Data mining methods in the prediction of Dementia: A real-data comparison of the accuracy, sensitivity and specificity of linear discriminant analysis, logistic regression, neural networks, support vector machines, classification trees and random forests”. BMC Research Notes, 2011, doi:10.1186/1756-0500-4-299.
146. Georgiou-Karistianis N. et al. “Automated differentiation of pre-diagnosis Huntington's disease from healthy control individuals based on quadratic discriminant analysis of the basal ganglia: The IMAGE-HD study”. Neurobiology of Disease 51, 2013, pp. 82 – 92.
147. Jombart et al. “Discriminant analysis of principal components: a new method for the analysis of genetically structured populations”. BMC Genetics, 2010, doi:10.1186/1471-2156-11-94.
148. Rosenblatt M. “Remarks on Some Nonparametric Estimates of a Density Function.” Annals of Mathematical Statistics 27, 1956, pp. 832 – 837.
149. Shang L., Chan K. P. “Nonparametric Discriminant HMM and Application to Facial Expression Recognition”. IEEE, 2009, pp. 2090 – 2096.
150. Khan N. M., Ksantini R., Ahmad I. S., Boufama B. “A novel SVM NDA model for classification with an application to face recognition”. Pattern Recognition 45, 2012, pp. 66 –79.
151. Xie X., Li B. “Kernel-Based Nonparametric Fisher Classifier for Hyperspectral Remote Sensing Imagery”. Journal of Information Hiding and Multimedia Signal Processing, Volume 6, Number 3, 2015, pp. 591 – 599.
152. Islam T. et al. “International Journal of Remote Sensing Non-parametric rain/no rain screening method for satellite-borne passive microwave radiometers at 19–85 GHz channels with the Random Forests algorithm” International Journal of Remote Sensing,35:9, 2014, pp. 3254-3267, DOI: 10.1080/01431161.2014.903444 2014 y.
153. Wu Y., Shi L. “Analysis of altered gait cycle duration in amyotrophic lateral sclerosis based on nonparametric probability density function estimation”. Medical Engineering & Physics 33, 2011, pp. 347 – 355.

154. Brasier A. R. “Discovery Proteomics and Nonparametric Modeling Pipeline in the Development of a Candidate Biomarker Panel for Dengue Hemorrhagic Fever”. CTS Journal, VOLUME 5, ISSUE 1, 2011, pp. 8 – 20.
155. Granata D. et al. “Evaluation of supervised methods for the classification of major tissues and subcortical structures in multispectral brain magnetic resonance images”. Computerized Medical Imaging and Graphics, 2014; 38(5):337–347, http://dx.doi.org/10.1016/j.compmedimag.2014.03.003.
156. Contrera J. F., Kruhlak N. L., Matthews E. J., Benz R.D. “Comparison of MC4PC and MDL-QSAR rodent carcinogenicity predictions and the enhancement of predictive performance by combining QSAR models”. Regulatory Toxicology and Pharmacology 49, 2007, pp. 172–182.
157. Contrera J. F., Matthews E. J., Kruhlak N. L., Benz R. D. “In Silico Screening of Chemicals for Genetic Toxicity Using MDL-QSAR, Nonparametric Discriminant Analysis, E-State, Connectivity, and Molecular Property Descriptors”. Toxicology Mechanisms and Methods, 2008, pp. 207–216.
158. Kruhlak N. L., Contrera J. F., Benz R. D., Matthews E. J. “Progress in QSAR toxicity screening of pharmaceutical impurities and other FDA regulated products”. Advanced Drug Delivery Reviews 59, 2007, pp. 43–55.
159. Osterhaus J. T., Purcaru O., Richard L. “Discriminant validity, responsiveness and reliability of the rheumatoid arthritis-specific Work Productivity Survey (WPS-RA)”. Arthritis Research & Therapy 2009, 11:R73, pp. 1 – 12. (doi:10.1186/ar2702) http://arthritis-research.com/content/11/3/R73 1-12
160. Rebmann V. et al. “Soluble MICA as an independent prognostic factor for the overall survival and progression-free survival of multiple myeloma patients”. Clinical Immunology, 2007, 123, pp. 114 — 120.
161. Sun X. M., Yu X. P., Liu Y., Xu L., Di D. L. “Combining bootstrap and uninformative variable elimination: Chemometric identification of metabonomic biomarkers by nonparametric analysis of discriminant partial least squares”. Chemometrics and Intelligent Laboratory Systems 115, 2012, pp. 37 – 43.
162. Cui Y., Zheng Ch. H., Yang J., Sha W. “Sparse maximum margin discriminant analysis for feature extraction and gene selection on gene expression data”. Computers inBiologyandMedicine43, 2013, pp. 933–941.
163. Ghosh D. “Penalized Discriminant Methods for the Classification of Tumours from Gene Expression Data”. Biometrics 59, 2003, pp. 992 – 1000.
164. Finn W. G. et al. “Analysis of Clinical Flow Cytometric Immunopheno typing Data by Clustering on Statistical Manifolds: Treating Flow Cytometry Data as High-Dimensional Objects”. Cytometry Part B (Clinical Cytometry), 2009, 76B, pp. 1–7.
165. Hallahan K. M. et al. “Discriminant Value of Custom Ocular Response Analyzer Waveform Derivatives in Keratoconus”. Ophthalmology, 2014, 121, pp. 459 - 468.
166. Käll L., Storey J. D., Noble W. S. “Non-parametric estimation of posterior error probabilities associated with peptides identified by tandem mass spectrometry” Bioinformatics, Vol. 24, 2008, pp. 142 – 148, doi:10.1093/bioinformatics/btn294.
167. Kurtulmus F., Lee W. S., Vardar A. “Immature peach detection in colour images acquired in natural illumination conditions using statistical classifiers and neural network”. Precision Agric, New York, 2013, doi 10.1007/s11119-013-9323-8.
168. Li B., Li J., Zhang X. P. “Nonparametric discriminant multi-manifold learning for dimensionality reduction”. Neurocomputing152, 2015, pp. 121–126.

169. Granados F. L. et al. “Multispectral classification of grass weeds and wheat (Triticum durum) using linear and nonparametric functional discriminant analysis and neural networks”. European Weed Research Society Weed Research 48, 2008, pp. 28 – 37.
170. Ren H., Ji H. “Nonparametric subspace analysis fused to 2DPCA for face recognition”. Optik 125, 2014, pp. 1922 – 1925.
171. Tarrı´o-Saavedra J. et al. “Functional nonparametric classification of wood species from thermal data”. J Therm Anal Calorim, 2011, pp. 87 – 100, DOI 10.1007/s10973-010-1157-2.
172. Wang P., Ji Q. “Multi-view face and eye detection using discriminant features”. Computer Vision and Image Understanding 105, 2007, pp. 99 – 111.
173. Xing K. et al. “A real-time EMG pattern recognition method for virtual myoelectrich and control”. Neurocomputing 136, 201, pp. 345 – 355.
174. Zhang J. et al. “Bayesian Nonparametric Model for the Validation of Peptide Identification in Shotgun Proteomics”. Molecular & Cellular Proteomics 8.3, pp. 547 – 557.
175. Marini F. “Classification Methods in Chemometrics”. Current Analytical Chemistry, 2010, 6, pp. 72 – 79.
176. Cook E. F., Goldman L. “Empiric comparison of multivariate analytic techniques: advantages and disadvantages of recursive partitioning analysis”. J Chron Dis Vol. 37, No. 9/10, 1984, pp. 721 – 731.
177. Li Z., Liu W., Lin D., Tang X. “Nonparametric Subspace Analysis for Face Recognition”.
178. Qiu X., Wu L.” Nonparametric maximum margin criterion for face recognition”. IEEE, 2005.
179. Kuo B. Ch., Landgrebe D. A. “Hyperspectral Data Classification Using Nonparametric Weighted Feature Extraction”. IEEE, 2002.
180. Li Z., Lin D., Tang X. “Nonparametric Discriminant Analysis for Face Recognition”. IEEE transactions on pattern analysis and machine intelligence, VOL. 31, NO. 4, 2009, pp. 755 – 761.
181. Yang J. M., Yu P. T., Kuo B. Ch. “A Nonparametric Feature Extraction and Its Application to Nearest Neighbour Classification for Hyperspectral Image Data”. IEEE transactions on geoscience and remote sensing, vol. 48, no. 3, 2010, pp. 1279 – 1293.
182. Bressan M., Vitri J. “Nonparametric discriminant analysis and nearest neighbor classification”. Pattern Recognition Letters 24, 2003, pp. 2743 – 2749.
183. Garcia-Pedrajas N., Maudes-Raedo J., Garcia-Osorio C., Rodriguez-Diez J. J. “Supervised subspace projections for constructing ensembles of classifiers”. Information Sciences 193, 2012, pp. 1 – 21.
184. Sadjadi S. O., Pelecanos J. W., Ganapathy S. “Nearest neighbor discriminant analysis for language recognition”. IEEE, 2015, pp. 4205 – 4209.
185. Fisher R. A. “The use of multiple measurements in taxonomic problems”. Ann. Eugen., 7, 1936, p. 179.
186. M. R. Chernick, V. K. Murthy, C. D. Nealy. “Estimation of error rate for linear discriminant functions by resampling: Non-Gaussian populations”. Computers & Mathematics with Applications, Volume 15, Issue 1, 1988, p. 29 - 37.
187. Mosteller, Wallace. “Inference in an authorship problem”. J. Amer. Statist. Ass., 58, pp. 275-309.
188. Stone M. “Cross-Validatory Choice and Assessment of Statistical Predictions”. Journal of the Royal Statistical Society. Series B (Methodological), Vol. 36, No. 2., 1974, pp. 111 - 147.
189. Lachenbruch P. A., Mickey M. R. “Estimation of error rates in discriminant analysis”. Technometrics 10, 1968, pp. 1 - 11.

190. Allen D. M. “The Relationship Between Variable Selection and Data Argumentation and a Method for Prediction”. Technometrics, 16:1, 1974, pp. 125 – 127.
191. Stone M. “Asymptotics for and against Cross-Validation”. Biometrika, Vol. 64, No. 1, 1977, pp. 29 - 35.
192. Geisser S. “The Predictive Sample Reuse Method with Applications”. Journal of the American Statistical Association, 70:350, 1975, pp. 320 – 328.
193. G. Wahba, S. Wold. “A completely automatic French curve: fitting spline functions by cross validation” Communications in Statistics, 4:1, 1975, pp. 1 – 17.
194. Picard R. R., Cook R. D. “Cross-Validation of Regression Models”. Journal of the American Statistical Association, 79:387, 1984, pp. 575 – 583.
195. Shao J. “Linear Model Selection by Cross-Validation”. Journal of the American Statistical Association. Vol. 88, No. 422, 1993, pp. 486 – 494.
196. Celisse A. “Optimal cross-validation in density estimation”. HAL Id: hal-00337058, https://hal.archives-ouvertes.fr/hal-00337058v3, 2008, p. 37.
197. Burman P. “Comparative study of Ordinary Cross-Validation, v-Fold Cross-Validation and the repeated Learning-Testing Methods”. Biometrika, 76(3), 1989, pp. 503 – 514.
198. Burman P. “Estimation of optimal transformation using v-fold cross-validation and repeated learning-testing methods”. Sankhya Ser. A, 52(3), 1990, pp. 314 – 345.
199. Glick N. “Additive Estimators for Probabilities of Correct Classification”. Pattern Recognition. 1978, 10, p. 211 – 222.
200. Hora S. C., Wilcox J. B. “Estimation of Error Rates in Several-Population Discriminant Analysis”. *Journal of Marketing Research.* 1982.
201. Akaike H. “A New Look at the Statistical Model Identification”. IEEE transactions on automatic control, vol. ac-19, no. 6, December 1974.
202. Stone M. “An Asymptotic Equivalence of Choice of Model by Cross-Validation and Akaike's Criterion”. Journal of the Royal Statistical Society. Series B (Methodological), Vol. 39, No. 1., 1977, pp. 44 - 47.
203. Mallows C. L. “Some Comments on C P”. Technometrics, Vol. 15, No. 4., 1973, pp. 661 - 675.
204. Herzberg A. M., Tsukanov A. V. “The Monte-Carlo comparison of two criteria for the selection of models”. Journal of Statistical Computation and Simulation, 22:2, 1985, pp. 113 – 126.
205. Efron B. “Estimating the error rate of a prediction rule: improvement on cross - validation”. Journal of the American Statistical Association, vol. 78, no. 382, 1983, pp. 316 – 331.
206. Kohavi R. “A study of cross – validation and bootstrap for accuracy estimation and model selection”. The international joint conference on artificial intelligence, 1995.
207. Pathak S.D., Chalana V., Kim Y.M. “Interactive automatic fetal head measurements from ultrasound images using multimedia computer technology”. Ultrasound in Medicine and Biology, 23, 1997. pp. 665 – 673.
208. Zimmerand Y., Tepper R., Akselrod S. “A two-dimensional extension of minimum cross entropy thresholding for the segmentation of ultrasound images”. Ultrasound Med. Biol., 22, 1996, pp. 1183 – 1190.
209. Yezzi A., Kichenassamy S., Kumar A., Olver P., Tannenbaum A. “A geometric snake model for segmentation of medical imagery”. IEEE T. Med. Imag., 16, 1997, pp. 199 – 209.
210. Sebbahi A., Herment A., A de Cesare, Mousseaux A. “Multimodality cardiovascular image segmentation using a deformable contour model”. Comput. Med. Im. Graph., 1997, 21, pp. 79 – 89.

211. Smith S. M., Brady J. M. “SUSAN—A New Approach to Low Level Image Processing”. International Journal of Computer Vision 23(1), 1997, pp. 45 – 78.
212. Bazi Y., Bruzzone L., Melgani F. “Image thresholding based on the EM algorithm and the generalized Gaussian distribution”. Pattern Recognition 40 2007, pp. 619 – 634.
213. McFadden D. “Conditional Logit Analysis of Qualitative Choice Behaviour”. Frontiers in Econometrics, New York: Academic Press, 1974, pp. 105 – 142.
214. McFadden D. “A comment on discriminant analysis “versus” logit analysis”. Annals of economic and social measurement, 5/4, 1976, pp. 511 – 523.
215. Efron B. “The Efficiency of Logistic Regression Compared to Normal Discriminant Analysis”. Journal of the American Statistical Association, Volume 70, Number 352, 1975, pp. 892 – 898.
216. Press S. J., Wilson S. “Choosing Between Logistic Regression and Discriminant Analysis”. Journal of the American Statistical Association, Vol. 73, No. 364, 1978, pp. 699 - 705.
217. Gordon T. “Hazards in the Use of the Logistic Function with Special Reference to Data from Prospective Cardiovascular Studies". Journal of Chronzc Diseases, 27, 1974, pp. 97 - 102.
218. Halperin M., Blacikwelder W. C., Verter J. I."Estimation of the Multivariate Logistic Risk Function: A Comparison of the Discriminant Function and Maximum Likelihood Approaches". Journal of Chronic Diseases, 24, 1971, pp. 125 - 158.
219. Dzung L. Pham Y, Chenyang Xu, Jerry L. Princ, “A survey of current methods in medical image segmentation”. Annual Review of Biomedical Engineering, January 19, 1998, pp. 1-27.
220. “Color Image Segmentation: A State-of-the-Art Survey”. New Delhi, India: Proc. Indian Nat. Science Academy, Mar. 2001, vol. 67 A, Arch Dermatol., pp. 998-1006.
221. M. Kass, A. Witkin, and D. Terzopoulos. “Snakes: Active contour models”. Int. J. Comput. Vis., vol. 1, no. 4, 1998, pp. 321–331.
222. Xu L., Jackowski M., Goshtasby A., Roseman D., Bines S., Yu C., Dhawan A. P., Huntley A. “Segmentation of skin cancer images”. Image Vis. Comput., vol. 17, 1999, pp. 65–74.
223. Sund T., Eilertsen K. “An algorithm for fast adaptive binarization with applications in radiotherapy imaging”. IEEE Trans. Med. Imaging 22, 2003, pp. 22–28.
224. Solihin Y, Leedham C. G. “Integral ratio: a new class of global thresholding techniques for handwriting images”. IEEE Trans. Pattern Anal. Mach. Intell. 21, 1999, pp. 761–768.
225. Bhanu B. “Automatic target recognition: state of the art survey”. IEEE Trans. Aerosp. Electron. Syst. AES-22, 1986, pp. 364–379.
226. Bruzzone L., Prieto D. F. “Automatic analysis of the difference image for unsupervised change detection”. IEEE Trans. Geosci. Remote Sensing 38, 2000, pp. 1171–1182.
227. Bruzzone L., Prieto D. F. “An adaptive and semiparametric and context-based approach to unsupervised change detection in multitemporal remote sensing image”. IEEE Trans. Image Process. 11, 2002, pp. 452–466.
228. Rosin P. L., Ioannidis E. “Evaluation of global image thresholding for change detection”. Pattern Recognition Lett. 24, 2003, pp. 2345–2356.
229. Palevicius P., Ragulskis M., Janusas G., Palevicius A. “A technique for the reconstruction of a map of continuous curves from interference fringes”. Proc. of SPIE Vol. 9286 92861G-8, 2014.
230. Tan K.S., Nor Ashidi Mat Isa. “Color image segmentation using histogram thresholding – Fuzzy C-means hybrid approach”. Pattern Recognition 44, 2011, pp. 1–15.

231. Bhandari A. K., Singh V. K, Kumar A., Singh G. K. “Cuckoo search algorithm and wind driven optimization based study of satellite image segmentation for multilevel thresholding using Kapur’s entropy”. Expert Systems with Applications 41, 2014, pp. 3538–3560.
232. Horng M. H. “Multilevel thresholding selection based on the artificial bee colony algorithm for image segmentation”. Expert Systems with Applications 38, 2011, pp. 13785 – 13791.
233. Vala H. J., Baxi A. “A Review on Otsu Image Segmentation Algorithm”. International Journal of Advanced Research in Computer Engineering & Technology (IJARCET) Volume 2, Issue 2, February 2013, ISSN: 2278 – 1323.
234. Sathya P.D., Kayalvizhi R. “Modified bacterial foraging algorithm based multilevel thresholding for image segmentation”. Engineering Applications of Artificial Intelligence 24, 2011, pp. 595 – 615.
235. Barbieri A. L., De Arruda G.F., Rodrigues F. A., Bruno O. M., L. da Fontoura Costa. “An entropy based approach to automatic image segmentation of satellite images”, Physica A 390, 2011, pp. 512 - 518.
236. Tang K., Yuan X., Sun T., Yang J., Gao S. “An improved scheme for minimum cross entropy threshold selection based on genetic algorithm”. Knowledge-Based Systems 24, 2011, pp. 1131 - 1138.
237. Gao H., Wenbo X., Sun J., Tang Y. “Multilevel thresholding for image segmentation through an improved quantum-behaved particle swarm algorithm”. IEEE Transaction of Instrumentation and Measurement 59 (4), 2010, pp. 934 - 946.
238. Bazi Y, Bruzzone L., Melgani F. “Image thresholding based on the EM algorithm and the generalized Gaussian distribution”. Pattern Recognition 40, 2007, pp. 619 – 634.
239. Vila J. P., Schniter P. “Expectation-maximization Gaussian-mixture Approximate Message Passing”. IEEE, pp. 1 – 15.
240. Pham D. L., Xu Ch., Prince J. L. “A survey of current methods in medical image segmentation”. Annual Review of Biomedical Engineering, 1998, pp. 27.
241. Tomas R. “The nonparametric estimation of multivariate distribution density applying clustering procedures”. Vilnius, 2007, pp. 12 - 13.
242. Dempster A.P., Laird N.M., Rubin D.B. “Maximum likelihood from incomplete data via the EM algorithm”. Journal of the Royal Statistical Society, B, 39, 1997, pp. 1 – 38.
243. Everitt B. S., Hand D. J. “Finite Mixture Distribution”. NY: John Wiley, 1981, ISBN 0-387-95457-0.
244. Jordan M.I., Xu L. “Convergence results for the EM approach to mixtures of expert architectures”. Neural Networks, vol. 8, 1995, 1409 – 131.
245. McLachlan G. J., Krishnan T. “The EM Algorithm and Extensions”. NY: John Wiley, 1997, p. 400.
246. Render R. A., Walker H. F. “Mixture densities, maximum likelihood and the EM algorithm”. SIAM Rev, vol. 26, 1984, pp. 195 – 239.
247. Tsuda K., Akaho S., Asai K. “The EM algorithm for kernel matrix completion with auxiliary data”. The Journal of Machine Learning Research, vol. 4, no. 1, 2004, pp. 67 – 81.
248. Tian G. J., Xia Y, Zhang Y., Feng D. “Hybrid Genetic and Variational Expectation-Maximization Algorithm for Gaussian-Mixture-Model-Based Brain MR Image Segmentation”. IEEE transactions on information technology in biomedicine, vol. 15, no. 3, 2011, pp. 373 – 380.

249. Lee G., Scott C. “EM algorithms for multivariate Gaussian mixture models with truncated and censored data”. Computational Statistics and Data Analysis 56, 2012, pp. 2816 – 2829.
250. Drulyte I., Ruzgas T., Raisutis R., Valiukeviciene S., Linkeviciute G. “Application of automatic statistical post–processing method for analysis of ultrasonic and digital dermatoscopy images”. Libyan Journal of Medicine. 2018, vol. 13, iss. 1. doi: 10.1080/19932820.2018.1479600
251. Fawcett T. “An introduction to ROC analysis”. Pattern Recognition Letters 27, 2006, pp. 861–874.
252. Mets CE. “ROC methodology in radiologic imaging”. Invest Radiol, 1986, 21, pp. 720 - 733.
253. Zweig M. H., Campbell G. “Receiver-Operating Characteristic (ROC) Plots: A Fundamental Evaluation Tool in Clinical Medicine”. Clin. Chem. 39/4, 1993, pp. 561 – 577.
254. Metz Ch. E., Herman B. A., Shen J. “Maximum likelihood estimation of receiver operating characteristic (ROC) curves from continuously-distributed data”. Statist. Med. 17, 1198, pp. 1033 – 1053.
255. Obuchowski N. A. “Nonparametric Analysis of Clustered ROC Curve”. Biometrics, Vol. 53, No. 2, 1997, pp. 567 – 578.
256. Swets J. A., Pickett R. M. “Evaluation of Diagnostic Systems: Methods from Signal Detection Theory”. New York: Academic Press, 1982.
257. DeLong E. R., DeLong D. M., Clarke-Pearson D. L. “Comparing the Areas under Two or More Correlated Receiver Operating Characteristic Curves: A Nonparametric Approach”. Biometrics, Vol. 44, No. 3,1988, pp. 837- 845.
258. Albert A., Harris E. K. “Multivariate interpretation of clinical laboratory data”. New York: Marcel Dekker, Inc., 1987. SAS Institute Inc. SUGI supplemental library user’s guide, version 5 ed. Cary, NC: SAS Institute, 1986, p. 273.
259. Lusted L. B. “Logical analysis in Roentgen diagnosis”. Radiology, 74, 1960, pp. 178 – 193.
260. Lusted L. B. “Introduction to Medical Decision Making”. Thomas Springfield, IL, 1968.
261. Lusted L. B. “Decision-making studies in patient management”. New England Journal of Medicine, 284, 1971, pp. 416 – 424.
262. Lusted L. B. “Signal detectability and medical decision-making”. Science, 171, 1971, pp. 1217 - 1219.
263. Swets J. A. “Signal detection in medical diagnosis”. Computer Diagnosis and Diagnostic Methods, Thomas Springfield, IL, 1972, pp. 8 - 28.
264. McNeil B. J., Keeler E., Adelstein, S. J. “Primer on certain elements of medical decision making”. New England Journal of Medicine, 293, 1975, pp. 211 – 215.
265. McNeil B. J., Adelstein S. J. “Determining the value of diagnostic and screening tests”. Journal of Nuclear Medicine, 17, 1976, pp. 439 – 448.
266. Weinstein M. C., Fineberg H. V. “Clinical Decision Analysis”. Saunders, Philadelphia, 1980.
267. Griner P. F., Mayewski R. J., Mushlin A. I., Greenland P. “Selection and interpretation of diagnostic tests and procedures: principles and applications”. Annals of Internal Medicine, 94, 1981, pp. 553 - 592.
268. Robertson E. A., Zweig M. H., Van Steirtghem A. C. “Evaluating the clinical efficacy of laboratory tests”. American Journal of Clinical Pathology, 79, 1983, pp. 78 - 86.
269. Swets, J. A. “Measuring the accuracy of diagnostic systems”. Science, 240, 1988, pp. 1285 -1293.

270. Zweig M. H., Campbell G. “Receiver-operating characteristic (ROC) plots: a fundamental evaluation tool in clinical medicine”. Clinical Chemistry, 39, 1993, pp. 561 - 577.
271. Wan Sh., Zhang B. “Smooth semiparametric receiver operating characteristic curves for continuous diagnostic tests”. Statist. Med. 2007; 26, pp. 2565 – 2586.
272. Alemayehu D., Zou K. H. “Applications of ROC Analysis in Medical Research: Recent Developments and Future Directions”. Academic Radiology, Vol 19, No 12, 2012 pp. 1457 – 1464.
273. Zou K. H., O’Malley A. J., Mauri L. “Receiver-Operating Characteristic Analysis for Evaluating Diagnostic Tests and Predictive Models”. Circulation. 2007, 115, pp. 654 -657.
274. Pencina M. J., D’Agostino R. B., Vasan R. S. “Evaluating the added predictive ability of a new marker: From area under the ROC curve to reclassification and beyond”. Statist. Med. 2008, 27, pp. 157 – 172.
275. Li J., Fine J. P. “ROC analysis with multiple classes and multiple tests: methodology and its application in microarray studies”. Biostatistics, 2008, 9, 3, pp. 566 – 576.
276. Ishwaran H., Gatsonis C. A. “A general class of hierarchical ordinal regression models with applications to correlated ROC analysis”. The Canadian Journal of Statistics, vol. 28, 2000, pp. 731 – 750.
277. Goodenough D. J., Rossmann K., Lusted L. B. “Radiographic applications of signal detection tTheory”. Radiology, 105, 1972, 199 – 200.
278. Goodenough D. J., Rossmann K., Lusted L. B. “Radiographic applications of receiver operating characteristic (ROC) analysis”. Radiology, 110, 1974, pp. 89 – 95.
279. Metz C. E. “Basic principles of ROC analysis”. Seminars in Nuclear Medicine, 8, 1978, pp. 283 – 298.
280. Swets J. A. “ROC analysis applied to the evaluation of medical imaging techniques”. Investigative Radiology, 14, 1979, 109 – 121.
281. Swets J. A., Pickett R. M. “Evaluation of Diagnostic Systems: Methods from Signal Detection theory”. Academic Press, New York, 1982.
282. Metz C. E. “ROC methodology in radiologic imaging”. Investigative Radiology, 21, 1986, pp. 720 – 733.
283. Metz C. E. “Some practical issues of experimental design and data analysis in radiological ROC studies”. Investigative Radiology, 24, 1989, pp. 234 – 245.
284. Hanley J. A. “Receiver operating characteristic (ROC) methodology: the state of art”. CRC Critical Reviews in Diagnostic Imaging, 29, 1989, pp. 307 – 335.
285. Hanley J. A., McNeil B. J. “The Meaning and Use of the Area under a Receiver Operating Characteristic (ROC) Curve”. Radiology 143, 1982, pp. 29-36.
286. McNeil B. J., Hanley J.A., Funkenstein H. H., Wallman J. “The use of paired ROC curves in studying the impact of history on radiography interpretation. CT of the head as a case study”. Radiology 149, 1983, pp. 75-77.
287. Duncan J. S., Ayache N. “Medical Image Analysis: Progress over Two Decades and the Challenges Ahead”. IEEE Transactions on pattern analysis and machine intelligence, vol. 22, no. 1, 2000, pp. 85 – 106.
288. Dreiseit S., Ohno-Machado L., Kittler H., Vinterbo S., Billhardt H., Binder M. “A Comparison of Machine Learning Methods for the Diagnosis of Pigmented Skin Lesions”. Journal of Biomedical Informatics 34, 2001, pp. 28 – 36.
289. Deichmann M., Kahle B., Moser K., Wacker J., Wu K. “Diagnosing melanoma patients entering American Joint Committee on Cancer stage IV, C-reactive protein in serum is superior to lactate dehydrogenase”. British Journal of Cancer, 2004, 91, pp. 699 – 702.

290. Findeisen P., Zapatka M., Peccerella T., Matzk H., Neumaier M., Schadendorf D., Ugurel S. “Serum Amyloid A As a Prognostic Marker in Melanoma Identified by Proteomic Profiling”. J Clin Oncol, 27, 2009, pp. 2199 - 2208.
291. Haniffa M.A., Lloyd J. J., Lawrence C. M. “The use of a spectrophotometric intracutaneous analysis device in the real-time diagnosis of melanoma in the setting of a melanoma screening clinic”.British Journal of Dermatology, 2007 156, pp. 1350 – 1352.
292. Henning J. S., Dusza S. W., Wang S. Q., Marghoob A. A., Rabinovitz H. S., Polsky D., Kopf A. W. “The CASH (color, architecture, symmetry, and homogeneity) algorithm for dermoscopy”. J Am Acad Dermatol, 2007, 56, pp. 45 - 52.
293. Lui H., Zhao J., McLean D., et al. “Real-time Raman Spectroscopy for In Vivo Skin Cancer Diagnosis”. Cancer Res, 2012, 72, pp. 2491 - 2500.
294. Pellacani G., Cesinaro A. M., Seidenari S. “Reflectance - mode confocal microscopy of pigmented skin lesions improvement in melanoma diagnostic specificity”. J Am Acad Dermatol, 2005, 53, pp. 979 - 985.
295. Sonego P., Kocsor A., Pongor S. “ROC analysis: applications to the classification of biological sequences and 3D structures”. Briefings in bioinformatics, vol 9. no 3, 2008, pp. 198 - 209.
296. Stoecker W. V., Gupta K., Stanley R. J., Moss R. H., Shrestha B. “Detection of asymmetric blotches (asymmetric structureless areas) in dermoscopy images of malignant melanoma using relative color”. Skin Research and Technology, 2005, 11, pp. 179 – 184.
297. Stoecker W. V. et al. “Detection of granularity in dermoscopy images of malignant melanoma using color and texture features”. Computerized Medical Imaging and Graphics, 35, 2011, pp. 144 – 147.
298. Edgeworth, F. Y. “On methods of ascertaining variations in the rate of births, deaths and marriages”. Journal of the Royal. Statistical Society, 48, 1985, pp. 628-649.
299. Brown, F.E. “Marketing Research: A Structure for Decision Making”. Addison Wesley: Reading, Massachusetts, USA, 1980, ISBN: 0-8442-3443-5
300. Parasuraman A. “Customer-oriented corporate cultures are crucial to services marketing success”. Journal of Services Marketing, 1987, pp. 139 - 146.
301. Wald A. “Tests of statistical hypotheses concerning several parameters when the number of observations is large”. Transactions of the American Mathematical Society 54, 1943, pp. 426 - 482.
302. Cox M. G., Harris P. M. "Measurement uncertainty and traceability", Meas. Sci. Technol. 17, 2006, pp. 533 – 540.
303. “Guide to the Expression of Uncertainty in Measurement, International Organization for Standardization”. 1995, ISBN 92-67r-r10188-9.
304. Sousa J A, Ribeiro A S. “The choice of method to the evaluation of measurement uncertainty in metrology”. ISBN 978-963-88410-0-1, 2009, Imeko, pp. 2388 – 2393.
305. Taylor B. N., Kuyatt Ch. E. NIST Technical Note 1297, 1994. Edition Guidelines for Evaluating and Expressing the Uncertainty of NIST Measurement Results NIST Technical Note 1297 1994 Edition Guidelines for Evaluating and Expressing the Uncertainty of NIST Measurement Results, 1994.
306. High R. “Plotting Differences among LSMEANS in Generalized Linear Models”. http://support.sas.com/resources/papers/proceedings14/1902-2014.pdf , pp. 1902 – 2014.
307. Julious S. A. “Using confidence intervals around individual means to assess statistical significance between two means”. Pharmaceutical Statistics, Vol. 3, 2004, pp. 217 – 222.
308. Goss S.A., Johnston R.L., Dunn F. 2Compilation of empirical ultrasonic properties of mammalian tissues”. J Acoust Soc, 1980, 68, pp. 93 – 108.

309. Escoffier C., Querleux B., De Rigal J. et al.” In vitro study of the velocity of ultrasound in the skin”. Bioeng Skin 1986, pp. 87 – 94.
310. Weichenthal M., Mohr P., Breitbart E. W. “The velocity of ultrasound in human primary melanoma tissue - implications for the clinical use of high resolution sonography”. BMC Dermatol. 2001, 1, doi: 10.1186/1471-5945-1-1.
311. Weichenthal M., Mohr P., Breitbart E. W. “The velocity of ultrasound in human primary melanoma tissue - implications for the clinical use of high resolution sonography”. BMC Dermatology, 2001, DOI: 10.1186/1471-5945-1-1.
312. Andria G., Savino M., Trotta A. “Windows and Interpolation Algorithms to Improve Electrical Measurement Accuracy”. 1989. 38(4), p. 856 – 863. DOI: 10.1109/19.31004.
313. BIPM, IEC, IFCC, ISO, IUPAC, IUPAP and OIML. Guide to the expression of uncertainty in measurement, 2006.
314. EA-4 / 02 M: 2013 Evaluation of the Uncertainty of Measurement in Calibration, 2013 (European accreditation source).

APPENDIX 1. ULTRASONIC AND DIGITAL DERMATSOCOPY IMAGES

Ultrasonic B-scan images (raw and processed) of skin melanoma, axes are in millimetres (1-pixel value for length is 0.033 mm, for depth – 0.0079 mm): ultrasonic raw B-scan image, binary B-scan image, detected informative region are presented in order.

IF011_5

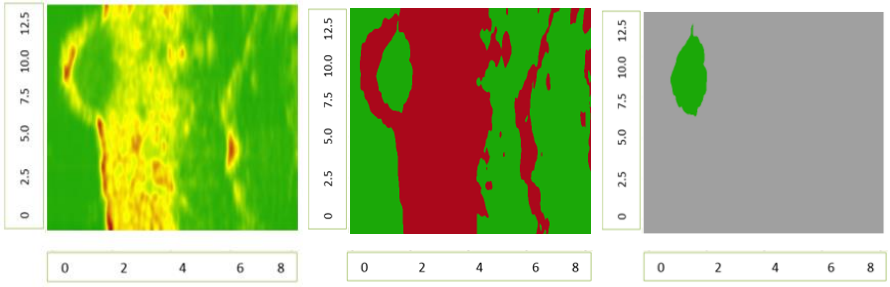

IF016

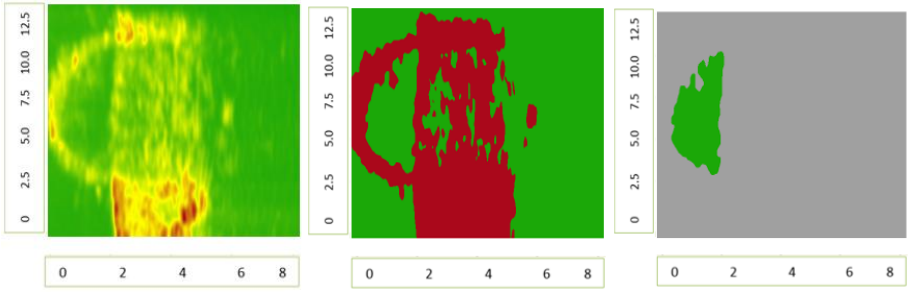

IF018_6

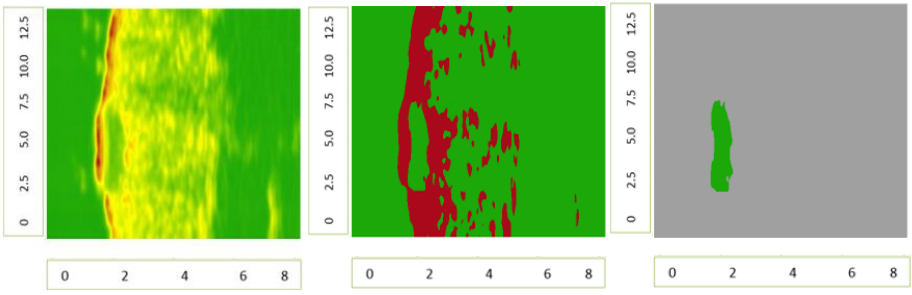

IF019

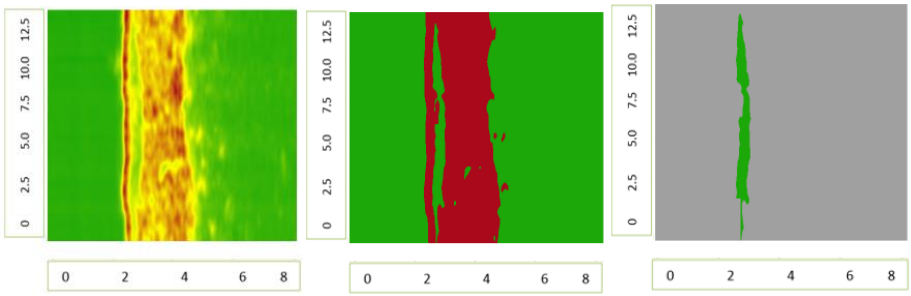

IF021

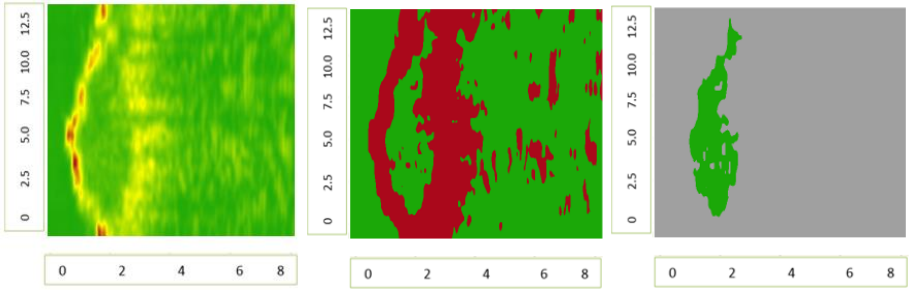

IF023

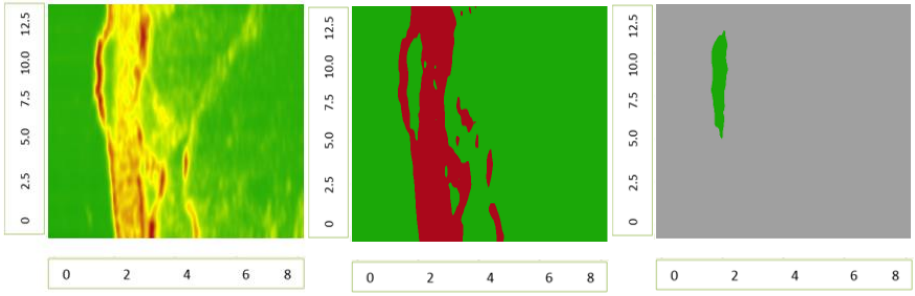

IF024

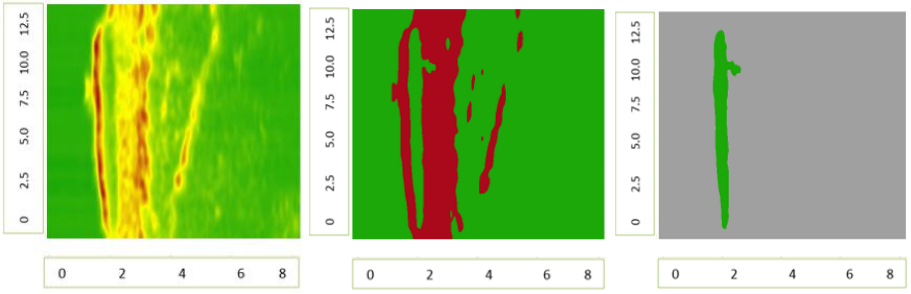

IF025

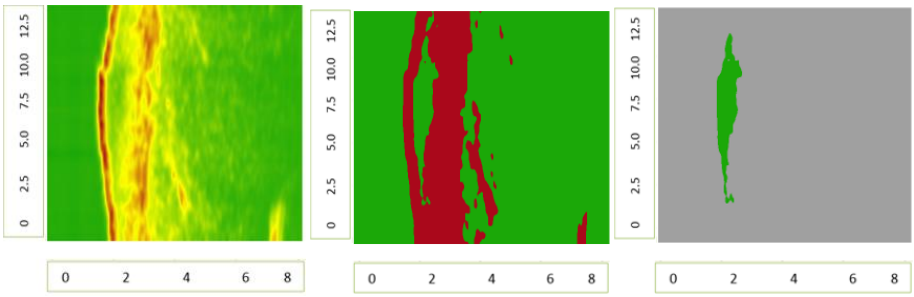

IF026_3

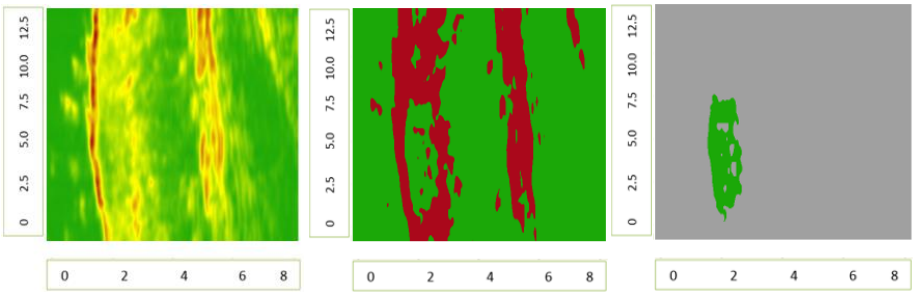

IF031

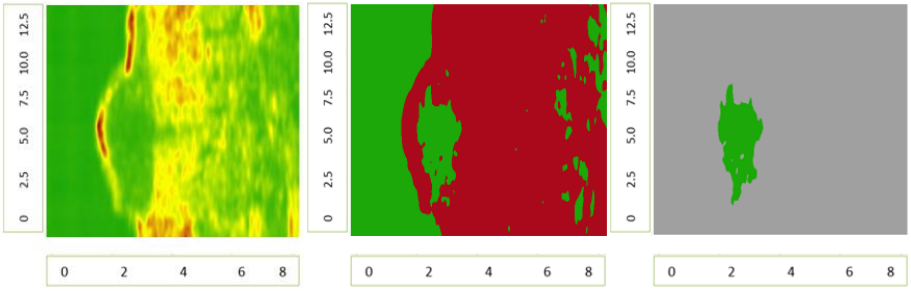

IF034

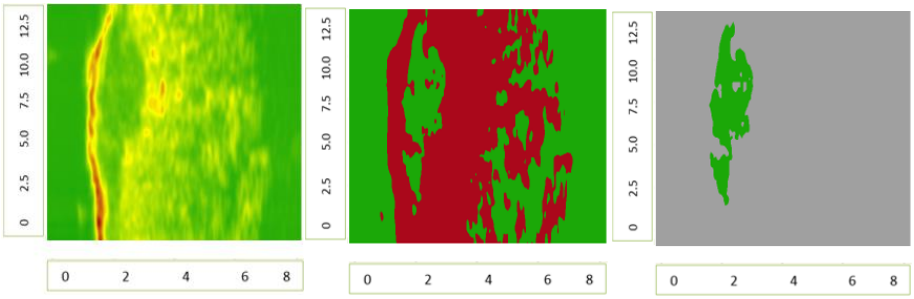

IF042

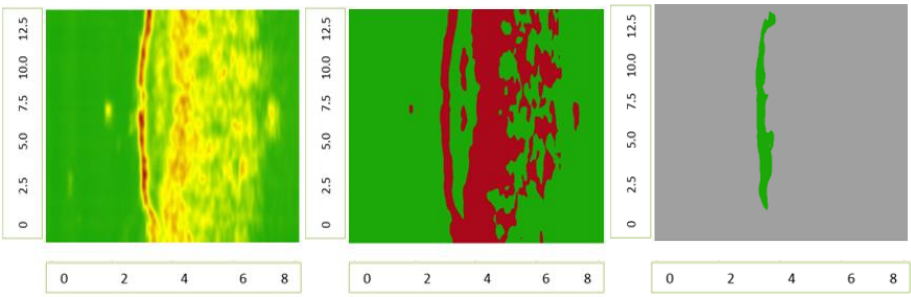

IF043

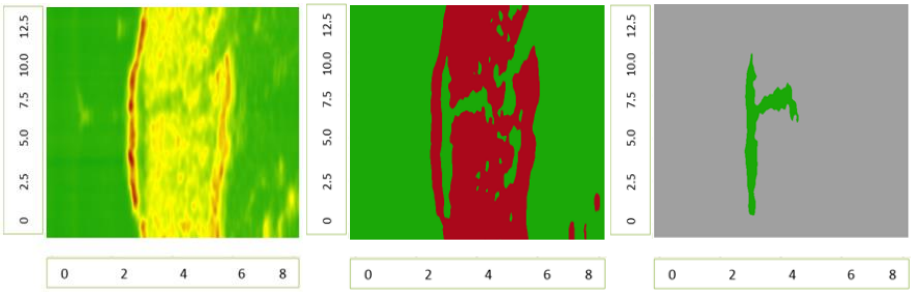

IF044

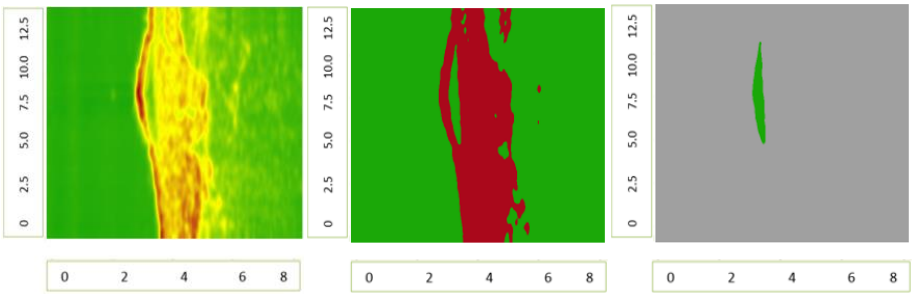

IF046

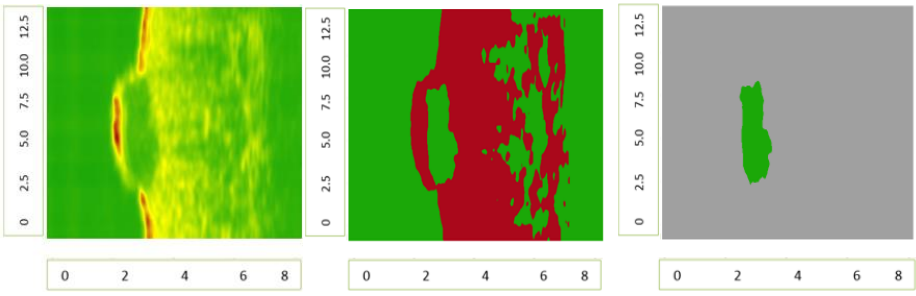

IF047

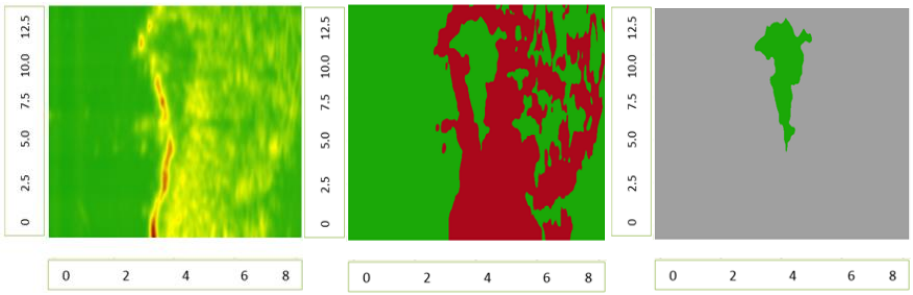

IF048

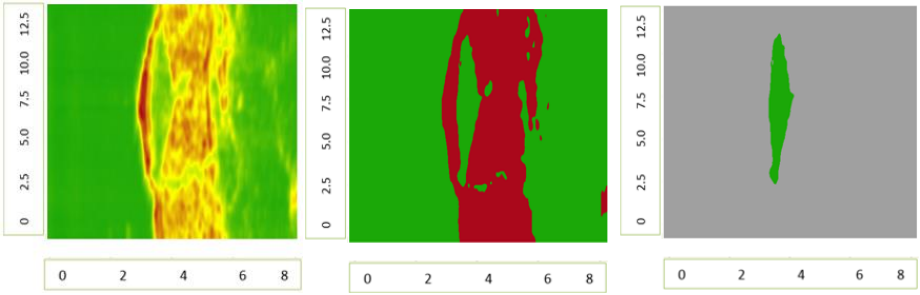

IF049

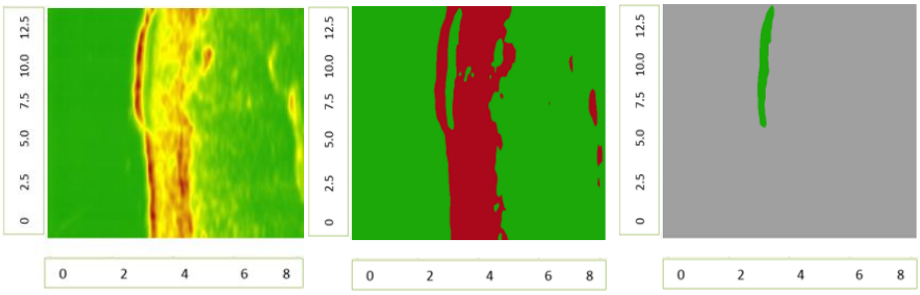

IF053

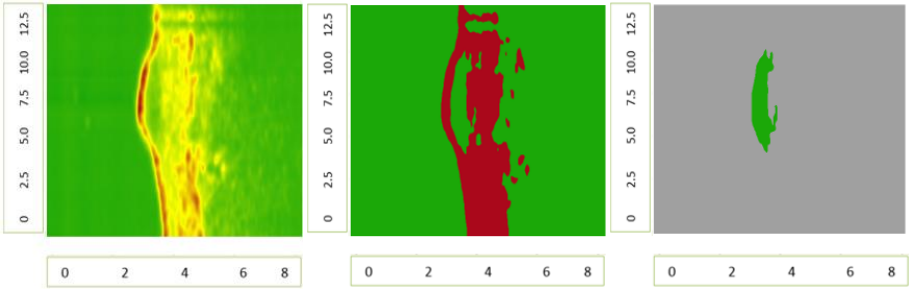

Digital Dermatoscopy Images (raw and processed) of skin melanoma, axes are in millimetres (1-pixel value 0.0071 mm): raw optical image, binary optical image, detected informative region are presented in order.

IF011_11g

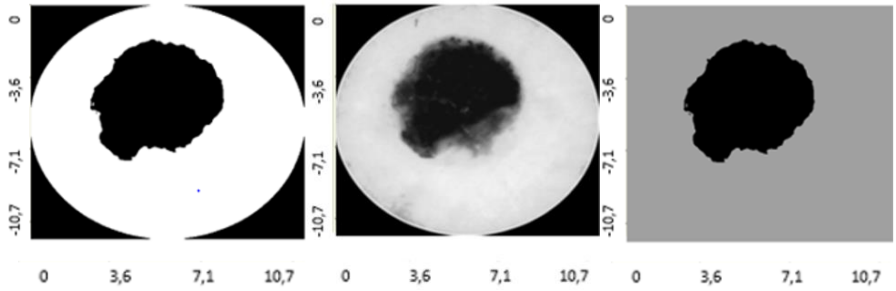

IF016_1g_hr

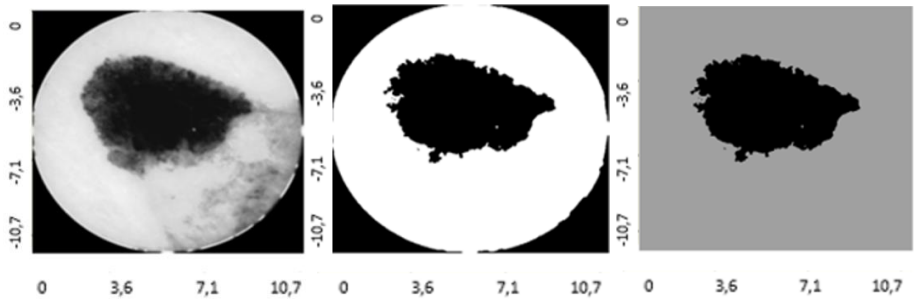

IF018_5g

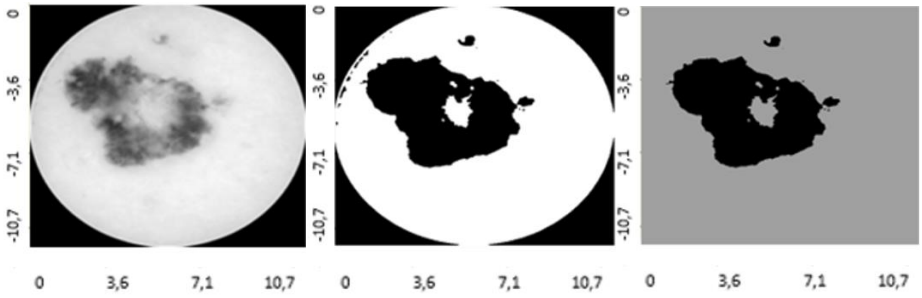

IF019_11g

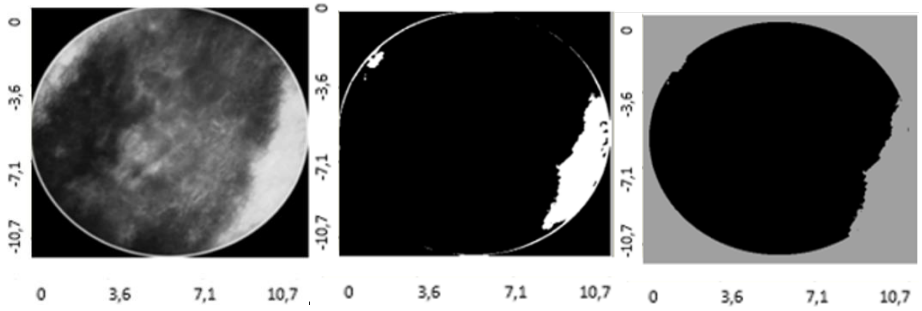

IF021_1g_hr

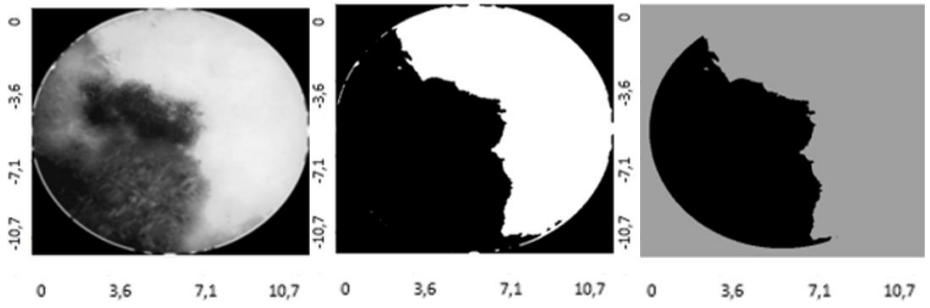

IF023_11g

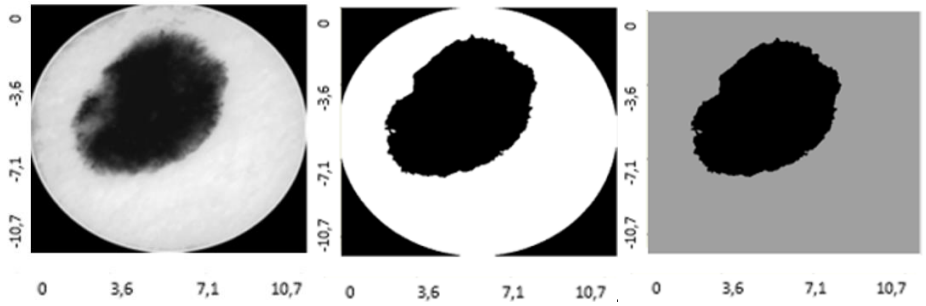

IF024_11g

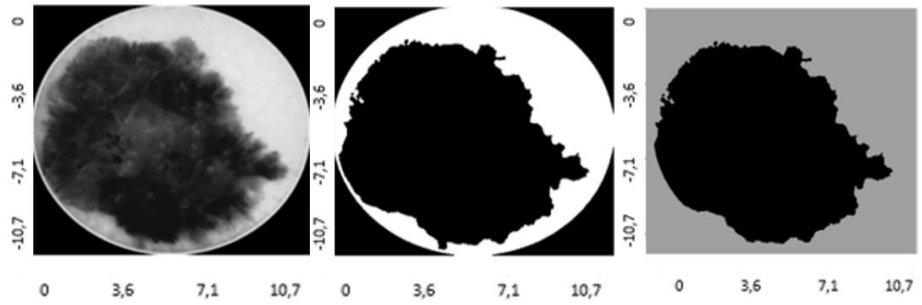

IF025_11g

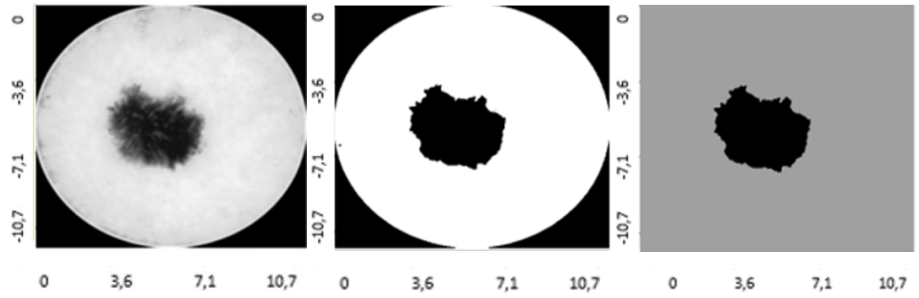

IF026_1g_hr

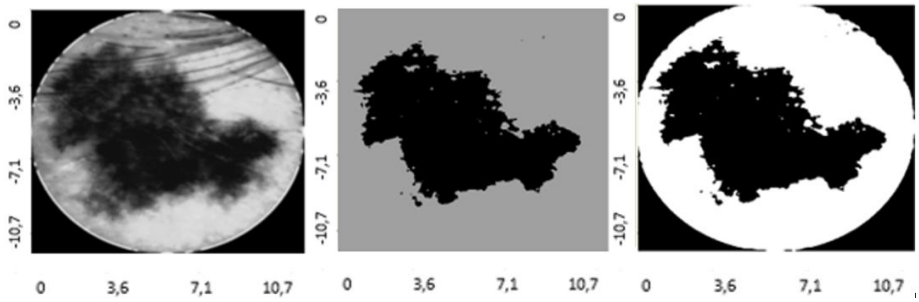

IF031_1g_hr

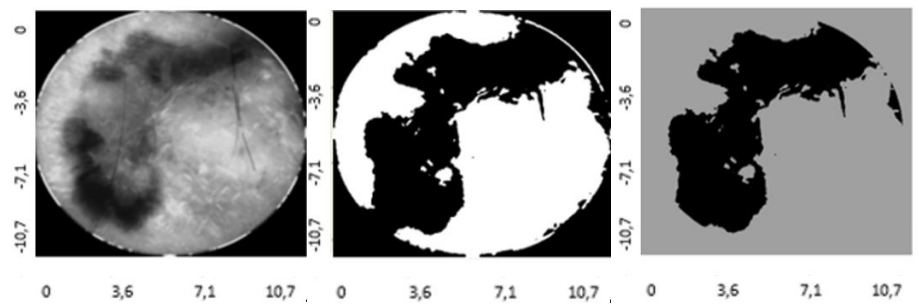

IF034_1g

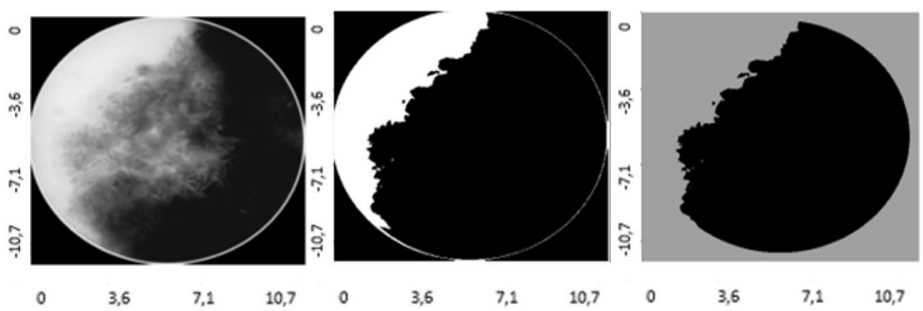

IF042_1g_hr

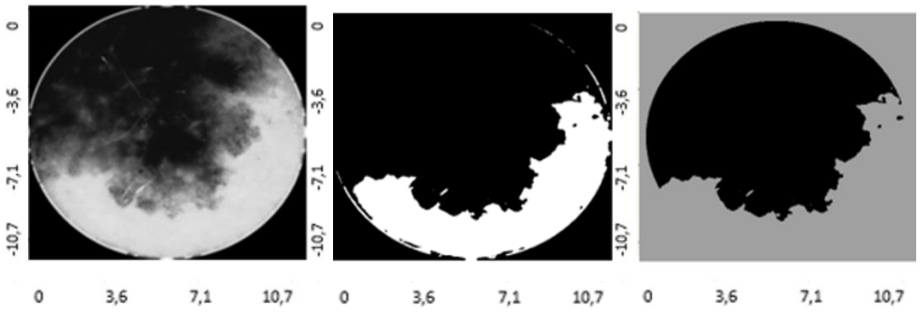

IF043_11g

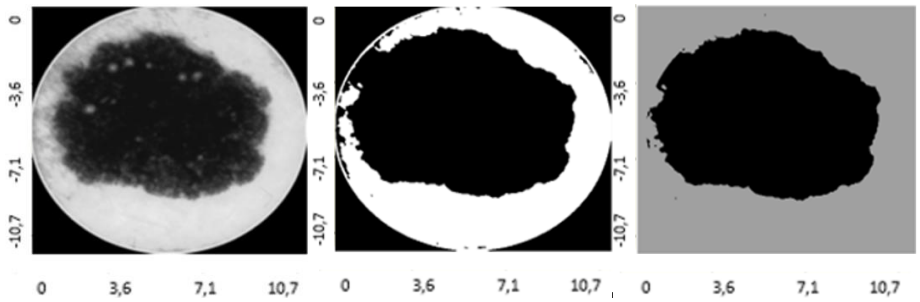

IF044_6g

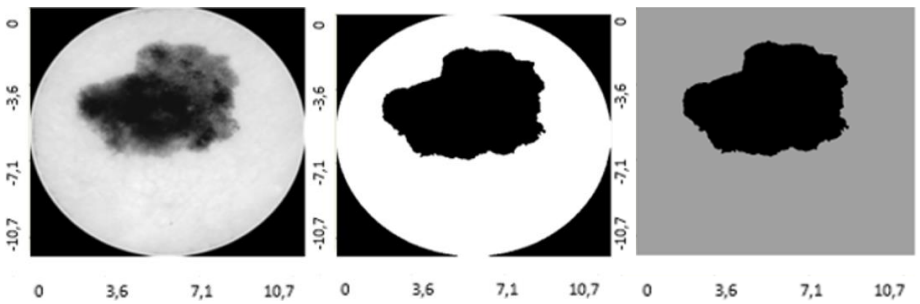

IF046_10g

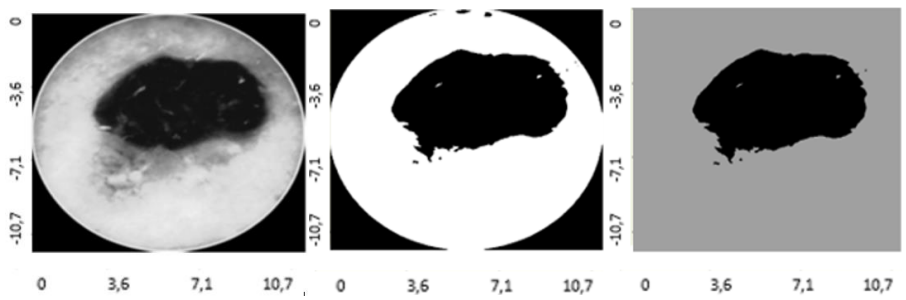

IF047_11

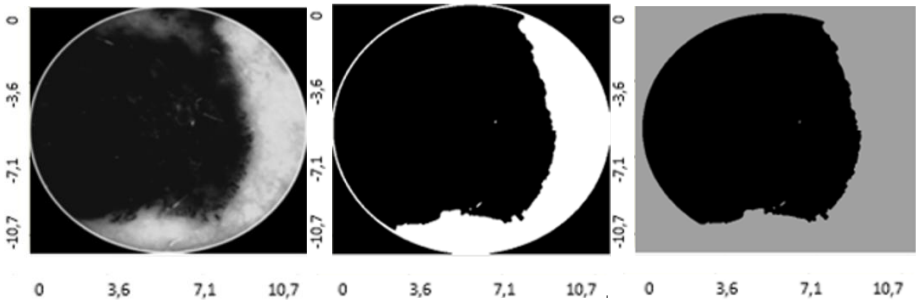

IF048_1g_hr

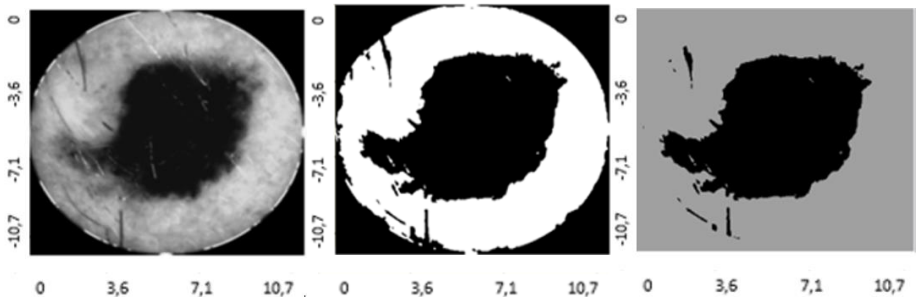

IF049_1g

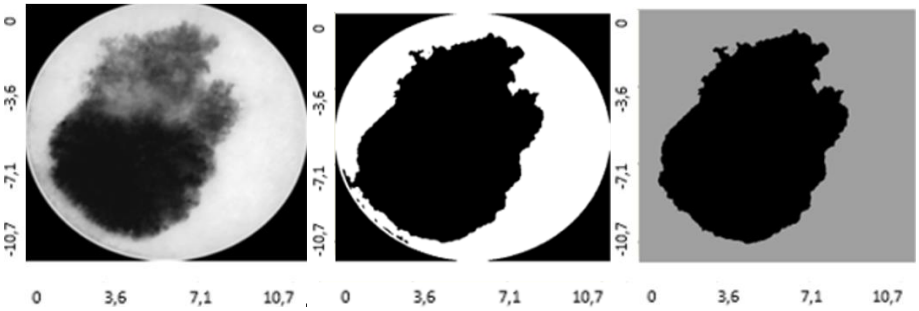

IF053_11g

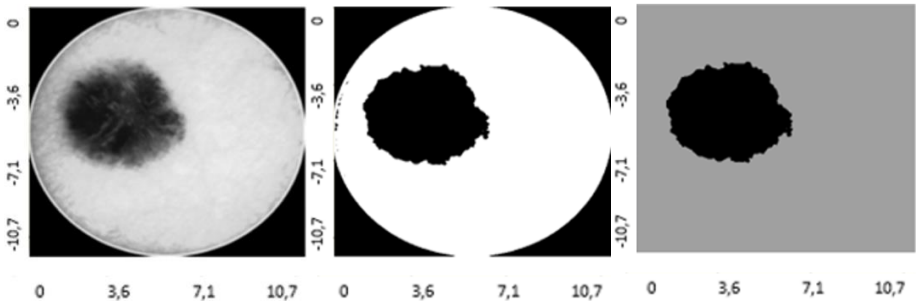

Ultrasonic B-scan images (raw and processed) of benign nevus, axes are in millimetres (1-pixel value for length is 0.033 mm, for depth – 0.0079 mm): ultrasonic raw B-scan image, binary B-scan image, detected informative region are presented in order.

IF009_2

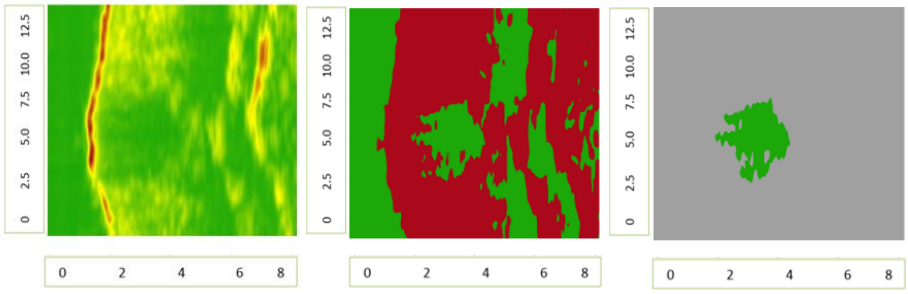

IF013_5

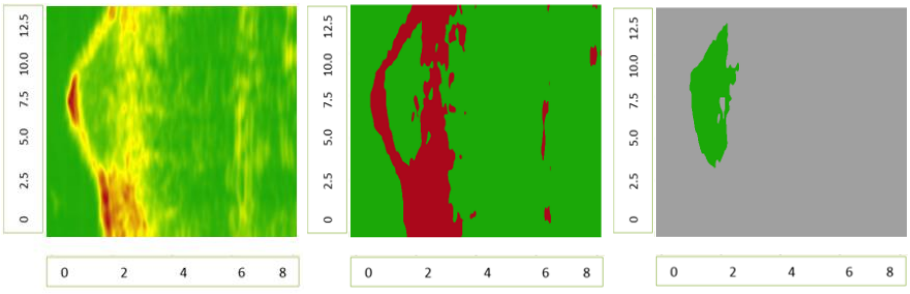

IF014_3

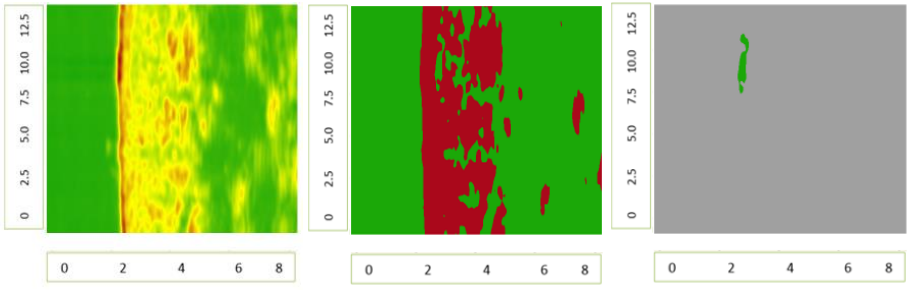

IF029

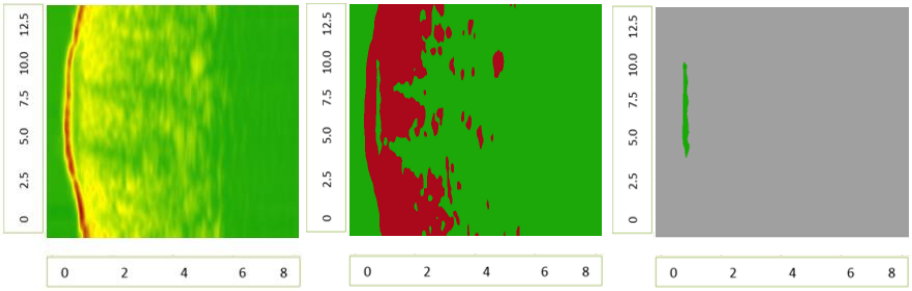

IF030

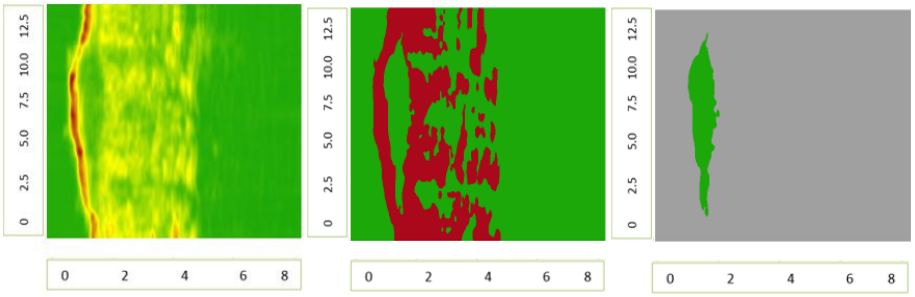

IF032_4

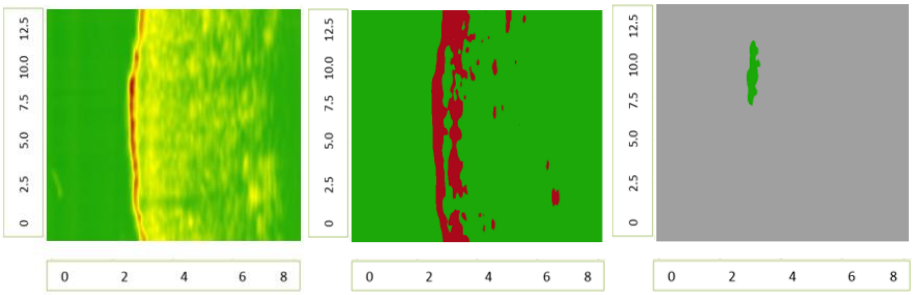

IF033

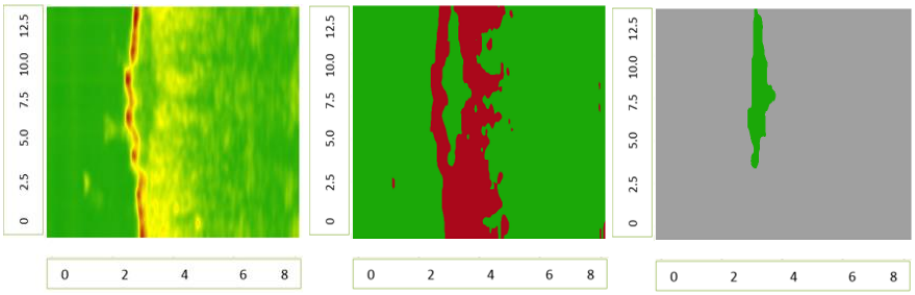

IF037

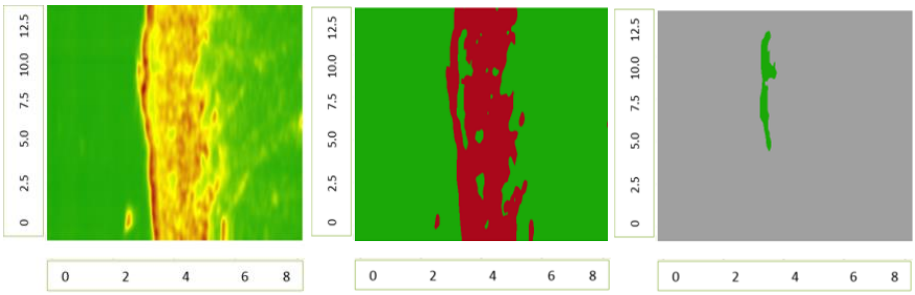

IF038

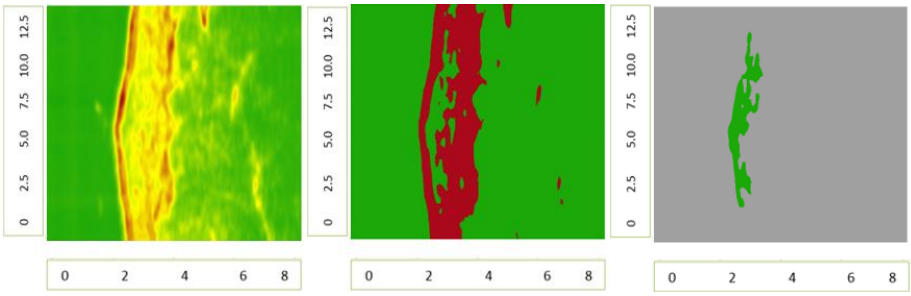

IF039

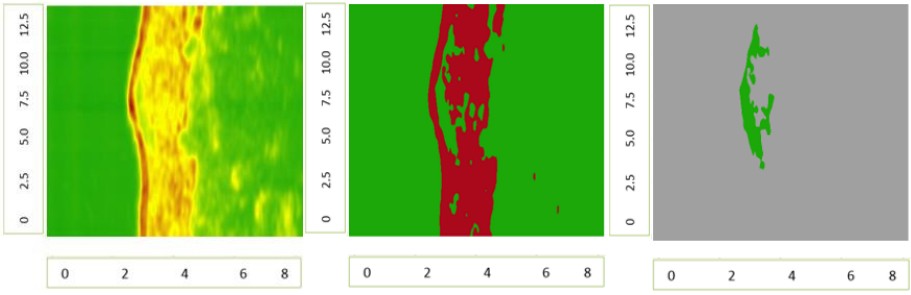

IF045

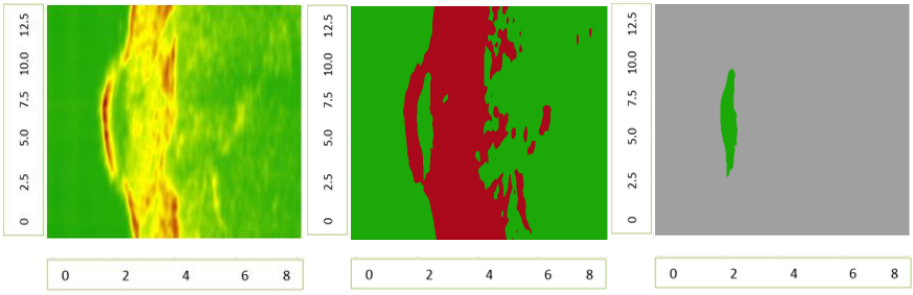

IF052

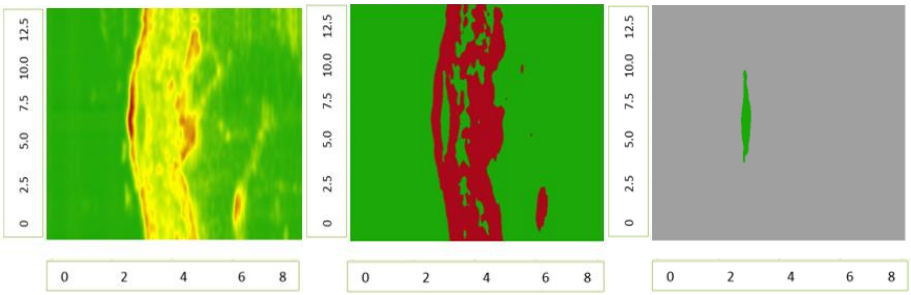

Digital Dermatoscopy Images (raw and processed) of benign nevus, axes are in millimetres (1-pixel value 0.0071 mm): raw optical image, binary optical image, detected informative region are presented in order.

IF009_1g_hr

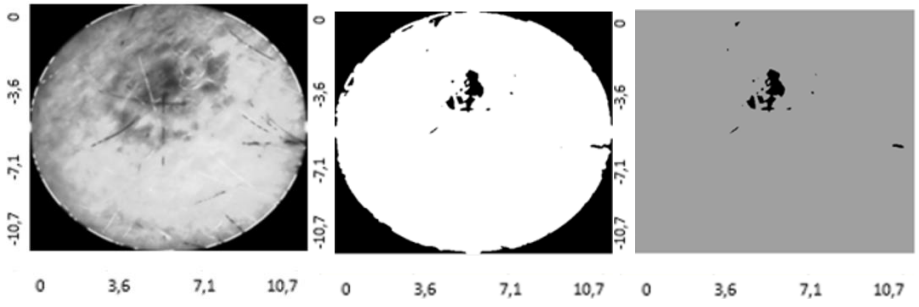

IF013_11g

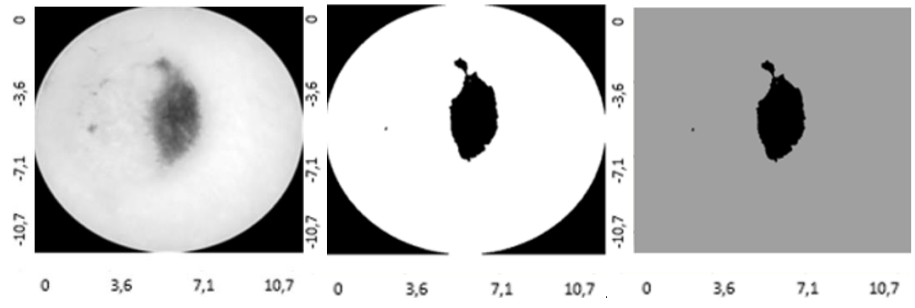

IF014_10g

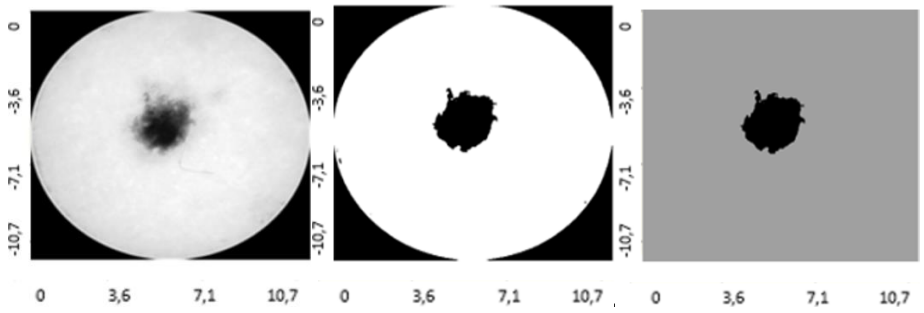

IF029_11g

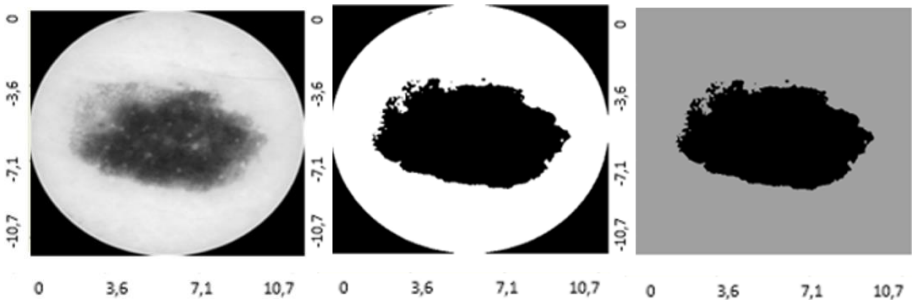

IF030_6g

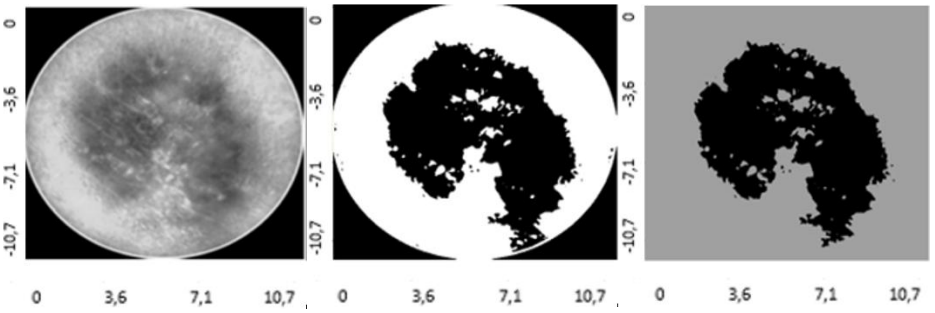

IF032_11g

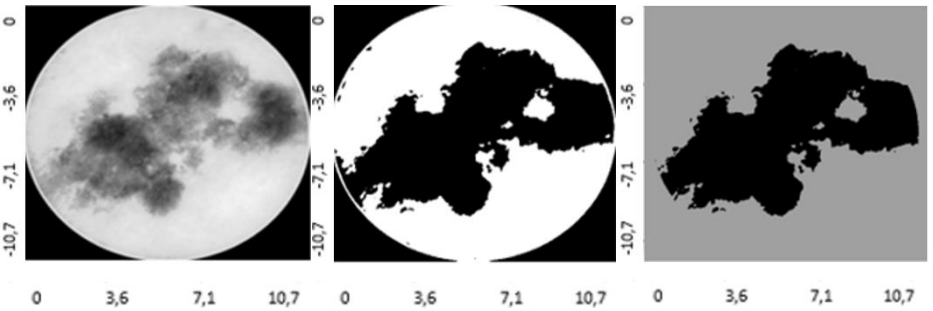

IF033_11g

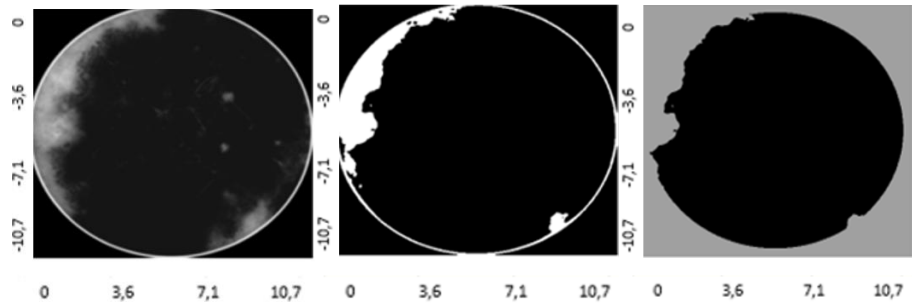

IF037_1g_hr

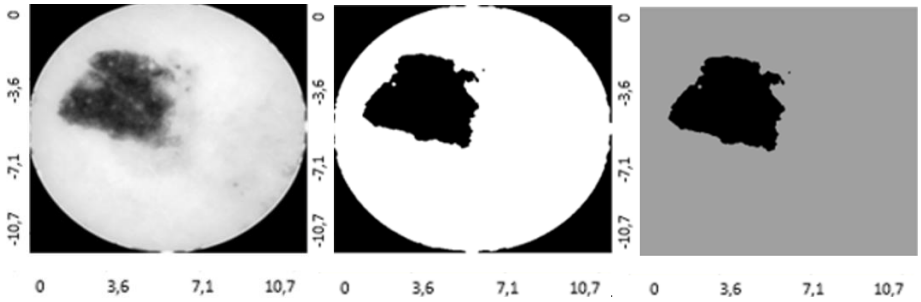

IF038_6g

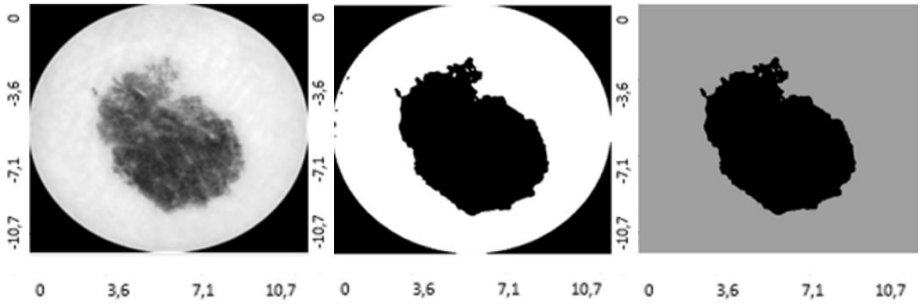

IF039_1g

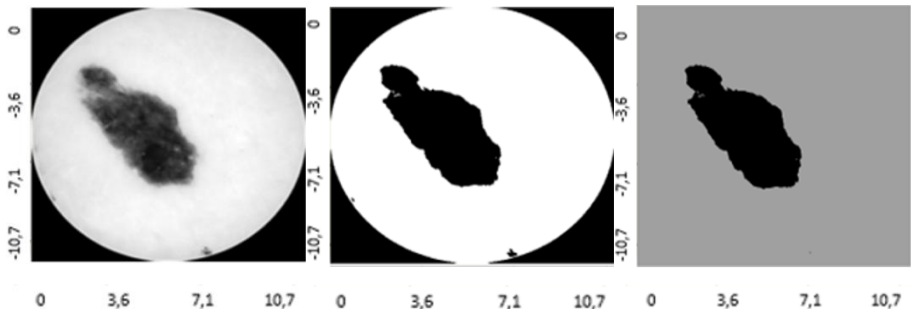

IF045_6g

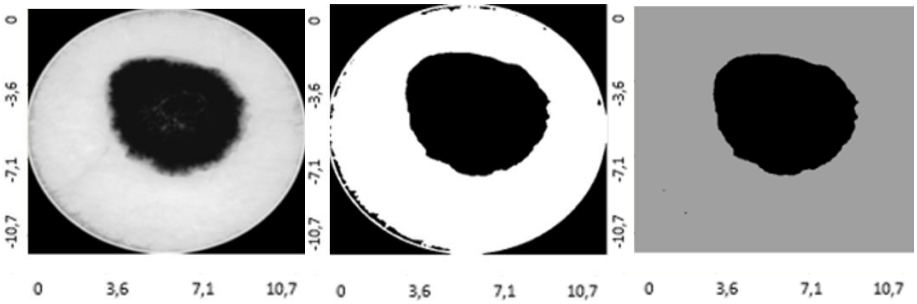

IF052_1g_hr

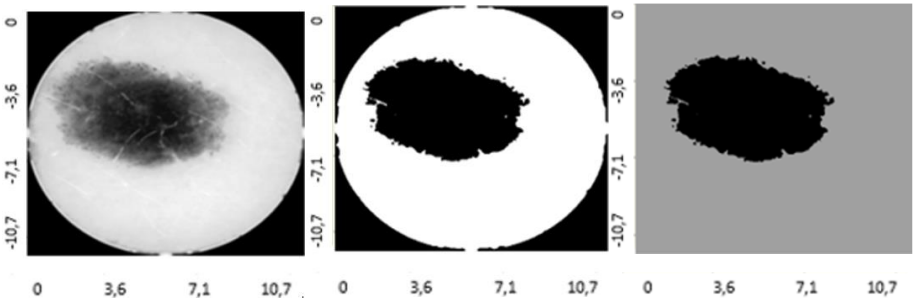

APPENDIX 2. DISTRIBUTIONS OF THE SIGNIFICANT PARAMETERS OF ULTRASONIC AND DIGITAL DERMATOSCOPY IMAGES

Fig. 1. – Fig. 5. represent the distributions of the significant parameters that are evaluated from the ultrasonic images by using the discriminant analysis model. Fig. 6. – Fig. 22. represent the distributions of the significant parameters that are evaluated from the digital dermatoscopy images by using the discriminant analysis model. Fig. 23. – Fig. 24. represent the distributions of the significant parameters that are evaluated from the ultrasonic images by using the logistic regression model. Fig. 25. – Fig. 26. represent the distributions of the significant parameters that are evaluated from the digital dermatoscopy images by using the logistic regression model.

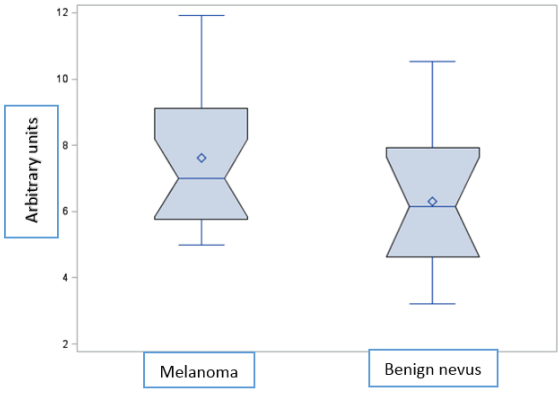

Fig. 1. Distribution of the maximum width by diagnosis evaluated from the ultrasonic images by using the discriminant analysis model. Mean of the maximum width for melanomas was equal to 7.621 millimetres, while mean of the maximum width for benign nevus was equal to 6.306 millimetres. Standard deviation for melanomas was equal to 2.089 millimetres, for benign nevus – 2.268 millimetres.

Diamonds show the mean of the maximum width of melanomas and benign nevus. For the melanomas, more observations are lower than the mean. For the benign nevus, more values are around the mean of maximum length.

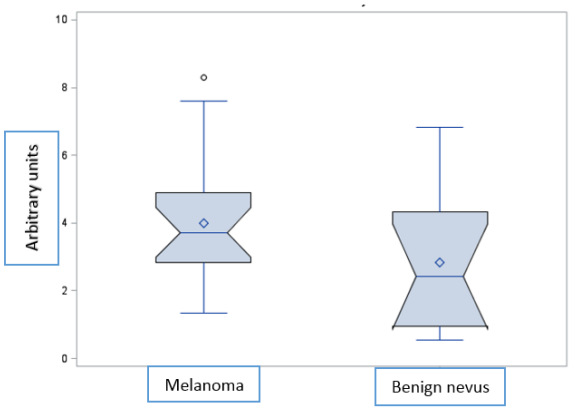

Fig. 2. Distribution of the area by diagnosis evaluated from the ultrasonic images by using the discriminant analysis model. Mean of the area for melanomas was equal to 3.997 squared millimetres, while mean of the area for benign nevus was equal to 2.845 squared millimetres. Standard deviation for melanomas was equal to 1.844 squared millimetres, for benign nevus – 2.111 squared millimetres.

Diamonds show the mean of the area. For melanomas and benign nevus, more values of the area are distributed under the mean.

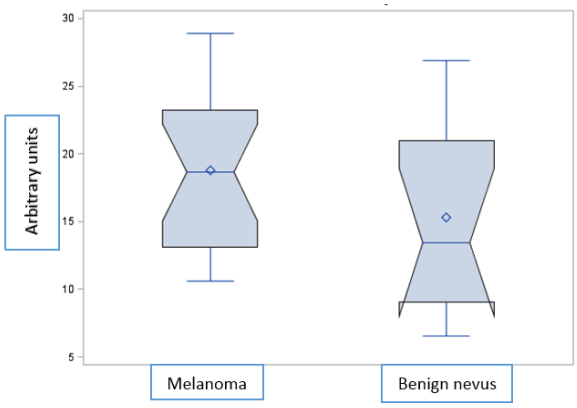

Fig. 3. Distribution of the perimeter by diagnosis evaluated from the ultrasonic images by using the discriminant analysis model. Mean of the perimeter for melanomas was equal to 18.761 millimetres, while mean of the perimeter for benign nevus was equal to 15.318 millimetres. Standard deviation for melanomas was equal to 5.773 millimetres, for benign nevus –7.385 millimetres.

Diamonds show the mean of the perimeter. The values of observations of melanoma are very close to the mean. In the case of the benign nevus, more values of area of observations are less than the mean.

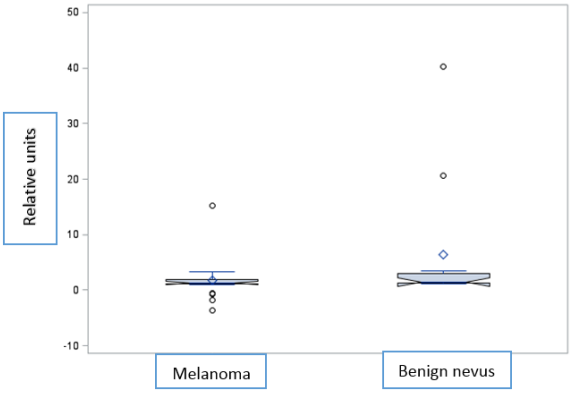

Fig. 4. Distribution of the ratio of average kurtosis (from 1000 directions) and maximum kurtosis by diagnosis evaluated from the ultrasonic images by using the discriminant analysis model. Mean of the ratio of average kurtosis (from 1000 directions) and maximum kurtosis for melanomas was equal to 1.711, while mean of the ratio of average kurtosis (from 1000 directions) and maximum kurtosis for benign nevus was equal to 6.463. Standard deviation for melanomas was equal to 3.562, for benign nevus – 11.962.

Diamonds show the mean of the ratio of average kurtosis (from 1000 directions) and maximum kurtosis by diagnosis. In the case of melanoma, more values are above the mean, while more values for the benign nevus are under the mean.

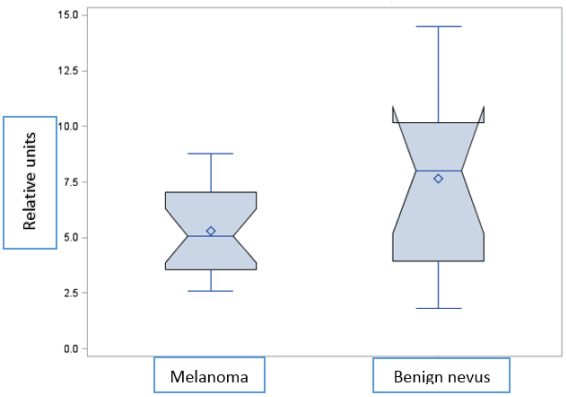

Fig. 5. Distribution of the ratio of perimeter and area by diagnosis evaluated from the ultrasonic images by using the discriminant analysis model. Mean of the ratio of perimeter and area for melanomas was equal to 5.290, while mean of the ratio of perimeter and area for benign nevus was equal to 7.670. Standard deviation for melanomas was equal to 1.962, for benign nevus – 4.048.

Diamonds show the mean of the ratio of perimeter and area. For melanomas, more values are distributed around the mean, while for benign nevus more values are above the mean.

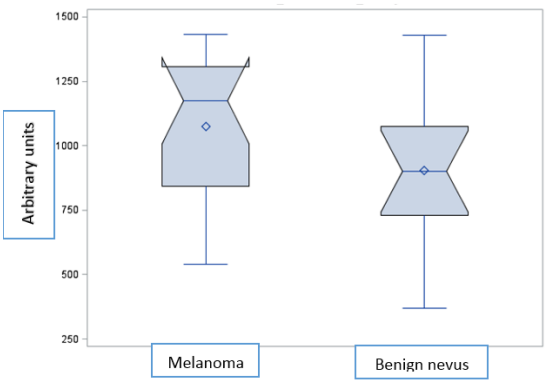

Fig. 6. Distribution of the average diameter by diagnosis evaluated from the digital dermatoscopy images by using the discriminant analysis model. Mean of the average diameter for melanomas was equal to 1074.410 millimetres, while mean of the average diameter for benign nevus was equal to 908.855 millimetres. Standard deviation for melanomas was equal to 273.421 millimetres, for benign nevus – 284.260 millimetres.

Diamonds show the mean of the average diameter. In the case of melanoma, a lot of the values are located above the mean, while the values for benign nevus are pretty much the same as the mean.

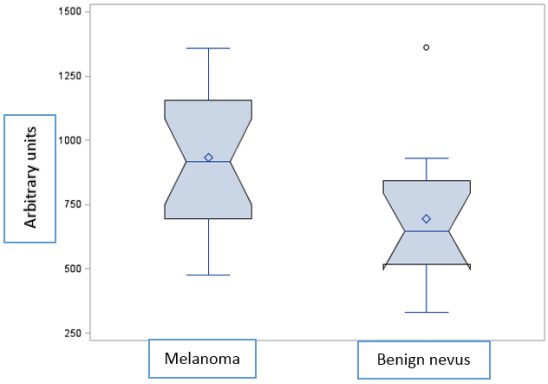

Fig. 7. Distribution of the minimum diameter by diagnosis evaluated from the digital dermatoscopy images by using the discriminant analysis model. Mean of the minimum diameter for melanomas was equal to 932.058 millimetres, while mean of the minimum diameter for benign nevus was equal to 695.872 millimetres. Standard deviation for melanomas was equal to 260.188 millimetres, for benign nevus – 275.939 millimetres.

Diamonds show the mean of the minimum diameter. For the melanomas, more values of parameter are distributed around the mean. Looking at the distribution of the benign nevus, more values are under the mean.

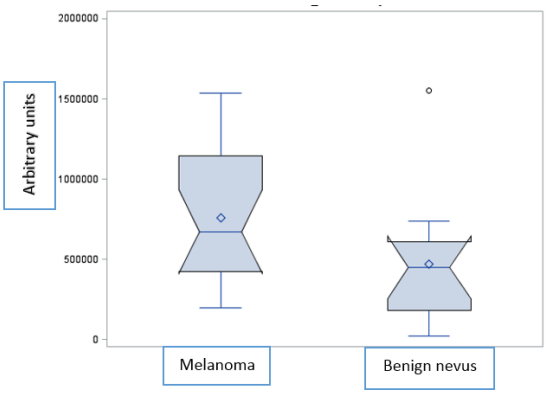

Fig. 8. Distribution of the area by diagnosis evaluated from the digital dermatoscopy images by using the discriminant analysis model. Mean of the area for melanomas was equal to 759201.740 squared millimetres, while mean of the area for benign nevus was equal to 470307.330 squared millimetres. Standard deviation for melanomas was equal to 388217.870 squared millimetres, for benign nevus – 412327.460 squared millimetres.

Diamonds show the mean of the area. For both types of the tumours, more values are less than the mean, but for the melanomas there are more observations that are under the mean.

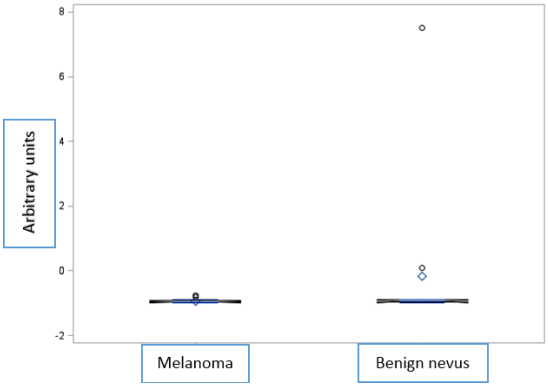

Fig. 9. Distribution of the average kurtosis (from 1000 directions) by diagnosis evaluated from the digital dermatoscopy images by using the discriminant analysis model. Mean of the average kurtosis (from 1000 directions) for melanomas was equal to -0.930 millimetres, while mean of the average kurtosis (from 1000 directions) for benign nevus was equal to -0.157 millimetres. Standard deviation for melanomas was equal to 0.075 millimetres, for benign nevus – 2.435 millimetres.

Diamonds show the mean of the average kurtosis (from 1000 directions). In the case of melanoma, the values are distributed very closely to the mean, while more observations of the benign nevus are below the mean.

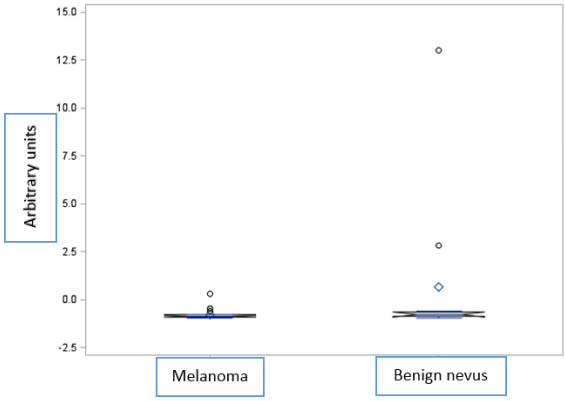

Fig. 10. Distribution of the maximum kurtosis by diagnosis evaluated from the digital dermatoscopy images by using the discriminant analysis model. Mean of the maximum kurtosis for melanomas was equal to -0.762 millimetres, while mean of the maximum kurtosis for benign nevus was equal to 0.651 millimetres. Standard deviation for melanomas was equal to 0.291 millimetres, for benign nevus – 4.036 millimetres.

Diamonds show the mean of the maximum kurtosis. In the case of melanoma, the values are distributed very closely to the mean, while more observations of the benign nevus are below the mean.

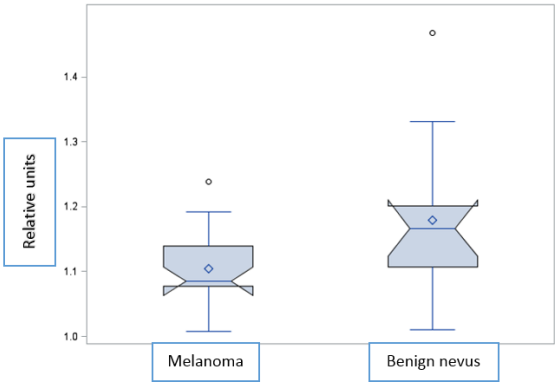

Fig. 11. Distribution of the ratio of maximum diameter and average diameter by diagnosis evaluated from the digital dermatoscopy images by using the discriminant analysis model. Mean of the ratio of maximum diameter and average diameter for melanomas was equal to 1.105, while mean of the ratio of maximum diameter and average diameter for benign nevus was equal to 1.178. Standard deviation for melanomas was equal to 0.054, for benign nevus – 0.122.

Diamonds show the mean of the ratio of maximum diameter and average diameter. For both types of the skin tumours, more observations are distribution below the mean.

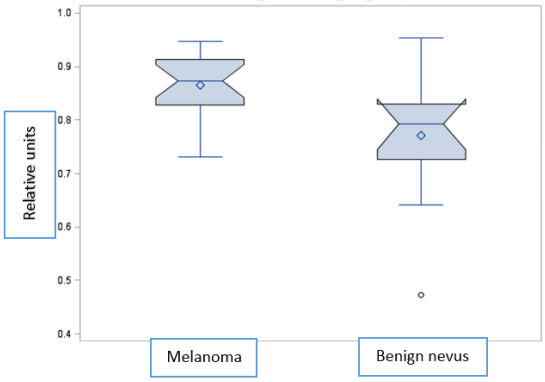

Fig. 12. Distribution of the ratio of minimum diameter and average diameter by diagnosis evaluated from the digital dermatoscopy images by using the discriminant analysis model. Mean of the ratio of the ratio of minimum diameter and average diameter for melanomas was equal to 0.865, while mean of the ratio of minimum diameter and average diameter for benign nevus was equal to 0.771. Standard deviation for melanomas was equal to 0.057, for benign nevus – 0.124.

Diamonds show the mean of the ratio of minimum diameter and average diameter. The values of the melanomas are more closely to the mean than the values of the benign nevus parameters, which are higher than the mean.

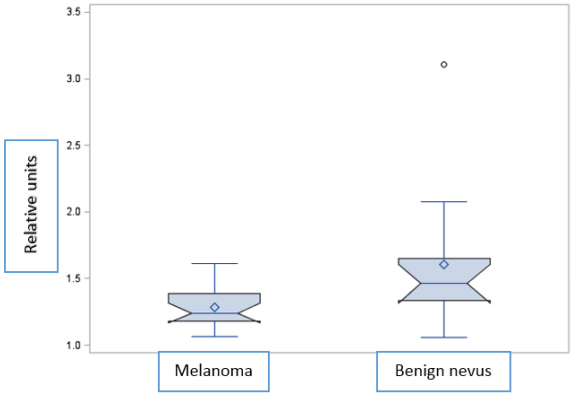

Fig. 13. Distribution of the ratio of maximum diameter and minimum diameter by diagnosis evaluated from the digital dermatoscopy images by using the discriminant analysis model. Mean of the ratio of minimum diameter and average diameter for melanomas was equal to 1.268, while mean of the ratio of minimum diameter and average diameter for benign nevus was equal to 1.606. Standard deviation for melanomas was equal to 0.145, for benign nevus – 0.537.

Diamonds show the mean of the ratio of maximum diameter and minimum diameter. More values are less than the mean of benign nevus parameters.

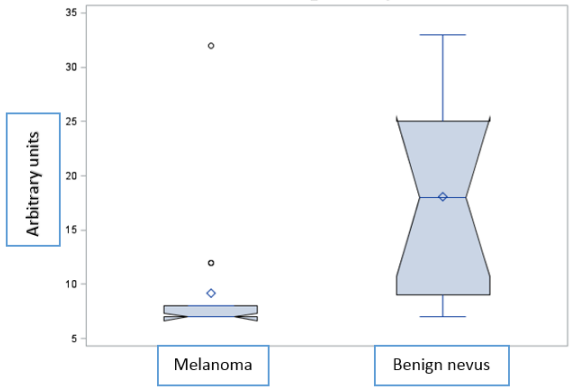

Fig. 14. Distribution of the 1st decile by diagnosis evaluated from the digital dermatoscopy images by using the discriminant analysis model. Mean of the 1st decile for melanomas was equal to 9.158 millimetres, while mean of the 1st decile for benign nevus was equal to 18.083 millimetres. Standard deviation for melanomas was equal to 5.833 millimetres, for benign nevus – 9.258 millimetres.

Diamonds show the mean of the 1st decile. In the case of melanoma, more values are distributed below the mean, while for the benign nevus values are placed very close to the mean.

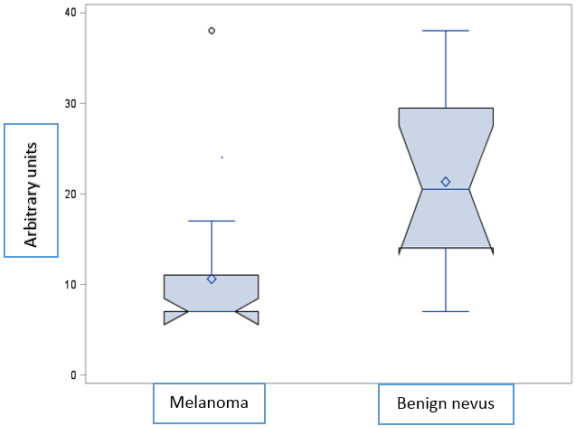

Fig. 15. Distribution of the 2nd decile by diagnosis evaluated from the digital dermatoscopy images by using the discriminant analysis model. Mean of the 2nd decile for melanomas was equal to 10.632 millimetres, while mean of the 2nd decile for benign nevus was equal to 21.333 millimetres. Standard deviation for melanomas was equal to 7.515 millimetres, for benign nevus – 10.228 millimetres.

Diamonds show the mean of the 2nd decile. For both types of the skin tumours, more values are distributed below the mean.

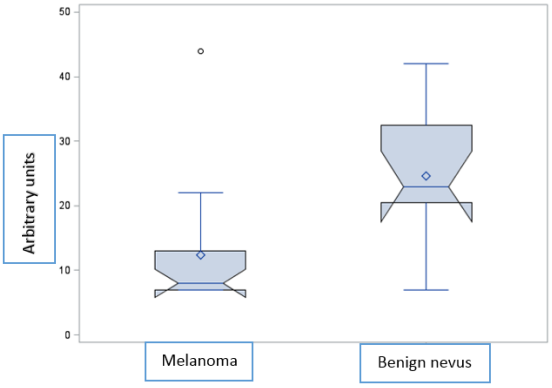

Fig. 16. Distribution of the 3rd decile by diagnosis evaluated from the digital dermatoscopy images by using the discriminant analysis model. Mean of the 3rd decile for melanomas was equal to 12.368 millimetres, while mean of the 3rd decile for benign nevus was equal to 24.583 millimetres. Standard deviation for melanomas was equal to 9.215 millimetres, for benign nevus – 10.933 millimetres.

Diamonds show the mean of the 3rd decile. For both types of the skin tumours, more values are distributed below the mean.

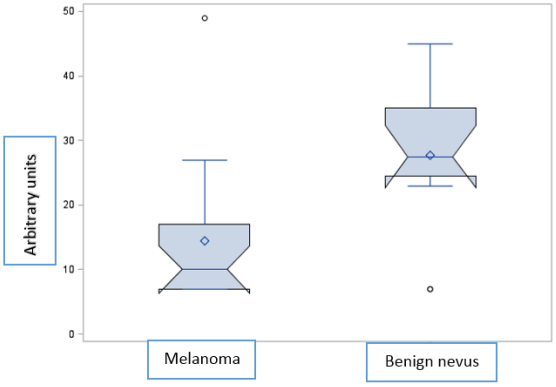

Fig. 17. Distribution of the 4th decile by diagnosis evaluated from the digital dermatoscopy images by using the discriminant analysis model. Mean of the 4th decile for melanomas was equal to 14.474 millimetres, while mean of the 4th decile for benign nevus was equal to 27.667 millimetres. Standard deviation for melanomas was equal to 10.637 millimetres, for benign nevus – 11.881 millimetres.

Diamonds show the mean of the 4th decile. For the melanomas, more values are under the mean. For the benign nevus, values are distributed around the mean.

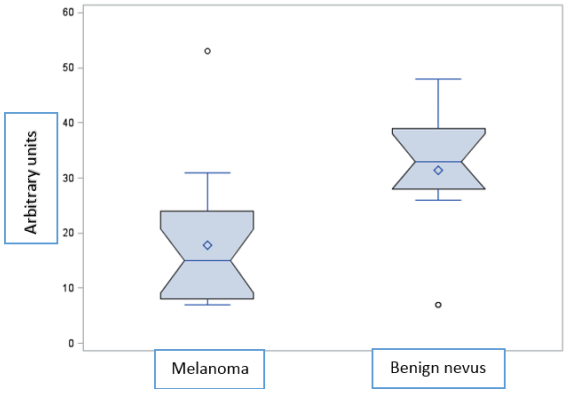

Fig. 18. Distribution of the 5th decile by diagnosis evaluated from the digital dermatoscopy images by using the discriminant analysis model. Mean of the 5th decile for melanomas was equal to 17.789 millimetres, while mean of the 5th decile for benign nevus was equal to 31.333 millimetres. Standard deviation for melanomas was equal to 11.583 millimetres, for benign nevus – 13.096 millimetres.

Diamonds show the mean of the 5th decile. For melanomas, values are distributed below the mean, while for the benign nevus, more values are distributed above the mean.

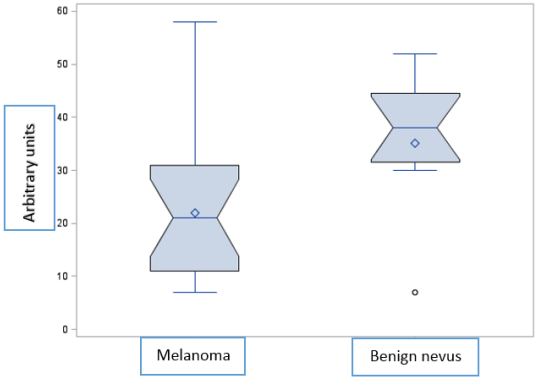

Fig. 19. Distribution of the 6th decile by diagnosis evaluated from the digital dermatoscopy images by using the discriminant analysis model. Mean of the 6th decile for melanomas was equal to 22.000 millimetres, while mean of the 6th decile for benign nevus was equal to 35.083 millimetres. Standard deviation for melanomas was equal to 12.987 millimetres, for benign nevus – 14.761 millimetres.

Diamonds show the mean of the 6th decile. For melanomas, more values are distributed below the mean, while for the benign nevus, more values are distributed above the mean.

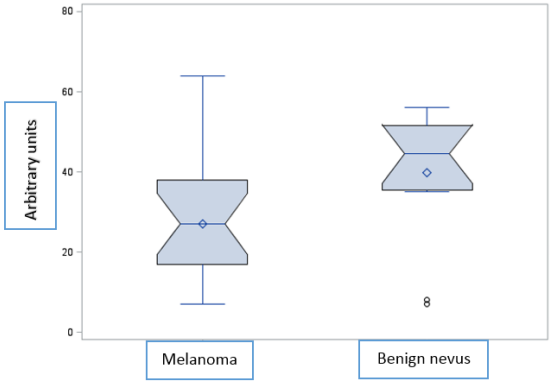

Fig. 20. Distribution of the 7th decile by diagnosis evaluated from the digital dermatoscopy images by using the discriminant analysis model. Mean of the 7th decile for melanomas was equal to 27.000 millimetres, while mean of the 7th decile for benign nevus was equal to 39.833 millimetres. Standard deviation for melanomas was equal to 14.079 millimetres, for benign nevus – 16.563 millimetres.

Diamonds show the mean of the 7th decile. In the case of melanoma, values of the parameters are distributed extremely close to the mean. For the benign nevus, more values are distributed above the mean.

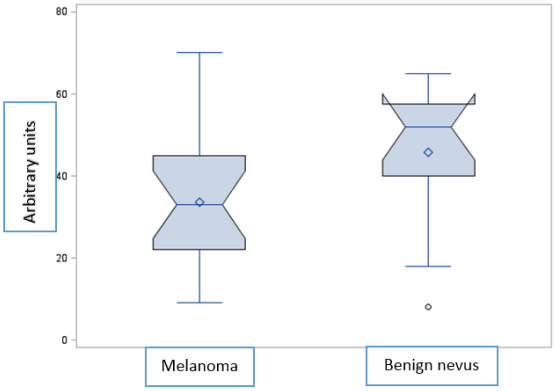

Fig. 21. Distribution of the 8th decile by diagnosis evaluated from the digital dermatoscopy images by using the discriminant analysis model. Mean of the 8th decile for melanomas was equal to 33.632 millimetres, while mean of the 8th decile for benign nevus was equal to 45.833 millimetres. Standard deviation for melanomas was equal to 14.720 millimetres, for benign nevus – 17.309 millimetres.

Diamonds show the mean of the 8th decile. In the case of melanoma, values of the parameters are distributed extremely close to the mean. For the benign nevus, more values are distributed above the mean.

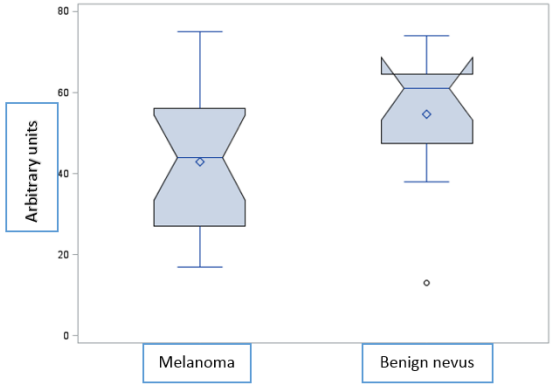

Fig. 22. Distribution of the 9th decile by diagnosis evaluated from the digital dermatoscopy images by using the discriminant analysis model. Mean of the 9th decile for melanomas was equal to 42.789 millimetres, while mean of the 9th decile for benign nevus was equal to 54.583 millimetres. Standard deviation for melanomas was equal to 15.109 millimetres, for benign nevus – 16.412 millimetres.

Diamonds show the mean of the 9th decile. For both graphs, more values are distributed above the mean.

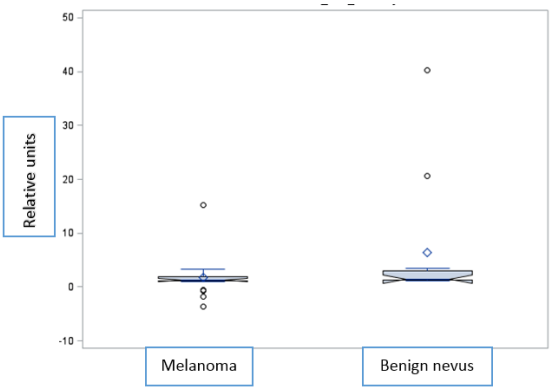

Fig. 23. Distribution of the ratio of average kurtosis (from 1000 directions) and maximum kurtosis by diagnosis evaluated from the ultrasonic images by using the logistic regression model. Mean of the ratio of average kurtosis (from 1000 directions) and maximum kurtosis for melanomas was equal to 1.711, while mean of the ratio of average kurtosis (from 1000 directions) and maximum kurtosis for benign nevus was equal to 6.463. Standard deviation for melanomas was equal to 3.562, for benign nevus – 11.962.

Diamonds show the mean Distribution of the ratio of average kurtosis (from 1000 directions) and maximum kurtosis. For the melanomas, more values are distributed above mean, while for the benign nevus, more values are distributed under the mean.

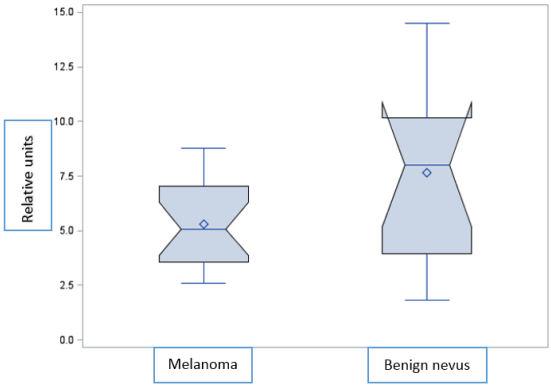

Fig. 24. Distribution of the ratio of perimeter and area by diagnosis evaluated from the ultrasonic images by using the logistic regression model. Mean of the ratio of perimeter and area for melanomas was equal to 5.290, while mean of the ratio of perimeter and area for benign nevus was equal to 7.670. Standard deviation for melanomas was equal to 1.962, for benign nevus – 4.048.

Diamonds show the mean of the ratio of perimeter and area. For the melanomas, more values are distributed below the mean and for the benign nevus, they are distributed above the mean.

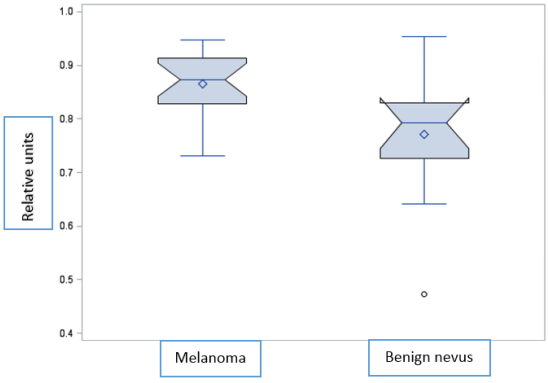

Fig. 25. Distribution of the ratio of minimum diameter and average diameter by diagnosis evaluated from the digital dermatoscopy images by using the logistic regression model. Mean of the ratio of minimum diameter and average diameter for melanomas was equal to 0.865, while mean of the 2nd decile for benign nevus was equal to 0.771. Standard deviation for melanomas was equal to 0.057, for benign nevus – 0.124.

Diamonds show the mean of the ratio of minimum diameter and average diameter. For the melanomas and for the benign nevus, more values are distributed above the mean.

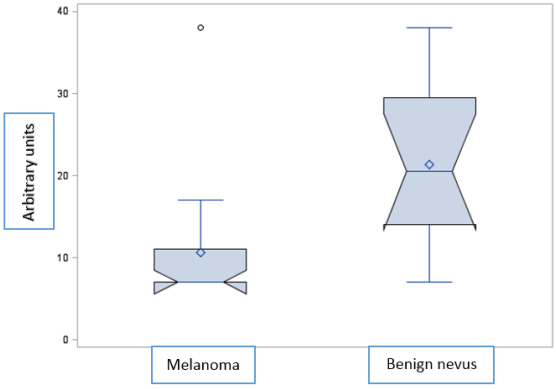

Fig. 26. Distribution of the 2nd decile by diagnosis evaluated from the digital dermatoscopy images by using the logistic regression model. Mean of the 2nd decile for melanomas was equal to 10.632 millimetres, while mean of the 2nd decile for benign nevus was equal to 21.333 millimetres. Standard deviation for melanomas was equal to 7.515 millimetres, for benign nevus – 10.228 millimetres.

Diamonds show the mean of the 2nd decile. In the case of melanomas, a lot more values are distributed below the mean than for the benign nevus.

LIST OF THE PUBLICATIONS

Publications referred in Journals from the master list of Thomson Reuters Web of Science (with impact factor)

1. **Drulytė, Indrė**; Ruzgas, Tomas; Raišutis, Renaldas; Valiukevičienė, Skaidra. Assessment and comparison of likely density distributions in the cases of thickness measurement of skin tumours by ultrasound examination and histological analysis // Journal of vibroengineering. Kaunas: JVE International. ISSN 1392-8716. 2016, vol. 18, iss. 5, p. 3279-3291. IF: 0,398 (2016).

2. **Drulytė, Indrė**; Ruzgas, Tomas; Raišutis, Renaldas; Valiukevičienė, Skaidra; Linkevičiūtė, Gintarė. Application of automatic statistical post–processing method for analysis of ultrasonic and digital dermatoscopy images // Libyan Journal of Medicine. Oxon: Taylor & Francis. ISSN 1993-2820. eISSN 1819-6357. 2018, vol. 13, iss. 1, art. no. 1479600, p. 1-11. DOI: 10.1080/19932820.2018.1479600. IF: 1,656 (2017).

Publications in Reviewed Proceedings of International Scientific Conferences

1. **Drulytė, Indrė**; Ruzgas, Tomas; Raišutis, Renaldas; Valiukevičienė, Skaidra; Linkevičiūtė, Gintarė. Automatic statistical post–processing method for analysis of ultrasonic and digital dermatoscopy measurements // Smithy of Ideas 19-21 May 2017, Valmiera, Latvia.

2. .**Drulytė, Indrė**; Ruzgas, Tomas; Raišutis, Renaldas; Valiukevičienė, Skaidra; Linkevičiūtė. Automatic method for assessment and integration of measurements performed by ultrasonic and spectrophotometric technologies in order to estimate the lesion parameters of the human tissue // Data analysis methods for software systems : 8th international workshop, Druskininkai, Lithuania, 1-3 December 2016 / Lithuanian Computer Society, Vilnius University Institute of Mathematics and Informatics, Lithuanian Academy of Sciences, 2016, ISBN 9789986680611. p. 18 – 19.

Publications in Reviewed Proceedings of National Scientific Conferences

1. **Drulytė, Indrė**; Ruzgas, Tomas; Raišutis, Renaldas; Valiukevičienė, Skaidra; Linkevičiūtė, Gintarė. Ultragarso ir skaitmeninės dermatoskopijos technologijomis gautų matavimo rezultatų apdorojimo metodas žmogaus odos pažeidimų parametrams vertinti // Mokslas - sveikatai : X nacionalinė doktorantų mokslinė konferencija, 7 April 2017, Kaunas : konferencijos tezių knyga / Lietuvos sveikatos mokslų universitetas. Kaunas: Lietuvos sveikatos mokslų universiteto Leidybos namai, 2017, ISBN 9789955154808. p. 9-10.

2. **Drulytė, Indrė**; Ruzgas, Tomas. Ultragarsinių vaizdų ir žmogaus odos struktūros pažeidimų parametrų vertinimas // Mokslas - sveikatai: IX nacionalinė doktorantų mokslinė konferencija, 13 April 2016, Kaunas: konferencijos tezių knyga

/ Lietuvos sveikatos mokslų universitetas. Kaunas: Lietuvos sveikatos mokslų universiteto Leidybos namai, 2016, ISBN 9789955154310. p. 8-9.

The results of the research presented in the scientific conferences

1. **Drulytė, Indrė**; Ruzgas, Tomas. 56th national conference of Lithuania mathematics association. Presentation of „Netiesinių statistikų taikymas ultragarso tyrimuose“, 2015, , KTU, Kaunas.
2. **Drulytė, Indrė**; Ruzgas, Tomas. IX national conference "mokslas - sveikatai". Presentation of „Ultragarsinių vaizdų ir žmogaus odos struktūros pažeidimų parametrų vertinimas.“ 13 April 2016, LSMU, Kaunas.
3. **Drulytė, Indrė**; Ruzgas, Tomas; Raišutis, Renaldas; Valiukevičienė, Skaidra. Data analysis methods for software systems : 8th international workshop. Presentation of “Automatic method for assessment and integration of measurements performed by ultrasonic and spectrophotometric technologies in order to estimate the lesion parameters of the human tissue.” 1-3 December 2016, Druskininkai.
4. **Drulytė, Indrė**; Ruzgas, Tomas; Raišutis, Renaldas; Valiukevičienė, Skaidra; Linkevičiūtė, Gintarė. X national conference "mokslas - sveikatai". Presentation of „Ultragarso ir skaitmeninės dermatoskopijos technologijomis gautų matavimo rezultatų apdorojimo metodas žmogaus odos pažeidimų parametrams vertinti”. 7 April 2017, LSMU, Kaunas.
5. **Drulytė, Indrė**; Ruzgas, Tomas; Raišutis, Renaldas; Valiukevičienė, Skaidra; Linkevičiūtė, Gintarė. International workshop conference „smithy of ideas 2017“. Presentation of “Automatic statistical post–processing method for analysis of ultrasonic and digital dermatoscopy measurements”. 19-21 May 2017, Valmiera, Latvia.

SL344. 2019-03-01, 18,75 leidyb. apsk. l. Tiražas 12 egz. Užsakymas 59.
Išleido Kauno technologijos universitetas, K. Donelaičio g. 73, 44249 Kaunas
Spausdino leidyklos „Technologija“ spaustuvė, Studentų g. 54, 51424 Kaunas